Resonant-state expansion and approximations for treating perturbations in the medium surrounding an optical system

by

Shaikhah Fahd Almousa

A Thesis submitted to Cardiff University
for the degree of Doctor of Philosophy

November 2023

Abstract

Developing a rigorous perturbation theory to treat changes in open optical systems may present a challenging task due to the leaky nature of such systems, in which the conventional conditions of Hermitian systems become inapplicable. Definitions of orthonormality and completeness have been reformulated for a special class of resonances, popularly known as resonant states or quasi-normal modes. Such resonances have been employed to develop modal expansion techniques for treating perturbations in open systems, such as the resonant-state expansion method (RSE). The RSE transforms Maxwell's equations into a linear eigenvalue problem, producing the perturbed modes with high accuracy and quick convergence. A major limitation of the RSE is that perturbations must be taken within the system where the resonant states are complete. In this thesis, we develop a rigorous theory based on the RSE to treat perturbations in the surrounding medium. This is achieved by performing a transformation to Maxwell's equations, which maps perturbations of the surrounding medium onto effective perturbations within the system where the resonant states are complete. By treating such perturbations rigorously with the RSE, we find the perturbed modes of the system for arbitrary homogeneous perturbations of the surrounding medium with any desired accuracy. We further develop approximations beyond the first-order accuracy using only one mode. We apply the developed approaches to accurately predict the resonance shift of highly responsive modes due to changes in the surrounding medium. We provide a special treatment to chiral systems that have a weak impact on the resonance shift. Such an impact is enhanced by deriving a linear splitting of quasi-degenerate modes in chirality. We illustrate such a splitting using quasi-degenerate modes deduced from our analysis of spherical systems.

Publications

Publications

- S. F. Almousa, and E. A. Muljarov. *Exact theory and approximations for optical resonators in a changing external medium.* Physical Review B 107, L081401 (2023).

- S. F. Almousa, T. Weiss and E. A. Muljarov. *Employing quasidegenerate optical modes for chiral sensing.* Physical Review B 109, L041410 (2024).

- S. Both, S. F. Almousa, H. Giessen, E. A. Muljarov, D. Shakirova, and T. Weiss. *Nanophotonic chiral sensing: How does it actually work?* META 2023 proceedings, ISSN 2429-1390 (2023).

Presentations

- *Employing quasi-degenerate modes for chirality sensing: extended*, Physics chat, Cardiff University (2023).

- *Employing quasi-degenerate modes for chirality sensing*, Photon, Nottingham, UK (2022).

- *Exact theory and approximations for optical resonators in a changing external medium*, NANOMETA, Seefeld in Tirol, Austria (2022).

- *An efficient way of treating changes of the medium surrounding an optical system*, The annual early career researcher poster competition, Cardiff University (2022).
- *Resonant-state expansion for perturbations in the surrounding medium of open optical systems*, Postgraduate conference, Cardiff University (2021).
- *Varying the medium surrounding an optical resonator: An efficient and rigorous way to calculate its spectral changes*, Physics chat, Cardiff University (2021).
- *Resonant states in dielectric core-shell systems*, Theory seminar, Cardiff University (2020).

Contents

Abstract **v**

Publications **vii**

Acknowledgements **xiii**

Introduction **1**

1 Resonant states **7**

1.1 Introduction 7

1.2 Orthogonality relation 12

1.3 Normalization conditions 13

1.4 Finding the resonant states 19

1.5 Resonant-state expansion (RSE) 23

1.6 First-order perturbation theory 30

1.7 Summary 32

2 RSE for perturbations in the surrounding medium **35**

2.1 Transformation matrix 35

2.2 Frequency dispersion of the optical system and the surrounding medium . . 42

2.3 Diagonal and first-order approximations 43

2.4 Effective-pole resonant states 45

2.5 Summary 49

3 Application of the RSE to refractive-index sensing **51**

3.1 Plasmonic nonoparticles 52

3.2 Microresonators 68
3.3 Summary 73

4 Regularization-based approaches 75
4.1 Orthonormality and Poynting's theorem for regularized resonant states . . 76
4.2 Regularized RSE 80
4.3 Regularized diagonal approximation 84
4.4 First-order approximation and comparison with Both and Weiss 86
4.5 Summary 89

5 Achieving degeneracy in spherical systems 91
5.1 General solution 92
5.2 An arbitrary magnetic sphere 96
5.3 A core-shell system 97
5.4 Introducing chirality to the magnetic sphere: resonant states and secular equation 105
5.5 Summary 108

6 Employing degenerate modes for chirality sensing 109
6.1 Motivation 109
6.2 Two-mode RSE 111
6.3 Chirality contribution in mode splitting 112
6.4 Application 1: a magnetic sphere 114
6.5 Application 2: a core-shell system 117
6.6 Summary 123

7 Conclusion 127
7.1 Thesis Overview 127
7.2 Future work 131

A Dielectric slab 132

B Matrix elements of the RSE **135**

B.1 Matrix elements for homogeneous chirality perturbations 135

B.2 Matrix elements for the point-like chiral perturber 137

C More results **141**

C.1 Effective-pole resonant states generated by Bessel function 141

C.2 Application of regularized diagonal approximation to refractive index sensing 141

"To mothers in science who carry family responsibilities on one shoulder and a mission in science on the other"

Acknowledgements

First and foremost, I would like to express my immense gratitude to King Saud University for supporting my higher education and for funding my postgraduate studies. I'm thankful to my supervisor, Dr. Sang Soon Oh, who helped me reach the finish line of my PhD journey. I am thankful for all the scientific communications and activities we had in group meetings and seminars. My sincere appreciation extends to my examiners, Dr. Francisco Rodríguez Fortuño and Dr. Leandro Beltrachini, for their constructive feedback and for the interesting discussions during the viva.

I would also like to extend my gratitude to my former supervisor, Dr. Egor Muljarov, for the scientific support. I am deeply appreciative of the invaluable support and advice I received from Dr. Matthew Smith, Prof. Wolfgang Langbein, and Dr. Cosimo Inserra throughout my PhD journey. A special thanks goes to Dr. Zeeshan Ahmad and Dr. Thomas Allcock for their feedback on my thesis, to Prof. Dr. Thomas Weiss for his feedback on the sixth chapter, to Prof. Haley Gomez for her instant response for suggestions of summer camps, which supported me with writing the first chapter, to Dr. Mark Doost for his generous discussions about his work on the RSE, and to Andrew Hannington for reviving the LaTeX template for PhD theses.

Words fall short in expressing my gratitude to my family—parents, husband, children, and siblings—for their endless support, understanding, and heartfelt prayers. My sincere gratitude extends to all my friends and to all my officemates in the TRH for fostering a supportive and inclusive environment, and to Luba, Tom, and Luke for our invented style in the theory literature discussion group. Lastly, I would like to thank my children's teachers for their continued support and for their exceptional solidarity during the lockdown days.

Introduction

Identifying materials and their chemical and physical properties is crucial for advancements in science and technology. Using the interaction of light with matter to obtain information about the properties of a material offers both efficiency and high precision. Detecting the material optically provides, for instance, non-contact measurements without physically or chemically disturbing the material. This becomes particularly useful for ensuring safety measures, close to explosive gases for example [1], or to avoid the necessity of blood samples, such as measuring the blood sugar in diabetic patients [2]. The strong light-matter interaction of optical resonators in nanophotonic systems enables ultra-sensitive resonance shifts in response to changes in their environment. Such detectable changes in the environment are often appear localized in a form of a molecule [3, 4] or delocalized in the entire environment [5] in various industrial applications, environmental monitoring, and medical diagnosis.

Sensing a molecule or substance surrounding an optical resonator by looking at the change in its eigenmodes, such as localized surface plasmon modes in metallic nanoparticles [6] or whispering gallery modes in dielectric microspheres [7], has recently become an important application of nanophotonics. However, modelling and optimization of optical resonators for sensing applications, as well as interpreting the sensing information, present complicated 'inverse' problems which require extensive and repetitive calculations. Theoretical approaches, in which the eigenmodes of the system are calculated only once and then used as a fixed basis for treating any changes in the environment, could reduce the computational time dramatically, by orders of magnitude [8]. At the same time, for a number of technologically crucial applications

of optical resonators, such as refractive index or chirality sensing, it is very important to develop a theory which would accurately and efficiently treat any changes of the medium and is not limited to first order. For example, the same optical resonator may be used as a sensor operating in different media surrounding it. However, developing a rigorous perturbation theory for external perturbations of an open optical system may present a fundamental challenge. In particular, treating the optical system through a class of eigenmodes, popularly known as resonant states, presents a challenge due to the divergence of the electromagnetic field of the eigenmodes with distance. Such divergence not only presents a challenge with the mode normalization, but also results in limited completeness of the eigenmodes outside the system [8, 9].

The resonant states of an optical system, also known as quasi-normal modes [10], are the eigen solutions to Maxwell's equations with purely outgoing wave boundary conditions. They fully describe the spectral properties of an optical system, providing direct access to its scattering matrix [11, 12]. Their normalization has been achieved either analytically or numerically [8, 10, 13]. Their analytical normalization consists of a sum of a volume integral of the square of the field of the resonant state with a material-dependent weight function, performed over any finite volume containing the system, and an integral of the fields over the volume surface [14–16]. Such an additional surface term compensates for the divergence of the field outside the system [13]. Owing to the well-defined boundaries of an optical system, the resonant states are complete at least within the minimal convex volume containing the system [14, 16].

The completeness of resonant states within the system is at the heart of the resonant-state expansion (RSE), a rigorous method recently developed for treating perturbations of arbitrary shape and strength by mapping Maxwell's equations onto a linear matrix eigenvalue problem [13, 14]. The RSE has been generalized to include frequency dispersion [17, 18] as well as magnetic, chiral, and bi-anisotropic materials [16] and was proven to be orders of magnitude more efficient than popular computational methods [14, 19]. However, a significant limitation of the RSE is that all perturbations must be contained within the basis system.

First- and second-order perturbation theories for open resonators treating finite-size volume perturbations [14, 20–22] or boundary perturbations [23] or both together [24] are available in the literature. However, these approaches are not suitable for treating homogeneous perturbations of the entire space surrounding the system, which often arise in sensing applications [25]. Recently, a first-order perturbation theory for homogeneous and isotropic perturbations of the surrounding medium has been developed [26]. This theory uses the analytic normalization of the resonant states but treats perturbations in a way entirely different from the RSE. Crucially, it is limited to small perturbations and predicts only linear changes of the frequencies of resonant states with the medium parameters, such as the permittivity. However, the optical modes can be extremely sensitive to even small changes of the environment. In plasmonic resonators, for example, this can be due to strong near fields and hot spots. Also, single-mode theories fail when two or more resonant states affected by perturbations are spectrally close to each other, such as in the examples considered in [27, 28]. At the same time, the same nanosensor may be operating in various solutions, with a difference in the refractive index going significantly beyond first order.

In this thesis, we present a rigorous RSE-based approach to treat any changes in the homogeneous isotropic medium surrounding an optical system. By developing a transformation matrix to Maxwell's equations, we map the changes of the surrounding medium onto effective perturbations of the system itself, which are treatable by the RSE. Additionally, we propose another RSE approach based on regularization to directly treat perturbations in the surrounding medium and test its convergence. The regularization-based approach yields a single-mode approximation for treating perturbations in the surrounding medium. We apply the RSE-based method and the developed approximations to a wide class of nanoresonators and microparticles to calculate the spectral changes of highly responsive modes caused by changing the dielectric properties of the surrounding medium. Through the RSE and the regularization-based approximation, we exhibit a linear splitting of quasi-degenerate modes due to a presence of a chiral medium or molecule, contrary to the expected quadratic contribution of chirality in the spectral changes. Employing single spherical

systems to achieve a linear splitting in chirality can provide insights for developing novel chiral sensing schemes. It also lifts the constraints of establishing chirality-induced strong coupling in comparison to prior efforts [29], in which a strong coupling between bound states in the continuum is demonstrated by introducing chirality in the vicinity of a metasurface.

This thesis is structured as follows:

1. In the first chapter, we introduce the concept of resonant states, present their orthogonality relation, normalization forms, and discuss analytical and numerical approaches for finding the resonant states in open optical systems. We then demonstrate the RSE, its development, and first-order perturbation theory in literature.

2. The second chapter introduces a transformation matrix to map the perturbation in the surrounding medium to effective perturbation inside the system to be treated by the RSE. We discuss the implications of the transformation for materials with dispersion. We then extract from the RSE the diagonal approximation and the first-order approximation.

3. In the third chapter, we apply the RSE-based approach and other approximations to experimentally relevant applications. Using the developed approaches, we calculate the frequency of the system as a function of the refractive index of the surrounding medium. We consider a wide class of plasmonic nonoparticles as well as microresonators.

4. In the fourth chapter, we propose an RSE method based on regularization and examine its convergence for perturbation outside the system. We develop a regularized diagonal approximation of single mode only to treat perturbations in the exterior medium. We compare our results with the best available approach in the literature and prove their equivalence in the first order.

5. In the fifth chapter, we analyze the analytical solution of spherical systems to

deduce conditions for achieving degeneracy in single spherical particles. In our discussion, we focus on a sphere and a core-shell system. We demonstrate quasi-degenerate modes in such systems.

6. The sixth chapter demonstrates a linear splitting of quasi-degenerate modes in chirality. We consider a presence of chirality perturbation with different possibilities, such as inside or outside the resonator, within the shell of a core-shell system, or inhomogeneously as a chiral molecule. We treat such perturbations with the RSE and the regularized diagonal approximation.

7. We conclude by presenting a thesis overview and an outlook on the presented work.

Chapter 1

Resonant states

1.1 Introduction

The eigen wavefunctions of conservative systems, such as a particle in an infinite square well, have oscillatory time dependence. Imposing outgoing boundary conditions at large distances outside the system results in complex eigenvalues, leading to exponential decay of their wavefunctions in time. The concept of considering purely outgoing boundary conditions outside the system to solve eigenvalue problems roots in nuclear physics in the early description of tunneling, particularly for the description of alpha decay, proposed by Gamow in 1921 [30]. Therefore, the solutions in these systems became known as Gamow states [31]. They are also known as decaying states or unstable states, characterising their finite lifetime, or more popularly later as resonant states, indicating their relation to the resonance of the system [32]. For a particle moving in a spherically symmetric potential $V(r)$ of a finite range such that $V(r) = 0$ for $r > R$, a simple case which can be given as an illustration is the S-waves, i.e., the angular momentum quantum number l is zero. The particle then has a solution $\Psi(r,t) = \psi(r)e^{-iEt}$, where $\psi(r)$ satisfies the time-independent Schrödinger equation [32],

$$\left[\frac{d^2}{dr^2} + E - V(r)\right]\psi(r) = 0, \tag{1.1}$$

in which for simplicity of presentation, we consider $\hbar = 1$ and $m = 1/2$. Considering purely outgoing boundary conditions in the region $r > R$ quantizes the energy of the particle E, and also requires it to be complex-valued with a negative imaginary part. Considering the region outside the potential range $r > R$, the wavefunction then has the solution

$$\Psi_n(r,t) = C_n e^{i(\sqrt{E_n}r - E_n t)}\,, \tag{1.2}$$

where C_n is the normalization constant and where the complex energy E_n can be expressed as $E_n = \mathcal{E} - i\frac{\Gamma}{2}$, with n labelling the state. Thus, the temporal part of the wavefunction decays as $e^{-\frac{\Gamma}{2}t}$. Although the decay factor Γ of the resonant states was satisfying because it interprets the finite lifetime of the decaying states, the spatial part, on the other side, grows exponentially at large distances in the region $r > R$. Consequently, the resonant states become non square-integrable and the properties of Hermitian systems that follows from Hilbert space, such as the orthogonality and completeness are no longer applicable, leading to challenges in their normalization.

The applications of the resonant states in physical processes, such as scattering and decay, called the attention to identify them in other realms of physics. In optics, one of the early adoption referred to the resonant states as morphology-dependent resonances [33], highlighting their dependence on the geometry and the material properties of the optical resonator. The resonant states are also popularly known as quasi-normal modes since, under certain treatment, they have orthogonality and completeness conditions analogous to those found for the normal modes in closed systems [9]. In all cases, they are the eigensolutions of the time-independent source-free Maxwell's equations, considering purely outgoing boundary conditions [9, 34]. For a simple optical system, such as a planar slab of thickness $2a$ in vacuum, having material properties described by permittivity along the z direction as [13]

$$\varepsilon(z) = \begin{cases} \varepsilon_s & \text{for } |z| < a \\ 1 & \text{for } |z| \geq a \end{cases} \tag{1.3}$$

and permeability $\mu = 1$ everywhere, the electric field polarized in the x direction and

having normal incidence is described by [13],

$$\left[\frac{d^2}{dz^2} + \varepsilon(z)k^2\right] E(z) = 0\,, \tag{1.4}$$

with k being the wavenumber. Here, the time dependence of the electric field $E(z)$ is given by $e^{-i\omega t}$, where $\omega = ck$, and c is the speed of light. The latter equation is a full analogy to the S-waves given by Eq. (1.1), where the quantum potential in the wave equation represents the permittivity in optics [35]. Considering purely outgoing boundary conditions in the Maxwell's equation Eq. (1.4) results in the following wavefunctions [13],

$$E_n(z) = \begin{cases} C_n e^{ik_n z} & \text{for } z \geq a \\ A_n(e^{i\sqrt{\varepsilon_s}k_n z} + (-1)^n e^{-i\sqrt{\varepsilon_s}k_n z}) & \text{for } |z| < a \\ (-1)^n C_n e^{-ik_n z} & \text{for } z \leq -a\,, \end{cases} \tag{1.5}$$

having a complex wavenumber given by,

$$k_n = \frac{1}{2a\sqrt{\varepsilon_s}}(n\pi - i\ln\alpha)\,, \qquad n = 0, \pm 1, \pm 2, \ldots. \tag{1.6}$$

with a negative imaginary part, where $\alpha = \frac{\sqrt{\varepsilon_s}+1}{\sqrt{\varepsilon_s}-1}$.

To illustrate the concept of resonate states, we consider an example of a dielectric slab with $\varepsilon_s = 2.5$, considering other boundary conditions in the field equation Eq. (1.4). These conditions are incoming boundary conditions, in which the waves travel to the system from both sides, and transparent boundary conditions, or non-reflecting boundaries, as the wave travels to the system and continues in the same direction to the other side of the system [36]. Imposing boundary conditions of purely incoming or purely outgoing waves, or even transparent conditions on the dielectric slab, quantizes the wavenumber to countable infinite number, with n labelling the state, see Appendix A for full analysis. The wavenumber for each condition is equidistantly distributed in the spectrum, as shown in the inset to the right of Fig. 1.1(a). The equidistant spectrum is physically arising from the constructive interference of the

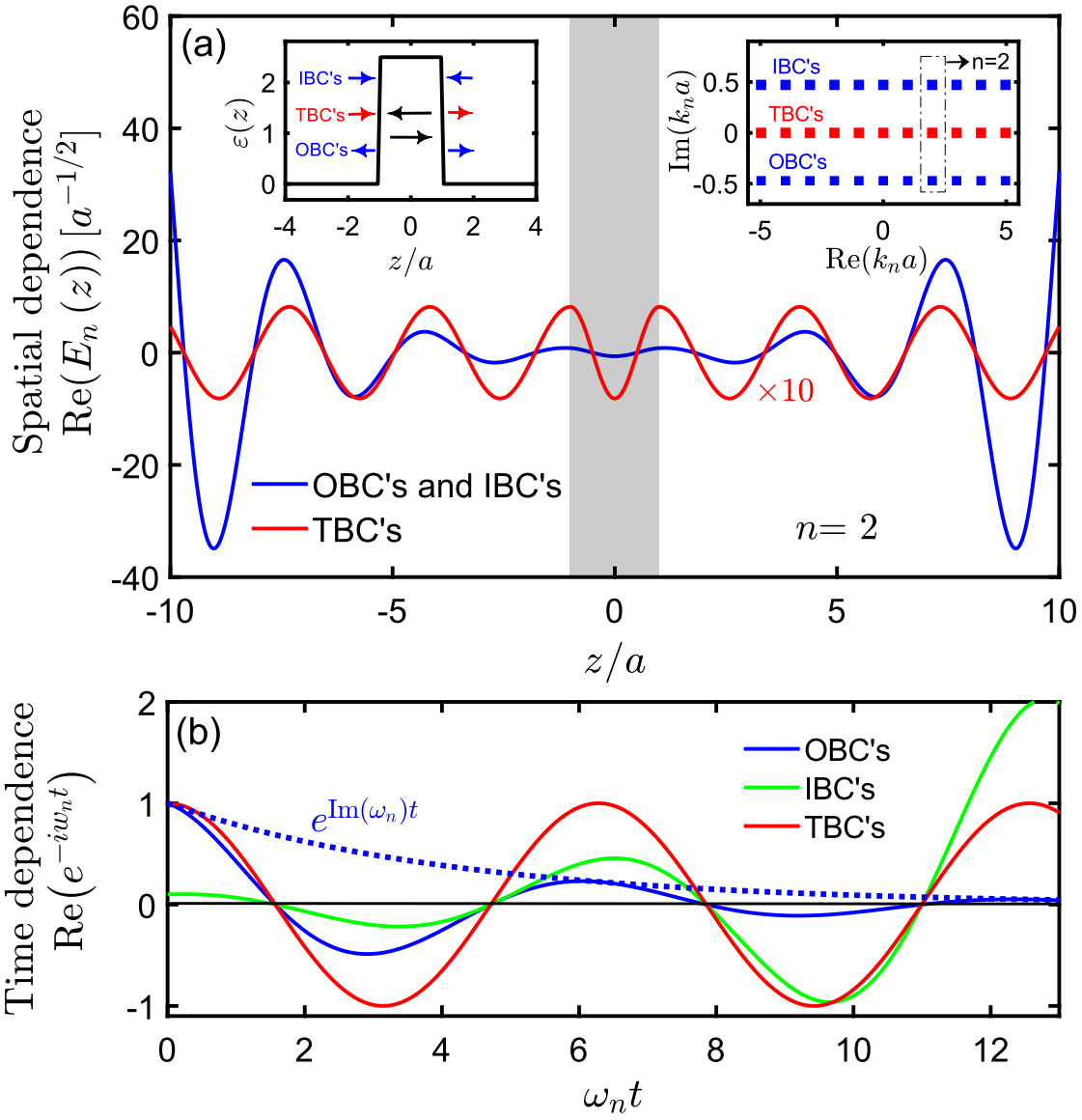

Figure 1.1. (a) The real spatial part of the electric field $\mathrm{Re}(E_n(z))$ of mode $n=2$ inside (shaded area) and outside a dielectric slab, considering three boundary conditions, incoming boundary conditions (IBCs) and outgoing boundary conditions (OBCs) (blue) and transparent boundary conditions (TBCs) (red), across a dielectric slab of width $2a$ and permittivity $\varepsilon=2$, as shown in the inset on the left of the permittivity function $\varepsilon(z)$, showing also schematics of the three boundary conditions. The eigen wavenumber k_n in the complex plane is shown in the inset on the right for the three conditions with the mode $n=2$ highlighted. (b) The real part of the time dependence $e^{-iw_n t}$ as a function of $\omega_n t$ of the OBCs (blue) with showing its exponentially decaying factor $e^{\mathrm{Im}(\omega_n)t}$ (dotted blue), IBCs (green), and TBCs (red).

waves multiply reflected from the slab surface, and thus denoted as Fabry-Perót modes for its similarities with the Fabry-Perót double-mirror resonator [37]. The wavenumber in the case of transparent boundary conditions is real while the wavenumbers of both the outgoing boundary conditions and incoming boundary conditions are complex with one being the complex conjugate of the other.

The real spatial part of the electric field $Re(E_n(z))$ and the real part of the time dependence $e^{-iw_n t}$, corresponding to $n = 2$ are shown in Fig. 1.1(a,b) for the three boundary conditions. The real wavenumber in the case of transparent conditions results in periodic oscillations of the field in both space and time as shown in Fig. 1.1(a,b). The complex wavenumber in the case of outgoing and incoming conditions results in exponential growth of the electric field outside the slab, as shown in Fig. 1.1(a). For the outgoing boundary conditions, the negative sign of the imaginary part of the wavenumber plays the role of the exponential decay in the time dependence of the field. The decay factor is given by $e^{\mathrm{Im}(\omega_n)t}$, where $\mathrm{Im}(w_n)$ is the imaginary part of the angular frequency $\omega_n = ck_n$, as shown in Fig. 1.1(b). The electric field in the case of outgoing boundary conditions resembles the oscillations of a classical damped oscillator. Hence, considering outgoing boundary conditions, not only quantizes the wavenumber, but also provides a finite lifetime to the wavefunction.

In general, the resonant states of an arbitrary linear medium are described by the following time-independent Maxwell's equations (Gaussian units) [38],

$$\nabla \cdot \mathbf{D} = 0\,, \qquad \nabla \cdot \mathbf{B} = 0\,, \tag{1.7}$$

$$\nabla \times \mathbf{E} = ik\mathbf{B}\,, \qquad \nabla \times \mathbf{H} = -ik\mathbf{D}\,, \tag{1.8}$$

considering outgoing boundary conditions, where k is the wavenumber, and the time dependence is given by $e^{-i\omega t}$, where $\omega = ck$. The response of the material is determined by the constitutive relations [39]

$$\mathbf{D} = \hat{\boldsymbol{\varepsilon}}(k, \mathbf{r})\mathbf{E} + \hat{\boldsymbol{\xi}}(k, \mathbf{r})\mathbf{H}\,, \tag{1.9}$$

$$\mathbf{B} = \hat{\boldsymbol{\mu}}(k, \mathbf{r})\mathbf{H} + \hat{\boldsymbol{\zeta}}(k, \mathbf{r})\mathbf{E}\,, \tag{1.10}$$

where $\hat{\boldsymbol{\varepsilon}}(k,\mathbf{r})$, $\hat{\boldsymbol{\mu}}(k,\mathbf{r})$, $\hat{\boldsymbol{\xi}}(k,\mathbf{r})$ and $\hat{\boldsymbol{\zeta}}(k,\mathbf{r})$ are, respectively, the permittivity, permeability and the bi-anisotropy 3×3 frequency-dependent tensors of the medium. We consider in our analysis reciprocal systems, i.e., $\hat{\boldsymbol{\varepsilon}}^{\mathrm{T}} = \hat{\boldsymbol{\varepsilon}}$, $\hat{\boldsymbol{\mu}}^{\mathrm{T}} = \hat{\boldsymbol{\mu}}$, and $\hat{\boldsymbol{\xi}}^{\mathrm{T}} = -\hat{\boldsymbol{\zeta}}$, where the superscript is for the matrix transpose [40]. For isotropic chiral media, $\hat{\boldsymbol{\xi}} = -i\kappa\hat{\mathbf{1}}$ and $\hat{\boldsymbol{\zeta}} = i\kappa\hat{\mathbf{1}}$, where κ is the Pasteur's parameter quantifying the system's chirality [39]. For simplicity in this introductory chapter, we consider $\hat{\boldsymbol{\mu}} = \hat{\mathbf{1}}$ and $\hat{\boldsymbol{\zeta}} = \hat{\boldsymbol{\xi}} = \hat{\mathbf{0}}$, where $\hat{\mathbf{0}}$ and $\hat{\mathbf{1}}$ are the 3×3 zero and unit tensors, respectively, and use the following form of Maxwell's equation,

$$-\nabla\times\nabla\times\mathbf{E}(\mathbf{r}) + k^2\hat{\boldsymbol{\varepsilon}}(\mathbf{r})\mathbf{E}(\mathbf{r}) = \mathbf{0}\,, \tag{1.11}$$

which can be obtained directly by using $\nabla\times\mathbf{H} = -ik\hat{\boldsymbol{\varepsilon}}\mathbf{E}$ in the curl of $\nabla\times\mathbf{E} = ik\mathbf{H}$. We also highlight that we define the system as the internal region of the compact permittivity throughout this thesis. As a final note, in the following chapters, we rely on the 6×6 compact form of Maxwell's equations introduced in [16], providing complete description of both the electric and magnetic fields in Eqs. (1.8), (1.9), and (1.10) of materials described by a generalized permittivity tensor. In the following section, we present the formulation of the orthogonality condition of resonant states.

1.2 Orthogonality relation

The conditions of orthogonality and normalization of the wavefunctions that follows from the inner product in Hermitian systems cannot be used for the resonant states due to their exponential growth with distance outside the resonator. The orthogonality of two resonant states having, respectively, k_n and k_m with $k_n \neq k_m$ can be derived in a direct way. We consider a resonant state satisfying

$$-\nabla\times\nabla\times\mathbf{E}_n(\mathbf{r}) + k_n^2\hat{\boldsymbol{\varepsilon}}(\mathbf{r})\mathbf{E}_n(\mathbf{r}) = \mathbf{0}\,, \tag{1.12}$$

and another resonant state with index m, which satisfies

$$-\nabla\times\nabla\times\mathbf{E}_m(\mathbf{r}) + k_m^2\hat{\boldsymbol{\varepsilon}}(\mathbf{r})\mathbf{E}_m(\mathbf{r}) = \mathbf{0}\,. \tag{1.13}$$

Multiplying Eq. (1.12) by $\mathbf{E}_m(\mathbf{r})$ and Eq. (1.13) by $\mathbf{E}_n(\mathbf{r})$, subtracting the two equations, using the vector identity $\nabla \times \nabla \times \mathbf{E} = \nabla(\nabla \cdot \mathbf{E}) - \nabla^2\mathbf{E}$, and integrating over a volume V containing all the system inhomogeneities, one now obtains

$$(k_m^2 - k_n^2) \int_V \mathbf{E}_n \cdot \hat{\boldsymbol{\varepsilon}} \mathbf{E}_m + \int_V \left[\mathbf{E}_n \cdot \nabla^2 \mathbf{E}_m - \mathbf{E}_m \cdot \nabla^2 \mathbf{E}_n \right] d\mathbf{r} = 0 \,, \tag{1.14}$$

where $\mathbf{r}$ dependence is dropped for brevity. The second term can be further treated by integrating by parts using [41]

$$\int_V f(\nabla \cdot \nabla g) d\mathbf{r} = \oint_{S_V} (f \nabla g) \cdot d\mathbf{S} - \int_V (\nabla f) \cdot \nabla g d\mathbf{r} \,, \tag{1.15}$$

where f and g represent any of the components of $\mathbf{E}_n$ and $\mathbf{E}_m$, respectively, and the surface integral in the first term is taken over the surface S_V of the volume V. This yields the orthogonality relation [8, 13]

$$\int_V \mathbf{E}_n \hat{\boldsymbol{\varepsilon}} \cdot \mathbf{E}_m d\mathbf{r} + \frac{\oint_{S_V} \left(\mathbf{E}_n \cdot \frac{\partial \mathbf{E}_m}{\partial s} - \mathbf{E}_m \cdot \frac{\partial \mathbf{E}_n}{\partial s} \right) dS}{(k_m^2 - k_n^2)} = 0 \,, \tag{1.16}$$

where the gradient $\frac{\partial}{\partial s}$ is taken normal to the surface S_V. Here, both the volume and surface terms depend on V, but there is an exact cancellation of the V-dependencies outside the system, which eliminates the divergence as $V \to \infty$. The final result is the orthogonality relation [8, 13].

1.3 Normalization conditions

Although several approaches for the normalization were proposed in quantum mechanics, the adaptation in optics was not a paved road and a long debate and different forms have been proposed since the beginning of 1990s [9]. Such an extended discussion may be attributed to the vectorial form of the wavefunctions and the Maxwellian's operators in optics which do not lead to the same forms used for scalar wavefunctions in quantum mechanics [9]. The normalization approaches presented in this section fall into three main categories stemming from the literature in quantum

mechanics. The first one is regularization-based approach, introduced first by Zeldovich in 1960s [42], and adopted in optics in [20, 43–47]. Another category is based on the outgoing Green's function as, for example, the work by García-Calderón in quantum mechanics [32, 48]. In optics, the normalization was achieved by considering an analytical continuation determined by the outgoing Green's function [8, 15, 16, 49]. The third category is the exterior scaling transformation [50] which is analogous to the perfectly matched layer (PML) normalization in electromagnetics [9, 51–53]. Although regularization was a general term used in [9] to describe mapping the resonant states into a Hilbert space where they become square integrable, we rather refer to the work that stems from Zeldovich normalization method in [42] as regularization. We discuss in the following the three categories with a main focus on the analytical normalization based on the Green's function as it is used to normalize the analytically solvable systems in this thesis.

1.3.1 Regularization-based forms

Zeldovich developed a first-order perturbation theory, using analytical continuation to find the first-order correction of the energy and linewidth of the resonant states, referred to as quasistationary states in that context. To treat the infinitely growing wavefunction outside as $r \to \infty$, he multiplied the integrand by a Gaussian-like factor $e^{-\alpha r^2}$ and took the limit as α goes to zero, such that this factor doesn't alter the wavefunction of the particle inside the compact potential $V(r)$. He specifically treated the limit,

$$\lim_{\alpha\to 0}\int_0^\infty e^{-\alpha r^2}e^{2ik_n r}dr = -\frac{1}{2ik_n}\,. \tag{1.17}$$

Adding and subtracting this limit from the diverging normalization integral,

$$\int_0^\infty \psi_n^2(r)dr \equiv \lim_{\alpha\to 0}\int_0^\infty e^{-\alpha r^2}\psi_n^2(r)dr\,, \tag{1.18}$$

leads to,

$$\int_0^\infty \psi_n^2(r)dr = \int_0^{r'} \psi_n^2(r)dr - \frac{(C_n e^{ik_n r'})^2}{2ik_n}\,, \tag{1.19}$$

where $k_n = \sqrt{E_n}$ in this context in accordance with Eq. (1.1). It's essential to notice that this integral is independent of the choice of r' because the second term always cancels out the integration in the first term evaluated at r'.

In one of the early adaptation of Zeldovich approach into optics by Leung *et al.*, the definition of a stable norm was achieved for one dimensional systems [54]. Their definition was extended to spherical systems with a volume and surface contributions, both are R-dependence and were given in the context of modes with high quality factor. This suggests in this case neglecting any diverging terms outside the system. Leung and Pang later added a limit to the normalization of the dielectric sphere, suggesting that the sum of the volume and surface terms at large volume is constant [20]. The same normalization condition was adopted in several works [45–47], and was demonstrated later that it is not generally correct [9, 55]. Most interestingly, Zeldovich presented in the same paper a regularized normalization condition for resonant states with higher angular momentum $l > 0$, having spherical Bessel function as a solution [56]. This case is analogous to the transverse electric (TE) resonant states of a dielectric sphere in optics, however this result was not extended nor was regularization explicitly implemented in any of Leung's work. A proper regularization, such as Zeldovich work or the one taken for spherical systems in [57], can be extended to develop a normalization integral for the electric field of TE polarization of a dielectric sphere. This normalization in this case converges to the analytical normalization presented in Sec. 1.3.2 for arbitrary optical systems surrounded by a homogeneous medium.

1.3.2 The analytical normalization

In 2010, an analytical form of the normalization for a non-magnetic, non-dispersive arbitrary three-dimensional geometries was presented by Muljarov *et al.* [13], and shown in the subsequent works that it is determined by the outgoing Green's function [14–16, 49] and benefited from its spectral representation in terms of the resonant states. We first present this representation, followed by an elaboration of the normalization and its evolution.

Owing to the Mittag-Leffler's theorem for meromorphic functions, the outgoing Green's function of the system, satisfying Maxwell's equation with a Dirac delta function source term [14],

$$-\nabla\times\nabla\times\hat{\mathbf{G}}_k\left(\mathbf{r},\mathbf{r}'\right)+k^2\hat{\boldsymbol{\varepsilon}}(\mathbf{r})\hat{\mathbf{G}}_k\left(\mathbf{r},\mathbf{r}'\right)=\hat{\mathbf{1}}\delta\left(\mathbf{r}-\mathbf{r}'\right)\,, \tag{1.20}$$

can be decomposed into a sum of partial fractions of its poles, being the wavenumbers of the resonant states, as follows [14, 49]

$$\hat{\mathbf{G}}_k\left(\mathbf{r},\mathbf{r}'\right)=\sum_n\frac{\mathbf{E}_n(\mathbf{r})\otimes\mathbf{E}_n\left(\mathbf{r}'\right)}{k_n\left(k-k_n\right)}\,, \tag{1.21}$$

provided that the system is surrounded by a homogeneous background. The Green's function Eq. (1.21) converges only inside the system as $k\to\infty$, and has $\mathbf{E}_n(\mathbf{r})\otimes\mathbf{E}_n\left(\mathbf{r}'\right)/k_n$ as the residues of the pole k_n, where $\otimes$ is the tensor product.

Now, the normalization relies on an analytical continuation $\mathbf{E}(k,\mathbf{r})$ of the form

$$\mathbf{E}(k,\mathbf{r})=\int_V\hat{\mathbf{G}}_k\left(\mathbf{r},\mathbf{r}'\right)\left(k^2-k_n^2\right)\boldsymbol{\sigma}\left(\mathbf{r}'\right)d\mathbf{r}'\,, \tag{1.22}$$

where V again is an arbitrary volume containing all the system's inhomogeneities of $\hat{\boldsymbol{\varepsilon}}(\mathbf{r})$, k is a complex wavenumber in the vicinity of the wavenumber of the resonant state k_n, and $\mathbf{E}(k,\mathbf{r})$ satisfies the following Maxwell's equation [8],

$$-\nabla\times\nabla\times\mathbf{E}(k,\mathbf{r})+k^2\hat{\boldsymbol{\varepsilon}}(\mathbf{r})\mathbf{E}(k,\mathbf{r})=\left(k^2-k_n^2\right)\boldsymbol{\sigma}(\mathbf{r})\,. \tag{1.23}$$

The arbitrary source $\boldsymbol{\sigma}(\mathbf{r})$ is vanishing outside the system to ensure that $\mathbf{E}(k,\mathbf{r})$ fulfills the outgoing boundary conditions, and it is normalized as $\int_V\mathbf{E}_n\cdot\boldsymbol{\sigma}d\mathbf{r}=1$, to ensure that in the limit $k\to k_n$, the analytical continuation $\mathbf{E}(k,\mathbf{r})$ transforms into a resonant state.

Following the same steps used previously to derive the orthogonality condition, but with the analytical continuation $\mathbf{E}(k,\mathbf{r})$ instead of $\mathbf{E}_m(\mathbf{r})$, then taking the limit as $k\to$

k_n, one obtains [14, 15]

$$\lim_{k\to k_n} \frac{\int_V 2\mathbf{E}\left(k^2\hat{\boldsymbol{\varepsilon}} - k_n^2\hat{\boldsymbol{\varepsilon}}\right)\cdot\mathbf{E}_n d\mathbf{r}}{k^2-k_n^2} + \lim_{k\to k_n} \frac{\oint_{S_V} 2\left(\mathbf{E}_n\cdot\frac{\partial\mathbf{E}}{\partial s} - \mathbf{E}\cdot\frac{\partial\mathbf{E}_n}{\partial s}\right)dS}{k^2-k_n^2} = 1\,. \tag{1.24}$$

The factor of 2 is artificial and was introduced in [16] and in all the subsequent work. By expanding the analytic continuation about $k= k_n$, the spectral derivative can be converted to a spatial derivative, the normalization for non-dispersive systems finally takes the form [18]

$$2\int_V \mathbf{E}_n\cdot\hat{\boldsymbol{\varepsilon}}\mathbf{E}_n d\mathbf{r} + \frac{1}{k_n^2}\oint_{S_V}\left[\mathbf{E}_n\cdot\frac{\partial\mathbf{E}_n'}{\partial s} - \frac{\partial\mathbf{E}_n}{\partial s}\cdot\mathbf{E}_n'\right]dS = 1\,, \tag{1.25}$$

where the derivative of the analytic continuation outside the system is given by $\mathbf{E}_n' = (\mathbf{r}\cdot\nabla)\mathbf{E}_n$, which becomes $\mathbf{E}_n' = r\frac{\partial\mathbf{E}_n}{\partial r}$ in spherical coordinates, where $r = |\mathbf{r}|$ is the radial coordinate. For a spherical enclosed boundary S_R of a spherical volume V_R centered at the origin, the partial derivative $\frac{\partial}{\partial s} = \frac{\partial}{\partial r}$ [8]. In other words, for such a spherical boundary, both derivatives $\mathbf{E}_n'$ and $\frac{\partial}{\partial s}$ are directional derivatives in the direction normal to the surface, resulting in a second order derivative for $\frac{\partial\mathbf{E}_n'}{\partial s}$, such that $\frac{\partial\mathbf{E}_n'}{\partial s} = \frac{\partial}{\partial r}r\frac{\partial\mathbf{E}_n}{\partial r}$. The normalization integral Eq. (1.25) is constant under any taken volume V because there is also an exact cancellation of the V-dependencies in the region outside the system.

Having frequency dispersion in the system introduces a factor of $\eta + 1$ in the volume integral, stemming from taking the limit $k \to k_n$. Similarly, dispersion in the surrounding medium introduces the same factor in the surface term, arising from expanding the analytic continuation about k_n, provided that the surrounding medium has uniform permittivity [15], the factor η is defined as

$$\eta = \frac{k}{2\hat{\boldsymbol{\varepsilon}}(k)}\frac{\partial\hat{\boldsymbol{\varepsilon}}(k)}{\partial k}\bigg|_{k=k_n}\,, \tag{1.26}$$

with noting that the factor $\eta + 1$ is conventionally written in the normalization integral for dispersive system as $\eta + 1 = \frac{1}{\hat{\boldsymbol{\varepsilon}}(k)}\frac{\partial k^2\hat{\boldsymbol{\varepsilon}}(k)}{\partial k^2}\Big|_{k=k_n}$. Later, the normalization integral was generalized to include magnetic, chiral, and bi-anisotropic materials, considering

frequency dispersion [16]:

$$\int_V \left[\mathbf{E}_n \cdot (k\hat{\boldsymbol{\varepsilon}})'\mathbf{E}_n + \mathbf{E}_n \cdot (k\hat{\boldsymbol{\xi}})'\mathbf{H}_n\right] d\mathbf{r} - \int_V \left[\mathbf{H}_n \cdot (k\hat{\boldsymbol{\zeta}})'\mathbf{E}_n + \mathbf{H}_n \cdot (k\hat{\boldsymbol{\mu}})'\mathbf{H}_n\right] d\mathbf{r} + \frac{i}{k_n} \oint_{S_V} \left[\mathbf{E}_n \times \mathbf{H}'_n + \mathbf{H}_n \times \mathbf{E}'_n\right] \cdot d\mathbf{S} = 1\,, \tag{1.27}$$

where the dependency on k is dropped from the material's tensors, and the prime refers to the derivative with respect to the frequency k at k_n, and $\mathbf{H}'_n = (\mathbf{r} \cdot \nabla)\mathbf{H}_n$. For non-dispersive systems with $\hat{\boldsymbol{\zeta}} = \hat{\boldsymbol{\xi}} = \hat{\mathbf{0}}$ and $\hat{\boldsymbol{\mu}} = \hat{\mathbf{1}}$, the normalization reduces to Eq. (1.25) [16].

The normalization integral Eq. (1.27) is a general normalization of resonant states in of a reciprocal system surrounded by a homogeneous medium, valid for any arbitrary three dimensional optical system [16]. It is important to note that the requirement of uniformity in the surrounding medium excludes systems on a substrate from the range of validity since substrates introduce inhomogeneity in the surrounding medium [9].

1.3.3 Perfectly-matched layer normalization

In computational methods, the PML is an essential tool for simulating systems with open boundaries. Unwanted reflections that may occur at the truncated computational region are minimized through the implementation of a PML domain at those boundaries. The essence of the PML is an analytical continuation of the waves in a complex infinite space in which the wave decays exponentially. Owing to the imaginary part of the complex coordinates, only outgoing waves are analytically continued in such a space. The complex space is then mapped into real coordinates, determining the finite thickness of the PML [58, 59]. The mapping may involve a transformation of the Maxwell's operator, the permittivity and permeability tensors, or the operator and the permittivity and permeability tensors together [51]. Thus, the resonant states can be found numerically by using an eigenmode solver for Maxwell's equation with defining a PML domain in the medium surrounding the resonator to consider only outgoing boundary conditions.

Hugonin and Lalanne demonstrated the PML machinery for nanophotonic applications and provided eigenfield normalization for systems bounded by a PML domain [10, 51]. Since the fields converge in the PML region, the normalization integral is taken as a volume integral over the entire computational domain, including the PML, as [9, 10]

$$\int_V \left[\mathbf{E}_n \cdot (k\hat{\boldsymbol{\varepsilon}})'\mathbf{E}_n - \mathbf{H}_n \cdot (k\hat{\boldsymbol{\mu}})'\mathbf{H}_n\right] d\mathbf{r} + \int_{V_{\text{pml}}} \left[\tilde{\mathbf{E}}_n \cdot (\tilde{k}\tilde{\hat{\boldsymbol{\varepsilon}}})'\tilde{\mathbf{E}}_n - \tilde{\mathbf{H}}_n \cdot (\tilde{k}\tilde{\hat{\boldsymbol{\mu}}})'\tilde{\mathbf{H}}_n\right] d\tilde{\mathbf{r}} = 1\,, \quad (1.28)$$

with V being the physical volume in the computational domain, V_{pml} is the volume of the PML in the new real coordinates, and the integrand is mapped into the new real coordinates of PML. The fields, permittivity, and permeability in the PML region are the transformed ones [10, 53]. The transformation is of key importance in the accuracy and convergence of the fields in the PML domain [51]. Thus, with using the PML normalization, the parameters of the system must be carefully chosen in order to guarantee its convergence. [34].

In this work, we employ the accuracy of the RSE-based theory for treating perturbation outside the system to normalize the electric fields of arbitrary shapes, including systems on a substrate. The method is detailed in the applications in Chapter 3.

1.4 Finding the resonant states

Resonant states are influenced by the system's morphology, encompassing both its geometric shape and material properties. Our discussion is divided into two parts: one dealing with easily solvable, symmetric systems, and the other with systems of arbitrary geometries, presenting more analytical challenges.

1.4.1 Analytically solvable systems

The resonant states of the one-dimensional slab presented in the introduction (Sec. 1.1) or three-dimensional symmetric systems located in a homogeneous surrounding medium can be found analytically [14, 49, 60]. The wavenumbers of the resonant states are determined from the secular equation obtained from applying Maxwell's boundary conditions, namely, the continuity of the tangential components of the electric field $\mathbf{E}(\mathbf{r})$ and the magnetic field $\mathbf{H}(\mathbf{r})$ across the boundaries [13, 14].

Spherically symmetric systems are reducible to one dimension, providing simplicity with rich features in the spectrum. The analytical solution of spherical systems is comprehensively discussed in Chapter 5, with the fields and secular equations for a sphere and a core-shell system. The given secular equations can be solved with the help of numerical methods, such as Newton–Raphson method, which is primarily used to find the *exact* modes of spherical systems in this work for a comparison with our results. Here, we devote a part of this section to introduce some features of the spectrum of spherical systems.

Owing to the spherical symmetry, Maxwell's equations distinguish two separate sets of equations for TE and transverse magnetic (TM) modes of non-chiral materials* [61]. The angular operator provides further quantization to the fields given by the index l and azimuthal index $m = -l, \ldots, l$, which are referred to as the angular momentum and magnetic quantum numbers, respectively [37]. Each polarization has $2l + 1$ degenerate modes for each l [14]. In addition to Fabry-Perót modes, additional modes with relatively high imaginary parts are created in the spectrum and denoted as leaky modes for their considerable loss [13]. Another class of modes, in contrary, are characterized by their low imaginary parts and thus longer lifetime, attributed to the total internal reflections along the concave surface [37]. These modes are known as whispering gallery modes, usually characterized by their high quality factor, measuring the ratio of their energy to their linewidth [62]. Both leaky modes and whispering gallery modes become

*Considering chirality in the system couples the electric and magnetic fields, making their Maxwell's equations inseparable, and the TE and TM modes become indistinguishable.

more prominent with higher angular momentum l [13], with exactly l and $l-1$ leaky modes for TE polarization and TM polarization, respectively.

TM polarization in spherical systems supports special modes. The mode marked by a peak in the spectrum corresponds to minimised reflectivity occurring at Brewster's angle between the incident TM wave and surface normal [37]. Additionally, TM polarization supports the presence of localized surface plasmon modes in metallic spherical systems described by Drude Lorentz model [18, 63].

As an illustration of spherical systems, we display the TE and TM modes of a dielectric sphere of radius R and $\varepsilon = 4$ in vacuum in Fig. 1.2(a), which exhibits the three main classes of modes for both $l = 5$ and $l = 10$, with the latter supporting more leaky modes and whispering gallery modes as expected. The Brewster's modes appear as peaks in the spectrum of TM polarization. Further, we show the radial dependence of the normal and tangential components of the normalized electric field of the TM polarization for one selected mode of each class for $l = 10$ in Fig. 1.2(b,c). The electric field of the lowest leaky mode at $k_n R \approx 7.55 - 4.17i$ is mostly situated outside the sphere, exhibiting rapid divergence. Conversely, the whispering gallery mode at $k_n R \approx 7.25 - 0.004i$, indicated as WGM, is concentrated around the sphere surface, with slower divergence outside the sphere. The oscillation of the electric field is more apparent inside the sphere for the Fabry-Perót (FP) mode at $k_n R \approx 27.78 - 0.3i$ [37]. For details on the radial dependence of the normal and tangential components of TM modes, expressed in a basis of vector spherical harmonics, see Sec. 5.1 and Sec. 5.2, and the normalization is discussed at the end of Sec. 5.3.2. As an additional note, the normal components of the electric field of the depicted modes exhibit discontinuities across the surface of the sphere, whereas the tangential components remain continuous as expected from Maxwell's boundary conditions.

1.4.2 Arbitrarily shaped structures

For systems with arbitrary geometries, one needs to use computational methods such as the finite element method (FEM) or Finite-Difference Time-Domain (FDTD). In the

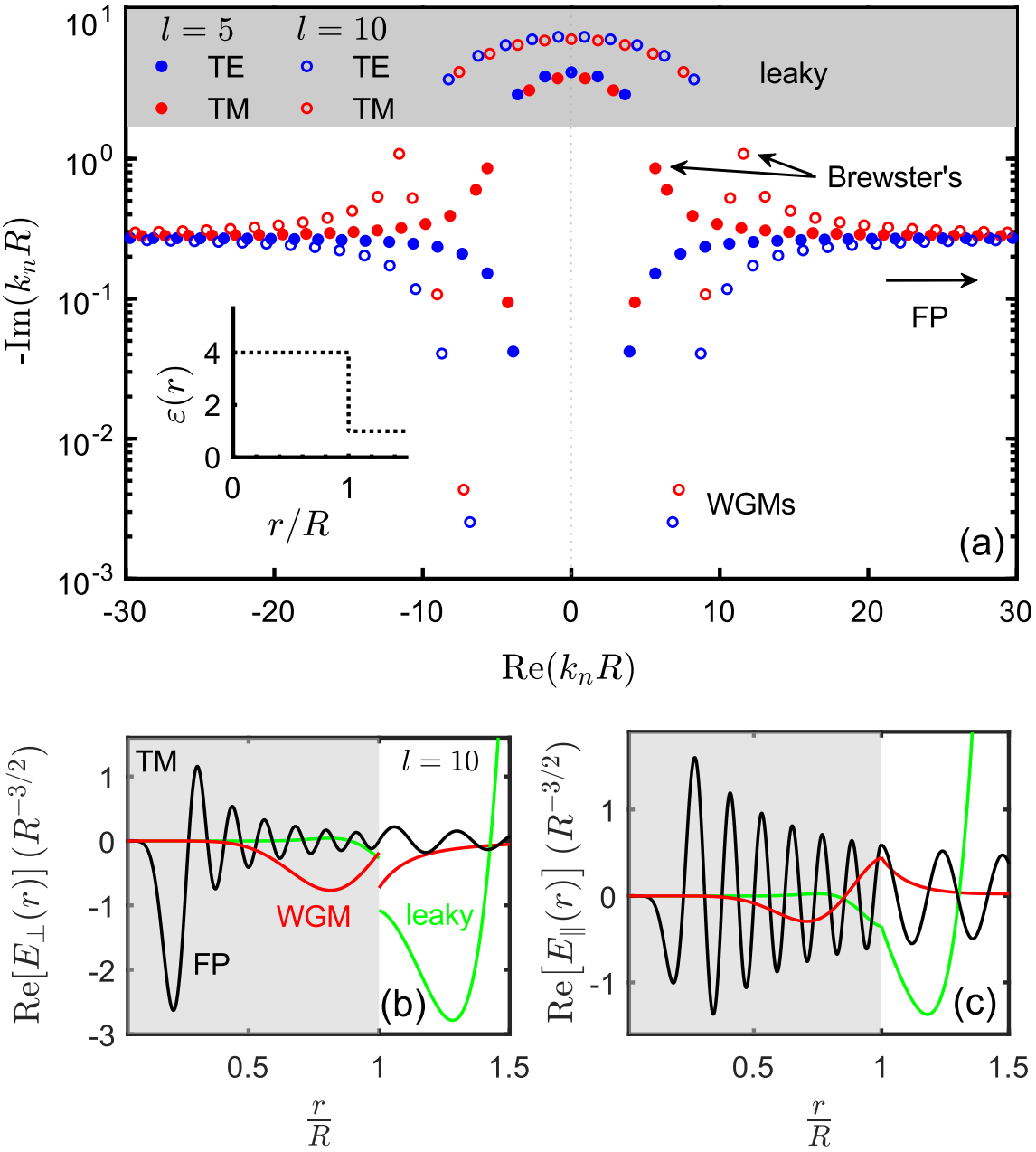

Figure 1.2. (a) The wavenumber of TE (blue) and TM (red) resonant states in the complex plane, calculated from the secular equation with l= 5 (filled circles) and l= 10 (empty circles) of a dielectric sphere of a permittivity profile shown in the inset. The real part of the radial dependence of (b) the normal component $E_\perp(r)$ and (c) tangential component $E_\parallel(r)$ of the electric field for one mode of each class: leaky mode at $k_n \approx 7.55 - 4.17i$ (green), whispering gallery mode (WGM) at $k_n \approx 7.25 - 0.004i$ (red) and Fabry-Perót (FP) mode at $k_n \approx 27.78 - 0.3i$ (black), for l= 10.

former, the open space is discretized into smaller elements in a form of a mesh, while the latter involves discretization of both space and time into a grid of so-called Yee cells, with iteratively updating electric and magnetic field values at discrete points in the grid [64]. In both, the discretization confines the system within finite PML domain which analytically continued the outgoing waves in a complex space, which replaces the exponential growth with exponential decay as explained in Sec. 1.3.3 [51]. An important note is that not all modes are sufficiently attenuated before being reflected from the PML wall. The fields of the modes that diverges quickly are mostly affected by the finite PML domain. Additional note is that the implementation of PML induces what is so-called Bérenger modes or PML modes. Such modes are sensitive to the PML parameters and can be distinguished from the other physical modes by changing, for example, the PML thickness. [10, 58]

In general, the computational approaches usually require repetitive optimization of computational parameters, such as initial values and PML thickness, that otherwise might lead to a confusion of the desired mode with other physical modes or unphysical modes, if they are around. The computational load for each operation is also a function of the number of other calculated modes, tolerance and size of the geometry.

The resonant states can be rigorously produced from an existing basis, calculated once, using the RSE, which maps Maxwell's equations into a linear eigenvalue problem. The RSE provides natural discretization of the system into its resonant states to calculate their changes caused by arbitrary perturbations (any strength) to any desirable accuracy determined by the basis size [13, 14, 18]. We demonstrate the RSE in the following section.

1.5 Resonant-state expansion (RSE)

The spectral representation of the outgoing Green's function of the system and completeness of the resonant states inside the system are the heart of the RSE [13]. The Green's function provides natural discretization of the system into its resonant states. Completeness, on the other hand, allows to convert Maxwell's equation into

a linear eigenvalue problem with quick convergence [18]. We present in this section the development of the RSE, started by treating perturbation of arbitrary strength in dielectrics [13] and generalized later to include dispersive systems [17, 18] as well as magnetic, chiral, and bi-anisotropic materials of reciprocal systems [16]. In this section, we first demonstrate the completeness of the resonant states inside the system and then present another form of the Green's function. The latter becomes useful in deriving the RSE equation. We follow that by demonstrating the RSE equation for non-dispersive and dispersive systems.

To demonstrate completeness, we use the Green's function Eq. (1.21) into Eq. (1.20), which with the help of Eq. (1.12) yields the closure relation [49],

$$\sum_n \hat{\boldsymbol{\varepsilon}}(\mathbf{r})\mathbf{E}_n(\mathbf{r}) \otimes \mathbf{E}_n(\mathbf{r}') = \hat{\mathbf{1}}\delta(\mathbf{r}-\mathbf{r}') \,, \tag{1.29}$$

provided the resonant states are taken inside the system surrounded by a uniform background as follows from the outgoing Green's function Eq. (1.21) [16, 34]. The Green's function Eq. (1.21) can also be taken in the following form

$$\mathbf{G}_k(\mathbf{r},\mathbf{r}') = \sum_n \frac{\mathbf{E}_n(\mathbf{r}) \otimes \mathbf{E}_n(\mathbf{r}')}{k(k-k_n)} \,, \tag{1.30}$$

which is obtained by combining the Green's function Eq. (1.21), presented earlier, with its sum rule [49]

$$\sum_n \frac{\mathbf{E}_n(\mathbf{r}) \otimes \mathbf{E}_n(\mathbf{r}')}{k_n} = 0 \,. \tag{1.31}$$

The spectral representation of the Green's function Eq. (1.30) is used in deriving the RSE equation.

Non-dispersive RSE

Now, to derive the RSE equation, let us assume first a non-dispersive, non-magnetic optical system, and its resonant states, described by Eq. (1.12), form the basis system. The system of our interest is modified by the perturbation $\Delta\hat{\boldsymbol{\varepsilon}}(\mathbf{r})$, and described by the

following Maxwell's equations,

$$-\nabla \times \nabla \times \mathbf{E}(\mathbf{r}) + k^2 \left[\hat{\boldsymbol{\varepsilon}}(\mathbf{r}) + \Delta\hat{\boldsymbol{\varepsilon}}(\mathbf{r})\right] \mathbf{E}(\mathbf{r}) = \mathbf{0}\,. \tag{1.32}$$

The above equation can be solved with the help of the Green's function Eq. (1.30) to obtain the electric field of the perturbed system $\mathbf{E}(\mathbf{r})$ as,

$$\mathbf{E}(\mathbf{r}) = -k^2 \int \mathbf{G}_k(\mathbf{r}, \mathbf{r}')\Delta\hat{\boldsymbol{\varepsilon}}(\mathbf{r}')\mathbf{E}(\mathbf{r}')d\mathbf{r}'\,. \tag{1.33}$$

Then, we employ the completeness of the resonant states inside the system to expand the electric field $\mathbf{E}(\mathbf{r})$ in terms of the unperturbed states as

$$\mathbf{E}(\mathbf{r}) = \sum_n c_n \mathbf{E}_n\,, \tag{1.34}$$

and use the expansion into Eq. (1.33), which leads after equating coefficients to a linear eigenvalue problem in a matrix form:

$$(k - k_n)c_n = -k \sum_m V_{nm} c_m\,, \tag{1.35}$$

where the matrix elements V_{nm} are given by

$$V_{nm} = \int_V \mathbf{E}_n(\mathbf{r}) \cdot \Delta\hat{\boldsymbol{\varepsilon}}(\mathbf{r})\mathbf{E}_m(\mathbf{r})d\mathbf{r}\,. \tag{1.36}$$

To obtain an explicit form of the eigenvalue problem, we divide Eq. (1.35) by k, and introduce new expansion coefficients $a_n = \sqrt{k_n}c_n$, such that [13, 65]

$$\frac{1}{k}a_n = \sum_m \left(\frac{\delta_{nm}}{k_n} + \frac{V_{nm}}{\sqrt{k_n k_m}}\right) a_m. \tag{1.37}$$

The eigen wavenumber k of the perturbed system and the expansion coefficients c_n can be obtained by diagonalizing Eq. (1.35), which is developed in literature as the RSE method. The RSE is described as exact, provided that all the resonant states are included in the basis. In practice, a finite number of the resonant states shows quick

convergence, given by $1/N^3$, where N is the number of the resonant states included in the basis. The RSE equation Eq. (1.35) is generalized to include magnetic, chiral and bi-anisotropic perturbations of the system which leads to the generalized matrix elements [16]

$$V_{nm} = \int_V \left[\mathbf{E}_n \cdot \Delta\hat{\boldsymbol{\varepsilon}} \mathbf{E}_m + \mathbf{E}_n \cdot \Delta\hat{\boldsymbol{\xi}} \mathbf{H}_m - \mathbf{H}_n \cdot \Delta\hat{\boldsymbol{\zeta}} \mathbf{E}_m - \mathbf{H}_n \cdot \Delta\hat{\boldsymbol{\mu}} \mathbf{H}_m \right] d\mathbf{r} \,. \tag{1.38}$$

Dispersive RSE

For systems with frequency dispersion, the RSE is based on the assumption that the frequency dispersion of the system is described by the generalized Drude-Lorentz model, most effective for describing dispersion of metals [18, 66]:

$$\hat{\boldsymbol{\varepsilon}}(k, \mathbf{r}) = \hat{\boldsymbol{\varepsilon}}_\infty(\mathbf{r}) + \sum_j \frac{i\hat{\boldsymbol{\sigma}}_j(\mathbf{r})}{k - \Omega_j} \,, \tag{1.39}$$

where $\hat{\boldsymbol{\varepsilon}}_\infty(\mathbf{r})$ is the high-frequency value of the permittivity tensor, Ω_j are the simple-pole positions of the permittivity in the complex wave number plane, and $\hat{\boldsymbol{\sigma}}_j(\mathbf{r})$ are the corresponding conductivities. Overall, Eq. (1.39) presents a Mittag-Leffler representation of $\hat{\boldsymbol{\varepsilon}}(k, \mathbf{r})$ treated as a function of a complex variable k [66].

The frequency dispersion introduces a weight factor in the Green's representation in Eq. (1.30) [18]. Such a modified representation of the Green's function of dispersive systems helps with mapping the Maxwell's equations of the perturbed system into a linear eigenvalue problem of the form

$$(k - k_n)c_n \;\; = \;\; -k \sum_m V_{nm}(\infty) c_m + k_n \sum_m \left[V_{nm}(\infty) - V_{nm}(k_n) \right] c_m \,, \tag{1.40}$$

where $V_{nm}(\infty)$ and $V_{nm}(k_n)$ are the matrix element evaluated with $\varepsilon(\infty, \mathbf{r})$ and $\varepsilon(k_n, \mathbf{r})$, respectively. The difference $V_{nm}(\infty) - V_{nm}(k_n)$ corresponds to the perturbation of the frequency-dependent part of the permittivity, and thus vanishes for non-dispersive systems leading to the RSE equation for non-dispersive systems Eq. (1.36). Most importantly, any non-zero pole of the permittivity results in a set of countable infinite

modes approaching that pole, and denoted as Drude resonant states (DRSs). These modes satisfy the secular equation of the system, and therefore they have to be included in the basis to complete it [18].

To illustrate the dispersive RSE for permittivity perturbations inside the system, we consider an isotropic gold sphere of $R = 200\,\text{nm}$, as a basis (unperturbed) system, described by Drude model,

$$\varepsilon(k) = \varepsilon_\infty + \frac{i\sigma}{k} - \frac{i\sigma}{k-\Omega}\,, \tag{1.41}$$

consisting of two poles $\Omega_0 = 0$ and $\Omega_1 = -i\gamma$, which correspond, respectively, to conductivities $\hat{\boldsymbol{\sigma}}_0(\mathbf{r}) = \sigma\hat{\mathbf{1}}$ and $\hat{\boldsymbol{\sigma}}_1(\mathbf{r}) = -\sigma\hat{\mathbf{1}}$, where σ is the DC conductivity and γ represents the frequency of collision of free electrons. While further refinement of the metal response can be obtained by including additional terms in the permittivity with poles of non-zero real parts to describe phonon and electron interband transitions [66], we rely on the Drude model to describe dispersion in metals in our illustrations for simplicity. The parameters of the Drude model are taken as $\varepsilon_\infty = 4$, $\hbar c\sigma = 957\,\text{eV}$, and $\hbar c\gamma = 0.084\,\text{eV}$, fitted to the Johnson and Christy data [67] with the help of the fit program provided in [66].

Considering TM polarization for $l = 1$, the normalized electric field of some selected modes is shown in Fig. 1.3(a,b), and the spectrum of the Drude gold sphere is shown in Fig. 1.3(c). In Fig. 1.3(a) and Fig. 1.3(b), we exhibit the normal and tangential components, respectively, of the radial dependence of the electric field of three modes: the surface plasmon (SP), the following mode in the spectrum (RS_1), and one of the DRSs, associated with the Drude pole $\Omega = -i\gamma$. Both normal and tangential components of the electric field of the surface plasmon, having energy $E_n = \hbar c k_n$ at $E_n \approx 0.88 - 0.43i\,\text{eV}$, are enhanced on the sphere surface. The following mode at $E_n \approx 4.64 - 0.15i\,\text{eV}$ exhibits higher oscillations in the electric field components inside the sphere. The electric field of the DRSs has a slightly different nature since it converges outside the sphere, as shown for both components in Fig. 1.3(a,b) for the lowest mode of DRSs at $E_n \approx -0.02i\,\text{eV}$. The convergence of the electric field of these modes outside the sphere is attributed to the purely imaginary part of their energies. Consequently,

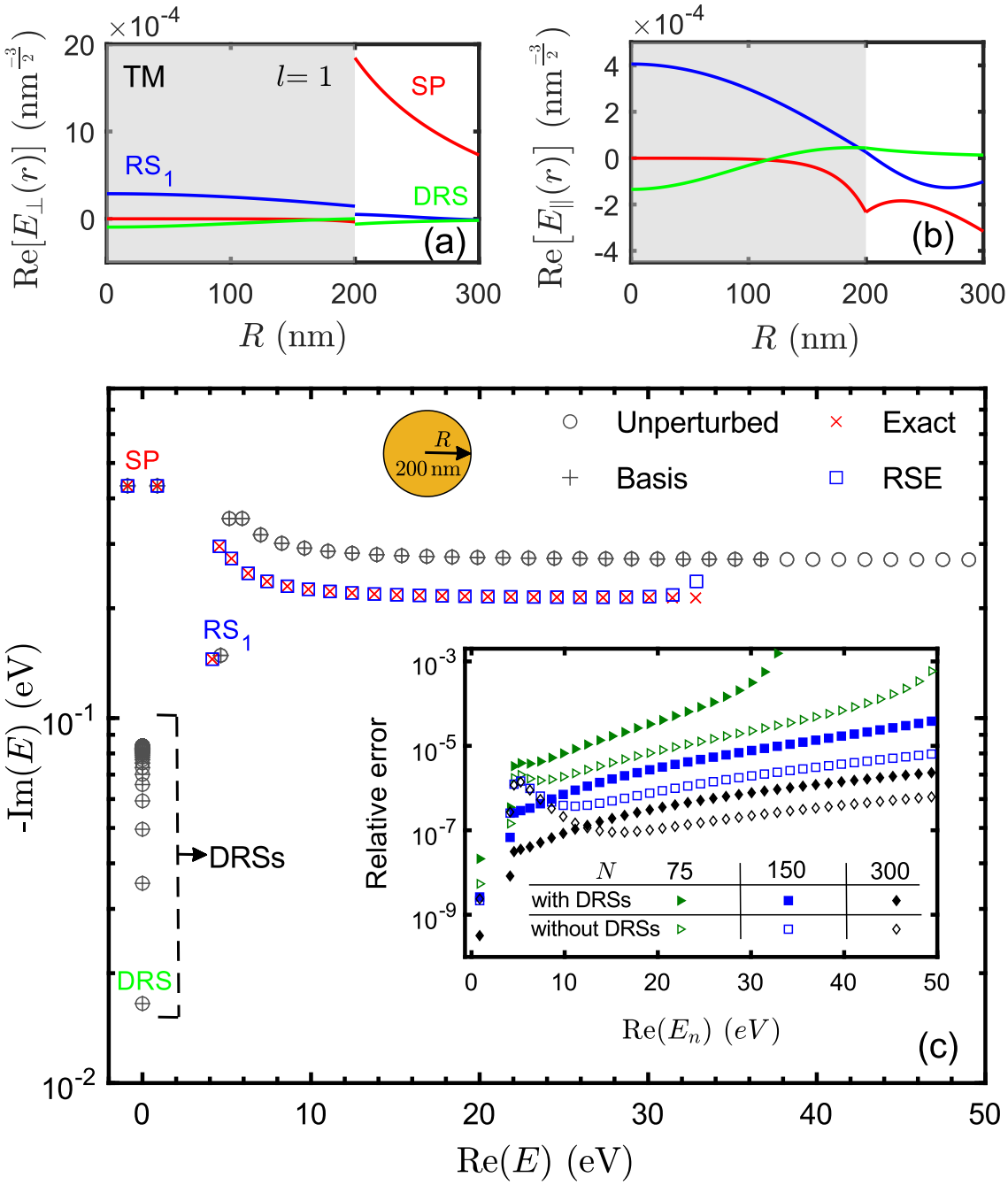

Figure 1.3. The TM resonant states of Drude gold nanosphere of radius R= 200 nm, mode order l=1, and Drude parameters ε_∞=4, $\hbar c\sigma$= 957 eV, and $\hbar c\gamma$= 0.084 eV. The real part of the radial dependence of (a) the normal component $E_\perp(r)$ and (b) tangential component $E_\parallel(r)$ of the electric field of the surface plasmon (SP) (red), the following mode (RS$_1$) (blue) and a DRS (green), where the fields of the SP and DRS are smaller by a factor of 10^2 and 10^4, respectively. (c) Complex energies $E = \hbar ck$ of a basis (grey pluses) of size $N = 75$ modes from the unperturbed energies (grey circles), including Drude poles (DRSs) and showing the positions of SP, RS$_1$ and DRS, are used in the RSE to calculate the energies of the perturbed system (blue squares), with a perturbation $\Delta\varepsilon_\infty = 1$, having exact values (red crosses) calculated from the secular equation. Inset: the error of the RSE results relative to the exact values using a basis size N= 75 (green triangles), N= 150 (blue squares), and N= 300 (black diamonds), including DRSs (filled) and excluding DRSs (empty).

the radial dependence of both components of the electric field is associated with the modified Bessel function [68]. As the energies of these modes approach the pole, their electric fields dramatically diminish due to diverging values of the permittivity at such energies. The normal and tangential components of the electric field are as presented in Sec. 5.1 and Sec. 5.2, but normalized according to [63], which considers the impact of dispersion in the normalization constants[†]. The distribution of the energies of the selected modes and other modes in the complex plane, including the DRSs, are shown in Fig. 1.3(c).

Now, we used the unperturbed modes as a basis in the RSE to produce the perturbed modes due to a change of the permittivity at high frequency. In Fig. 1.3(c), the perturbed modes were produced from the unperturbed ones using a basis of $N = 75$ in the dispersive RSE equation due to permittivity perturbation $\Delta\varepsilon_\infty = 1$. The RSE results show a good agreement with the exact modes, obtained from the secular equation. Crucially, including DRSs in the basis of the dispersive RSE is essential to obtain the convergence as N^{-3} for all the modes as shown in the relative error for different basis size N with and without DRSs in the inset of Fig. 1.3(c).

Infinitesimal-dispersive RSE

The infinitesimal-dispersive RSE has to be applied when an additional pole is introduced by the perturbation $\Delta\varepsilon(k, \mathbf{r})$. Such an additional pole requires including a degenerate set, denoted as pole resonant states (pRSs), in the basis [63]. This set has the frequency of the pole and weight tending to zero in the permittivity. Following the description used in [63], pRSs for the dispersion Eq. (1.39) are found by taking the limit $\xi \to 0$ both in the conductivity $i\hat{\boldsymbol{\sigma}}_j(\mathbf{r}) = \xi\hat{\boldsymbol{s}}_j(\mathbf{r})$, where $\hat{\boldsymbol{s}}_j(\mathbf{r})$ can be taken as $\hat{\mathbf{1}}$ without loss of generality, and in the mode wavenumber $k_m = \Omega_j + \xi q_m$, where the index m is used to label the pRS. The quantum numbers q_m are finite and are related to effective

[†]Note that in order to use the normalization constants in [63], the wavefunction in Eq. (5.22) is divided by spherical Riccati-Bessel function of the first kind $J(\sqrt{\varepsilon(k_n)}k_n r)$ inside the sphere and the spherical Riccati-Hankel function of the first kind $H(k_n r)$ outside the sphere. Such definition leads to identical normalization constants at the boundary R. Additionally, note that the radius R in the normalization constant mentioned in [63] requires correction to R^3.

permittivities $\hat{\varepsilon}_m$ of the pRSs, according to

$$\hat{\boldsymbol{\varepsilon}}_m(k,\mathbf{r}) = \hat{\boldsymbol{\varepsilon}}_\infty + \sum_{j'\neq j} \frac{i\hat{\boldsymbol{\sigma}}_{j'}(\mathbf{r})}{\Omega_j - \Omega'_j} + \frac{\hat{\boldsymbol{s}}_j(\mathbf{r})}{q_m}\,. \tag{1.42}$$

Note that while all pRS are degenerate, i.e. $k_m = \Omega_j$, different pRSs have different values of q_m and consequently ε_m. The latter determines the spatial distribution of the pRS fields within the basis system while the former contribute to their normalization and depends on the geometry of the considered system [63].

The infinitesimal-dispersive RSE is illustrated in Fig. 1.4 for the same gold sphere displayed in Fig. 1.3. The unperturbed complex energies $E_n = \hbar c k_n$ are used as a basis to calculate the modes due to perturbation of the pole $\Delta\Omega = -0.035i\,\mathrm{eV}$. Figure 1.4 (a) shows that the modes are responsive to such a small variation of the pole. The pRSs of the new (perturbed) pole $\Omega'_1 = -0.119i\,\mathrm{eV}$ are added to the basis, and the values of their refractive indices Eq. (1.42), where $n_r = \sqrt{\varepsilon_m}$ are shown in the inset of Fig. 1.4 (a). Including both DRSs in the basis as well as the pRSs is crucial to obtain the convergence as shown Fig. 1.4(b), displaying the relative error for different basis size N with or without the pRSs. The relative error for the first few modes, including the surface plasmon, dose not exceed 10^{-4} without the pRSs. We provide more details on the calculation of such modes in Chapter 2.

1.6 First-order perturbation theory

Finding the changes of the wavenumber of resonant states in the first-order is proposed in literature for weak perturbations $\delta\hat{\boldsymbol{\varepsilon}}(\mathbf{r})$. The linear shift can be derived from the RSE equation by neglecting all the off-diagonal elements from the RSE matrix, which yields [27, 63, 69]

$$k \approx \frac{k_n}{1+V_{nn}}\,. \tag{1.43}$$

The shift in the first-order then becomes

$$\delta k \approx -k_n \int_V \mathbf{E}_n(\mathbf{r})\delta\hat{\boldsymbol{\varepsilon}}(\mathbf{r})\mathbf{E}_n(\mathbf{r})d\mathbf{r}\,. \tag{1.44}$$

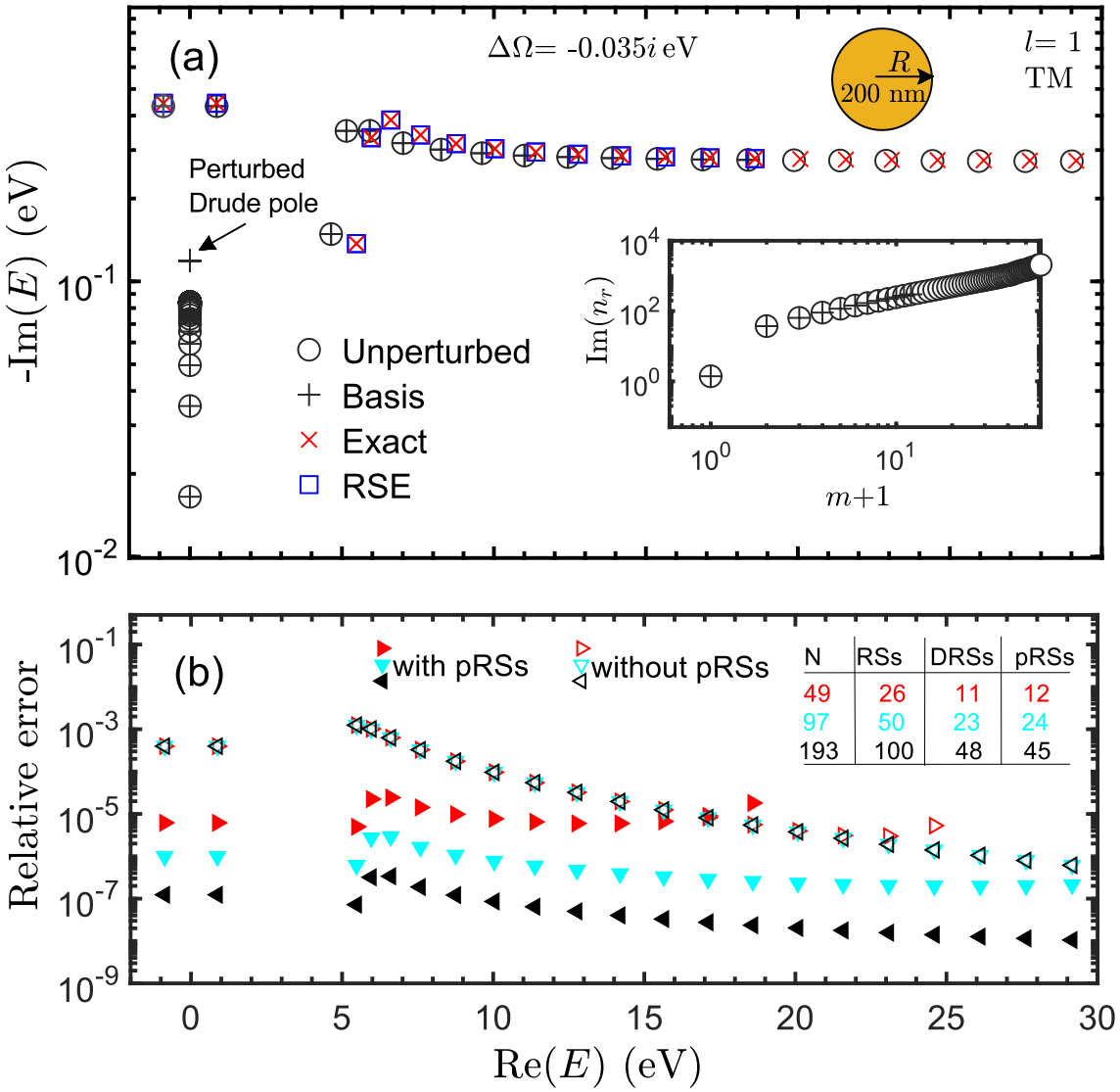

Figure 1.4. (a) As Fig. 1.3 but for perturbation of Drude pole $\Delta\Omega = -0.035i\,\text{eV}$. Inset: the imaginary parts of the refractive index n_r of the degenerate set pRSs, corresponding to the frequency of the perturbed Drude pole $\Omega_1' = -0.119i\,\text{eV}$. (b) The relative error of different basis sizes $N = 49$ (red), $N = 97$ (cyan), and $N = 193$ (black), with pRSs (filled) and without pRSs (empty).

This truncation of the RSE matrix to have only one mode in the basis can also be justified by the Rayleigh-Schrödinger perturbation theory based on the RSE [8]. In this theory the perturbed wavenumber k is expanded to the second order in terms of the RSE matrix. This expansion up to first-order correction provides exactly the perturbed wavenumber Eq. (1.44), provided that the overlap of the mode of interest

n and all other modes m in the matrix elements V_{nm} in Eq. (1.36) are negligible and the distances to other modes m in the complex plane are much larger than the mode shift δk. While this form is derived from the RSE and expected to be valid for perturbations inside the system only, it was demonstrated that it predicts linear shifts of the frequency of resonant states due to perturbations in the close vicinity of the system [70]. Furthermore, existing literature includes first- and second-order perturbation theories for open systems, addressing perturbations related to finite-size volume [14, 20, 22], boundary [23], or a combination of both [24]. However, these approaches are not suitable for treating homogeneous perturbations of the entire space surrounding the system which occurs in sensing applications [25]. The best available approach for treating perturbations in the surrounding medium is provided by Both and Weiss for homogeneous perturbation of permittivity or permeability [26]. The RSE-based method developed in this thesis provides the frequency shift to any desired accuracy, and its diagonal approximation predicts shifts beyond the first-order in the considered examples. Additionally, we develop a simpler analog to Both and Weiss based on regularization, and prove their equivalence in the first order.

1.7 Summary

Resonant states are the eigensolutions to the time-independent, sourceless Maxwell's equations, considering solely outgoing boundary conditions. Such consideration results in exponential decay of the electromagnetic fields in time and exponential growth with distance in the region outside the system. In the orthonormality conditions, this catastrophic growth with distance is compensated analytically by a surface term. Computationally, the infinite growth is compensated by a volume integral over a PML domain. For simple one-dimensional systems or those reducible to one-dimensional, the resonant states can be found by solving Maxwell's equations analytically. In such cases, the eigenvalues (wavenumbers) can be found from the secular equation obtained from the continuity of the tangential components of the electric and magnetic fields. For more complex systems, the resonant states can be found computationally using

an eigenmode solver for Maxwell's equations. In this case, the outgoing boundary conditions are satisfied by defining a PML domain enclosing the system. Owing to the boundaries in optical systems, the resonant states are complete inside the system, which allowed for the development of the RSE theory. The RSE is a perturbation theory in which the perturbed modes can be reproduced efficiently from a fixed basis of the unperturbed modes. Instead of solving Maxwell's equations, one only needs a fixed basis of normalized resonant states obtained analytically or numerically to reproduce perturbed resonant states using the RSE equation with a quick convergence as N^{-3}, where N is the basis size, to any desired accuracy or perturbation strength. The RSE can treat dispersive systems described by a generalized Drude-Lorentz model. For such systems, any permittivity pole of finite weight or zero weight requires adding a set of resonant states to the basis to obtain the convergence. Using only single mode in the RSE basis leads to a first-order theory for treating weak perturbations inside the system. For perturbations outside the system, the RSE fails, and the only available approach is a first-order theory by Both and Weiss for treating homogeneous perturbations outside the system [26].

Chapter 2

RSE for perturbations in the surrounding medium

In this chapter, we develop an approach based on the RSE to treat homogeneous perturbations in the medium surrounding an optical system [71]. To achieve that, we develop a transformation matrix that maps perturbations in the exterior medium to effective perturbations inside the system where the resonant states are complete. By treating the effective perturbations with the RSE, we find the perturbed modes of the system for arbitrary strength of homogeneous perturbations in the surrounding medium. We follow this with a discussion of the implications of the transformation in dispersive systems and environments. We then present approximations deduced from the introduced theory: the diagonal approximation, the simple-diagonal, and the first-order approximation.

2.1 Transformation matrix

To begin with, we assume that the relevant resonant states of a basis system are known. This basis system is an optical resonator described by generally dispersive permittivity, permeability, and bi-anisotropy tensors, respectively, $\hat{\boldsymbol{\varepsilon}}(k, \mathbf{r})$, $\hat{\boldsymbol{\mu}}(k, \mathbf{r})$, and $\hat{\boldsymbol{\zeta}}(k, \mathbf{r})$ and $\hat{\boldsymbol{\xi}}(k, \mathbf{r})$. The resonant states of the basis system are solutions to Maxwell's

equations [16],

$$\left[k_n\hat{\mathbb{P}}_0(k_n,\mathbf{r})-\hat{\mathbb{D}}(\mathbf{r})\right]\vec{\mathbb{F}}_n(\mathbf{r})=\vec{\mathbb{0}}\,, \tag{2.1}$$

satisfying outgoing boundary conditions. We use here the 6×6 compact form of Maxwell's equations, where

$$\hat{\mathbb{P}}_0(k,\mathbf{r})=\begin{pmatrix}\hat{\boldsymbol{\varepsilon}} & -i\hat{\boldsymbol{\xi}}\\ i\hat{\boldsymbol{\zeta}} & \hat{\boldsymbol{\mu}}\end{pmatrix},\quad \hat{\mathbb{D}}(\mathbf{r})=\begin{pmatrix}0 & \nabla\times\\ \nabla\times & 0\end{pmatrix}, \tag{2.2}$$

are, respectively, the 6×6 generalized permittivity and curl operators, and $\vec{\mathbb{F}}_n(\mathbf{r})$ is a 6×1 column vector with components of the electric field $\mathbf{E}_n(\mathbf{r})$ and magnetic field $i\mathbf{H}_n(\mathbf{r})$,

$$\vec{\mathbb{F}}_n(\mathbf{r})=\begin{pmatrix}\mathbf{E}_n\\ i\mathbf{H}_n\end{pmatrix}. \tag{2.3}$$

Let us use $\mathcal{V}_{\text{in}}$ and $\mathcal{V}_{\text{out}}$ to denote, respectively, the system volume and the rest of space. For $\mathcal{V}_{\text{out}}$, the basis system is surrounded by an isotropic homogeneous medium described by

$$\hat{\mathbb{P}}_0(k,\mathbf{r})=\begin{pmatrix}\varepsilon_{b_0}\hat{\mathbf{1}} & -\kappa_{b_0}\hat{\mathbf{1}}\\ -\kappa_{b_0}\hat{\mathbf{1}} & \mu_{b_0}\hat{\mathbf{1}}\end{pmatrix}, \tag{2.4}$$

where ε_{b_0} and μ_{b_0} are, respectively, the surrounding medium permittivity and permeability, and since it is isotropic, its bi-anisotropy tensors become $\hat{\boldsymbol{\xi}}_{b_0}=-i\kappa_{b_0}\hat{\mathbf{1}}$ and $\hat{\boldsymbol{\zeta}}_{b_0}=i\kappa_{b_0}\hat{\mathbf{1}}$. Note that the surrounding medium is also assumed to be non-dispersive. We discuss the implication of dispersion in the environment in Sec. 2.2.

Now, we consider a perturbed system which is the same optical resonator but placed in a different environment, so its resonant states (labelled with an index ν) are modified and satisfy perturbed Maxwell's equations

$$\left[k_\nu\hat{\mathbb{P}}(k_\nu,\mathbf{r})-\hat{\mathbb{D}}(\mathbf{r})\right]\vec{\mathbb{F}}_\nu(\mathbf{r})=\vec{\mathbb{0}}\,, \tag{2.5}$$

with

$$\hat{\mathbb{P}}(k,\mathbf{r})=\hat{\mathbb{P}}_0(k,\mathbf{r})=\begin{pmatrix}\hat{\boldsymbol{\varepsilon}} & -i\hat{\boldsymbol{\xi}}\\ i\hat{\boldsymbol{\zeta}} & \hat{\boldsymbol{\mu}}\end{pmatrix} \tag{2.6}$$

for $\mathbf{r} \in \mathcal{V}_{\text{in}}$ and

$$\hat{\mathbb{P}}(k, \mathbf{r}) = \begin{pmatrix} \varepsilon_b \hat{\mathbf{1}} & -\kappa_b \hat{\mathbf{1}} \\ -\kappa_b \hat{\mathbf{1}} & \mu_b \hat{\mathbf{1}} \end{pmatrix} \tag{2.7}$$

for $\mathbf{r} \in \mathcal{V}_{\text{out}}$, and ε_b, μ_b, and κ_b being the isotropic parameters for the perturbed surrounding medium.

Now, we start developing the transformation by introducing a linear transformation which keeps the operator $\hat{\mathbb{D}}$ in Eq. (2.1) unchanged. It is defined by

$$T \begin{pmatrix} 0 & 1 \\ 1 & 0 \end{pmatrix} S = \begin{pmatrix} 0 & 1 \\ 1 & 0 \end{pmatrix} , \tag{2.8}$$

where T and S are 2×2 matrices having a general form

$$T = \frac{1}{\sqrt{\Delta}} \begin{pmatrix} \alpha & i\gamma \\ -i\delta & \beta \end{pmatrix} , \qquad S = \frac{1}{\sqrt{\Delta}} \begin{pmatrix} \alpha & i\delta \\ -i\gamma & \beta \end{pmatrix} , \tag{2.9}$$

with

$$\Delta = \alpha\beta - \gamma\delta \, , \tag{2.10}$$

and α, β, γ, and δ are arbitrary real constants, and $T = S^{\dagger}$, where $S^{\dagger}$ is the conjugate transpose of S. Then, a reduced 2×2 matrix of the perturbed generalized permittivity $\hat{\mathbb{P}}(k, \mathbf{r})$,

$$P_b = \begin{pmatrix} \varepsilon_b & -\kappa_b \\ -\kappa_b & \mu_b \end{pmatrix} , \tag{2.11}$$

for $\mathbf{r} \in \mathcal{V}_{\text{out}}$, is transformed according to

$$P_b' = TP_bS \;\; = \;\; \frac{1}{\Delta} \begin{pmatrix} \alpha & i\gamma \\ -i\delta & \beta \end{pmatrix} \begin{pmatrix} \varepsilon_b & -\kappa_b \\ -\kappa_b & \mu_b \end{pmatrix} \begin{pmatrix} \alpha & i\delta \\ -i\gamma & \beta \end{pmatrix} , \tag{2.12}$$

which yields

$$P_b' = \frac{1}{\Delta} \begin{pmatrix} \alpha^2\varepsilon_b + \gamma^2\mu_b & i(\alpha\delta\varepsilon_b + \gamma\beta\mu_b) + (\gamma\delta - \alpha\beta)\kappa_b \\ -i(\alpha\delta\varepsilon_b + \gamma\beta\mu_b) + (\gamma\delta - \alpha\beta)\kappa_b & \delta^2\varepsilon_b + \beta^2\mu_b \end{pmatrix} . \tag{2.13}$$

To complete the transformation of Eq. (2.1), we also introduce wavenumber scaling,

$$k = \Gamma\tilde{k}\,, \tag{2.14}$$

and require that

$$\tilde{P}_b = \Gamma P_b' = P_{b_0} \equiv \begin{pmatrix} \varepsilon_{b_0} & -\kappa_{b_0} \\ -\kappa_{b_0} & \mu_{b_0} \end{pmatrix} . \tag{2.15}$$

This results in the following four equations determining the scaling factor Γ, and the matrix parameters α, β, γ, and δ:

$$\begin{aligned} \varepsilon_{b_0} &= \frac{\Gamma}{\Delta}\left(\alpha^2\varepsilon_b + \gamma^2\mu_b\right) , \qquad \kappa_{b_0} = \Gamma\kappa_b\,, \\ \mu_{b_0} &= \frac{\Gamma}{\Delta}\left(\delta^2\varepsilon_b + \beta^2\mu_b\right) , \qquad 0 = \alpha\delta\varepsilon_b + \gamma\beta\mu_b\,. \end{aligned} \tag{2.16}$$

Note that α, β, γ, and δ are defined up to an arbitrary constant factor, so that the number of the above equations is equal to the number of unknowns.

After applying the above transformation, the perturbed Maxwell's equations in the surrounding medium take exactly the same form as the unperturbed ones,

$$\tilde{k}\begin{pmatrix} \varepsilon_{b_0}\hat{\mathbf{1}} & -\kappa_{b_0}\hat{\mathbf{1}} \\ -\kappa_{b_0}\hat{\mathbf{1}} & \mu_{b_0}\hat{\mathbf{1}} \end{pmatrix}\begin{pmatrix} \tilde{\mathbf{E}} \\ i\tilde{\mathbf{H}} \end{pmatrix} - \begin{pmatrix} 0 & \nabla\times \\ \nabla\times & 0 \end{pmatrix}\begin{pmatrix} \tilde{\mathbf{E}} \\ i\tilde{\mathbf{H}} \end{pmatrix} = \begin{pmatrix} \mathbf{0} \\ \mathbf{0} \end{pmatrix} , \tag{2.17}$$

provided that the electromagnetic fields are also transformed according to

$$\begin{pmatrix} \mathbf{E}_\nu \\ i\mathbf{H}_\nu \end{pmatrix} = \frac{1}{\sqrt{\Delta}}\begin{pmatrix} \alpha & i\delta \\ -i\gamma & \beta \end{pmatrix}\begin{pmatrix} \tilde{\mathbf{E}} \\ i\tilde{\mathbf{H}} \end{pmatrix} = \frac{1}{\sqrt{\Delta}}\begin{pmatrix} \alpha\tilde{\mathbf{E}} - \delta\tilde{\mathbf{H}} \\ -i\gamma\tilde{\mathbf{E}} + i\beta\tilde{\mathbf{H}} \end{pmatrix} . \tag{2.18}$$

Note that Eq. (2.18) determines the field transformation over the entire space. Therefore, within the system, the transformed Maxwell's equations for a perturbed resonant state with the wavenumber $k_\nu = \Gamma\tilde{k}$ and the field $\vec{\mathbb{F}}_\nu = \hat{\mathbb{S}}\tilde{\vec{\mathbb{F}}}$ become

$$\tilde{k}\hat{\tilde{\mathbb{P}}}(\Gamma\tilde{k}, \mathbf{r})\tilde{\vec{\mathbb{F}}}(\mathbf{r}) - \hat{\mathbb{D}}(\mathbf{r})\tilde{\vec{\mathbb{F}}}(\mathbf{r}) = \vec{\mathbb{0}}\,, \tag{2.19}$$

where the generalized permittivity tensor,

$$\tilde{\hat{\mathbb{P}}}(k,\mathbf{r}) = \Gamma\hat{\mathbb{S}}^{\dagger}\hat{\mathbb{P}}_0(k,\mathbf{r})\hat{\mathbb{S}} = \frac{\Gamma}{\Delta}\begin{pmatrix} \alpha\hat{\mathbf{1}} & i\gamma\hat{\mathbf{1}} \\ -i\delta\hat{\mathbf{1}} & \beta\hat{\mathbf{1}} \end{pmatrix}\begin{pmatrix} \hat{\boldsymbol{\varepsilon}} & -i\hat{\boldsymbol{\xi}} \\ i\hat{\boldsymbol{\zeta}} & \hat{\boldsymbol{\mu}} \end{pmatrix}\begin{pmatrix} \alpha\hat{\mathbf{1}} & i\delta\hat{\mathbf{1}} \\ -i\gamma\hat{\mathbf{1}} & \beta\hat{\mathbf{1}} \end{pmatrix}, \tag{2.20}$$

describes an effective perturbed system surrounded by the unperturbed homogeneous medium. Here,

$$\hat{\mathbb{S}} = \frac{1}{\sqrt{\Delta}}\begin{pmatrix} \alpha\hat{\mathbf{1}} & i\delta\hat{\mathbf{1}} \\ -i\gamma\hat{\mathbf{1}} & \beta\hat{\mathbf{1}} \end{pmatrix},$$

is the transformation matrix, and Γ is the scaling factor determined by Eq. (2.16) as well as α, β, γ, and δ.

Thus, if we know the resonant states of an optical system described by tensors $\hat{\boldsymbol{\varepsilon}}$, $\hat{\boldsymbol{\mu}}$, $\hat{\boldsymbol{\xi}}$ and $\hat{\boldsymbol{\zeta}}$, and surrounded by a medium with isotropic parameters ε_{b_0}, μ_{b_0} and κ_{b_0}, and if these parameters of the medium are perturbed to, respectively, ε_b, μ_b, and κ_b, we transform Maxwell's equations according to Eqs. (2.13), (2.14), and (2.15), bringing the perturbed medium back to the unperturbed one at the cost of changing the system to an effective one, which is described by the generalized permittivity tensor $\tilde{\hat{\mathbb{P}}}$ given by Eq. (2.20). In other words, by introducing the perturbation of the surrounding medium, we effectively modify the system itself, and therefore can apply the standard dispersive RSE [16, 18] for treating the perturbation

$$\Delta\hat{\mathbb{P}}(\tilde{k},\mathbf{r}) = \tilde{\hat{\mathbb{P}}}(\Gamma\tilde{k},\mathbf{r}) - \hat{\mathbb{P}}_0(\tilde{k},\mathbf{r}) \tag{2.21}$$

which is nonzero only within the optical system. Note that the transformed Maxwell's equations Eq. (2.19) present a nonlinear eigenvalue problem for $\tilde{k}$. Expanding within the system volume the transformed electromagnetic field $\tilde{\vec{\mathbb{F}}}$ of a perturbed resonant state with the wavenumber k_ν (transformed to $\tilde{k}$) into a complete set of the resonant states of the unperturbed system,

$$\tilde{\vec{\mathbb{F}}}(\mathbf{r}) = \sum_n c_n\vec{\mathbb{F}}_n(\mathbf{r}), \tag{2.22}$$

the nonlinear Eq. (2.19) is then mapped onto a linear matrix eigenvalue problem,

$$(\tilde{k} - k_n)c_n = -\tilde{k}\sum_m V_{nm}(\infty)c_m + k_n \sum_m \left[V_{nm}(\infty) - V_{nm}(k_n)\right] c_m \,, \tag{2.23}$$

where the matrix elements of the perturbation are given by

$$V_{nm}(k) = \int \vec{\mathbb{F}}_n(\mathbf{r}) \cdot \Delta\hat{\mathbb{P}}(k, \mathbf{r})\vec{\mathbb{F}}_m(\mathbf{r}) d\mathbf{r} \,, \tag{2.24}$$

in which $\Delta\hat{\mathbb{P}}(k, \mathbf{r})$, defined by Eq. (2.21), is used for $k = k_n$ and $k = \infty$. Equation (2.23) is an exact result provided that all the resonant states are included in the basis. In this way, the standard dispersive RSE, originally valid only for perturbations within the system, is now used for finding the resonant states of an optical system in a modified (perturbed) environment surrounding it. To treat chirality perturbations in the surrounding medium, we note that the transformation method would work only if the unperturbed surrounding medium is chiral, i.e., if $\kappa_{b_0} \neq 0$. In the following, we determine the parameters of the transformation matrix, and provide the effective permittivity for systems and environments having non-chiral properties, with or without magnetic properties.

Non-chiral media

In the case of a non-chiral surrounding medium, i.e., $\kappa_b = \kappa_{b_0} = 0$, we find from Eq. (2.16) a set of equations

$$\varepsilon_{b_0} = \frac{\Gamma}{\Delta}\left(\alpha^2\varepsilon_b + \gamma^2\mu_b\right) \,, \tag{2.25}$$

$$\mu_{b_0} = \frac{\Gamma}{\Delta}\left(\delta^2\varepsilon_b + \beta^2\mu_b\right) \,, \tag{2.26}$$

$$0 = \alpha\delta\varepsilon_b + \gamma\beta\mu_b \,, \tag{2.27}$$

which has a general solution (with $\Gamma > 0$):

$$\Gamma = \sqrt{\frac{\varepsilon_{b_0}}{\varepsilon_b}\frac{\mu_{b_0}}{\mu_b}} \,, \qquad \frac{\delta}{\gamma} = \sqrt{\frac{\mu_b\mu_{b_0}}{\varepsilon_b\varepsilon_{b_0}}} \,, \qquad \frac{\beta}{\alpha} = \sqrt{\frac{\varepsilon_b}{\varepsilon_{b_0}}\frac{\mu_{b_0}}{\mu_b}} \,. \tag{2.28}$$

One can take a simple special case of Eq. (2.28):

$$\alpha = \sqrt{\frac{\varepsilon_{b_0}}{\varepsilon_b}}\ , \qquad \beta = \sqrt{\frac{\mu_{b_0}}{\mu_b}}\,, \qquad \gamma = 0\,, \qquad \delta = 0\,, \tag{2.29}$$

leading to a transformation

$$k_\nu = \Gamma\tilde{k}\,, \qquad \mathbf{E}_\nu(\mathbf{r}) = \alpha\tilde{\mathbf{E}}(\mathbf{r})\,, \qquad \mathbf{H}_\nu(\mathbf{r}) = \beta\tilde{\mathbf{H}}(\mathbf{r})\,, \tag{2.30}$$

and an effective generalized permittivity within the system volume

$$\tilde{\hat{\mathbb{P}}}(k,\mathbf{r}) = \begin{pmatrix} \alpha^2\hat{\boldsymbol{\varepsilon}} & -i\Gamma\hat{\boldsymbol{\xi}} \\ i\Gamma\hat{\boldsymbol{\zeta}} & \beta^2\hat{\boldsymbol{\mu}} \end{pmatrix}. \tag{2.31}$$

Now, considering non-chiral systems as well ($\hat{\boldsymbol{\zeta}} = \hat{\boldsymbol{\xi}} = \hat{\mathbf{0}}$), the off-diagonal elements of the effective permittivity $\tilde{\hat{\mathbb{P}}}(k,\mathbf{r})$ become zero.

Non-magnetic media

Clearly, when both the system and its surrounding medium are non-chiral and non-magnetic, it follows from Eqs. (2.28) and (2.29)

$$\Gamma = \alpha = \sqrt{\frac{\varepsilon_{b_0}}{\varepsilon_b}}\ , \qquad \beta = 1\,, \tag{2.32}$$

leading to the following transformation

$$k_\nu = \sqrt{\frac{\varepsilon_{b_0}}{\varepsilon_b}}\tilde{k}\,, \qquad \mathbf{E}_\nu(\mathbf{r}) = \sqrt{\frac{\varepsilon_{b_0}}{\varepsilon_b}}\tilde{\mathbf{E}}(\mathbf{r})\,, \qquad \mathbf{H}_\nu(\mathbf{r}) = \tilde{\mathbf{H}}(\mathbf{r})\,, \tag{2.33}$$

with the effective permittivity simply becomes

$$\tilde{\hat{\boldsymbol{\varepsilon}}}(k,\mathbf{r}) = \frac{\varepsilon_{b_0}}{\varepsilon_b}\hat{\boldsymbol{\varepsilon}}(k,\mathbf{r})\,. \tag{2.34}$$

2.2 Frequency dispersion of the optical system and the surrounding medium

The dispersive RSE given by Eq. (2.23) is based on the assumption that the frequency dispersion of the system is described by a generalized Drude-Lorentz model [16, 18, 66],

$$\hat{\mathbb{P}}_0(k,\mathbf{r}) = \hat{\mathbb{P}}_\infty(\mathbf{r}) + \sum_j \frac{\hat{\mathbb{Q}}_j(\mathbf{r})}{k-\Omega_j}\,, \tag{2.35}$$

where $\hat{\mathbb{P}}_\infty(\mathbf{r})$ is the high-frequency value of the generalized permittivity, Ω_j are its simple-pole positions in the complex wavenumber plane, and $\hat{\mathbb{Q}}_j(\mathbf{r})$ are the corresponding residues.

Clearly, the perturbation Eq. (2.21), which includes the transformation of the wavenumber Eq. (2.14), contains both the original poles at $\tilde{k} = \Omega_j$ of the unperturbed system in the second term of Eq. (2.21) and shifted poles at $\tilde{k} = \Omega_j/\Gamma$ in the first term. One therefore has to apply the infinitesimal-dispersive RSE [63], which requires the inclusion of new pRSs in the RSE basis. The latter are however dependent on the perturbation through the scaling factor Γ. This could make using the RSE potentially inefficient, as the infinitesimal-pole basis states have to be recalculated every time when the perturbation (i.e. the properties of the surrounding medium) changes. In order to avoid this complication, we have introduced a simple transformation of the original pole modes of the basis system which produces an alternative set of basis states replacing the new pRSs. This transformation does not require calculating new basis states every time but instead uses the same fixed set of states of the basis system, by simply re-scaling them in space. This is described in more detail in Sec. 2.4 and illustrated there using an example of a Drude model of gold.

Let us finally note that if any of the parameters describing the surrounding medium, such as ε_b and μ_b as well as ε_{b_0} and μ_{b_0}, depend on the wavenumber k, the general

transformation method becomes state dependent. This can be easily seen for a non-magnetic and non-chiral medium, in which case the scaling factor

$$\Gamma(k, k_\nu) = \sqrt{\frac{\varepsilon_{b_0}(k)}{\varepsilon_b(k_\nu)}} \tag{2.36}$$

becomes state dependent, as it explicitly depends on k_ν and is thus different for different states. In this case, one may consider applying the transformation to both the unperturbed and perturbed systems, which may work for some cases to some extent. Nevertheless, dispersive surrounding media can be treated by means of resonant-state regularization as described in Chapter 4, leading to analytic results which in first order coincide with those reported in [26].

2.3 Diagonal and first-order approximations

Now we aim to obtain from the RSE a first order approximation in terms of the perturbation parameters. To do this, we first consider the diagonal version of the RSE in Eq. (2.23) which results from keeping only the diagonal terms, leading to a single-mode approximation:

$$k_\nu = \Gamma\tilde{k} \approx \Gamma k_n \frac{1 + V_{nn}(\infty) - V_{nn}(k_n)}{1 + V_{nn}(\infty)}\,, \tag{2.37}$$

which turns out to be surprisingly accurate for a large class of plasmonic nano-resonators, as we demonstrate later in Chapter 3. In fact, neglecting any matrix elements of the effective perturbation in Eq. (2.37) leads to $\tilde{k} \approx k_n$ and thus to a much simplified version of the diagonal approximation:

$$k_\nu \approx \Gamma k_n\,, \tag{2.38}$$

which we refer to later as the simple diagonal approximation.

Now, to extract the first-order approximation from the diagonal approximation Eq. (2.37), we need to keep in the expression for the perturbed resonant state's

wavenumber k_ν only terms linear in δ_ε, δ_μ, and δ_κ, where

$$\delta_\varepsilon = \varepsilon_b/\varepsilon_{b_0} - 1\,, \qquad \delta_\mu = \mu_b/\mu_{b_0} - 1\,, \qquad \delta_\kappa = \kappa_b/\kappa_{b_0} - 1\,. \tag{2.39}$$

However, for clarity of presentation, we assume hereafter that both the system and its environment are non-chiral with or without perturbation ($\hat{\boldsymbol{\zeta}} = \hat{\boldsymbol{\xi}} = \hat{\mathbf{0}}$ and $\kappa_b = \kappa_{b_0} = 0$) in the diagonal RSE, taking the form

$$\frac{k_\nu}{k_n} \approx \frac{n_{b_0}}{n_b}\frac{1 + V_{nn}(\infty) - V_{nn}(k_n)}{1 + V_{nn}(\infty)}\,. \tag{2.40}$$

By noting that $\varepsilon_{b_0}/\varepsilon_b \approx 1 - \delta_\varepsilon$ and $\mu_{b_0}/\mu_b \approx 1 - \delta_\mu$, as well as

$$\Gamma = \frac{n_{b_0}}{n_b} \approx 1 - \frac{1}{2}\left(\delta_\varepsilon + \delta_\mu\right)\,, \tag{2.41}$$

where $n_{b_0} = \sqrt{\varepsilon_{b_0}\mu_{b_0}}$ and $n_b = \sqrt{\varepsilon_b\mu_b}$, are calculated to first order. Also, taking into account that in this limit $V_{nn}(\infty)$ is linear in δ_ε and δ_μ, we find from Eq. (2.40)

$$\frac{k_\nu}{k_n} \approx 1 - V_{nn}(k_n) - \frac{1}{2}\left(\delta_\varepsilon + \delta_\mu\right)\,. \tag{2.42}$$

Let us now evaluate $V_{nn}(k_n)$ to first order. The permittivity perturbation contributing to $V_{nn}(k_n)$ has the form [see Eq. (2.21)]:

$$\Delta\hat{\boldsymbol{\varepsilon}}(\tilde{k}, \mathbf{r}) = \hat{\boldsymbol{\varepsilon}}(k, \mathbf{r})\frac{\varepsilon_{b_0}}{\varepsilon_b} - \hat{\boldsymbol{\varepsilon}}(\tilde{k}, \mathbf{r})\,, \tag{2.43}$$

where $\tilde{k} = k/\Gamma = k_n$, from what we find

$$k - k_n = k_n(\Gamma - 1) \approx -\frac{k_n}{2}(\delta_\varepsilon + \delta_\mu)\,, \tag{2.44}$$

to first order. Expanding also to first order $\hat{\boldsymbol{\varepsilon}}(k, \mathbf{r}) \approx \hat{\boldsymbol{\varepsilon}}(k_n, \mathbf{r}) + \hat{\boldsymbol{\varepsilon}}'(k_n, \mathbf{r})(k - k_n)$, where the prime means the derivative with respect to k, we find

$$\Delta\hat{\boldsymbol{\varepsilon}}(k_n, \mathbf{r}) \approx -\hat{\boldsymbol{\varepsilon}}(k_n, \mathbf{r})\delta_\varepsilon - \hat{\boldsymbol{\varepsilon}}'(k_n, \mathbf{r})\frac{k_n}{2}(\delta_\varepsilon + \delta_\mu)\,. \tag{2.45}$$

Similarly,

$$\Delta\hat{\boldsymbol{\mu}}(k_n,\mathbf{r}) \approx -\hat{\boldsymbol{\mu}}(k_n,\mathbf{r})\delta_\mu - \hat{\boldsymbol{\mu}}'(k_n,\mathbf{r})\frac{k_n}{2}(\delta_\varepsilon+\delta_\mu)\,. \tag{2.46}$$

Introducing integrals over the system volume $\mathcal{V}_{\text{in}}$,

$$I^E_{nm} = \int_{\mathcal{V}_{\text{in}}} \mathbf{E}_n\cdot\hat{\boldsymbol{\varepsilon}}(k_n,\mathbf{r})\mathbf{E}_m d\mathbf{r}, \qquad J^E_n = k_n\int_{\mathcal{V}_{\text{in}}} \mathbf{E}_n\cdot\hat{\boldsymbol{\varepsilon}}'(k_n,\mathbf{r})\mathbf{E}_n d\mathbf{r}\,, \tag{2.47}$$

$$I^H_{nm} = \int_{\mathcal{V}_{\text{in}}} \mathbf{H}_n\cdot\hat{\boldsymbol{\mu}}(k_n,\mathbf{r})\mathbf{H}_m d\mathbf{r}, \qquad J^H_n = k_n\int_{\mathcal{V}_{\text{in}}} \mathbf{H}_n\cdot\hat{\boldsymbol{\mu}}'(k_n,\mathbf{r})\mathbf{H}_n d\mathbf{r}\,, \tag{2.48}$$

the diagonal matrix element of the perturbation takes the form

$$V_{nn}(k_n) \approx -I^E_{nn}\delta_\varepsilon + I^H_{nn}\delta_\mu + (-J^E_n + J^H_n)\frac{1}{2}(\delta_\varepsilon+\delta_\mu)\,, \tag{2.49}$$

so that finally the first-order approximation takes the form

$$\frac{k_n-k_\nu}{k_n} \approx \frac{1}{2}\left(1-2I^E_{nn}-J^E_n+J^H_n\right)\delta_\varepsilon + \frac{1}{2}\left(1+2I^H_{nn}-J^E_n+J^H_n\right)\delta_\mu\,. \tag{2.50}$$

It is convenient, for the purpose of comparison with other approaches which is done in Chapter 4, to introduce

$$A_n = I^E_{nn}+J^E_n-I^H_{nn}-J^H_n\,, \qquad B_n = I^E_{nn}+I^H_{nn}\,, \tag{2.51}$$

so that Eq. (2.50) can be written as

$$\frac{k_n-k_\nu}{k_n} \approx \frac{1-A_n}{2}(\delta_\varepsilon+\delta_\mu) - \frac{B_n}{2}(\delta_\varepsilon-\delta_\mu)\,. \tag{2.52}$$

Clearly, for non-dispersive systems $J^E_n = J^H_n = 0$, and A_n simplifies to $A_n = I^E_{nn} - I^H_{nn}$.

2.4 Effective-pole resonant states

As already mentioned in Sec. 2.2, the transformation Eq. (2.14) of the wavenumber leads in dispersive systems to a shift of the pole positions in the permittivity, which in turn results in a need of introducing degenerate pRSs. This may potentially lead to an

inefficiency of applying the RSE to systems with gradual changes of the environment, since every time when the environment is changed, the pRSs have to be recalculated for a changed position of the permittivity pole. To mitigate this complication, we introduce here an alternative approach based on a simple, good quality approximation in which the effective (shifted) pRSs are replaced with some effective pRSs generated by the unperturbed permittivity.

The pRSs are determined by the secular equation of the system. Considering a spherical system to illustrate the above idea, the secular equation of an isotropic sphere in an isotropic surrounding medium is given by

$$\beta J'(n_r z)H(n_b z) = \beta_b J(n_r z)H'(n_b z)\,, \qquad \text{for TE} \tag{2.53}$$

$$\beta_b J'(n_r z)H(n_b z) = \beta J(n_r z)H'(n_b z)\,, \qquad \text{for TM} \tag{2.54}$$

which are very similar to the secular equations in [61], but with taking into account permittivity for the surrounding medium other than vacuum. Here, $J(x) = xj_l(x)$ and $H(x) = xh_l^{(1)}(x)$, where $j_l(x)$ and $h_l^{(1)}(x)$ are, respectively, the spherical Bessel function and Hankel function of first kind, primes mean the derivatives of functions with respect to their arguments, $z = k_n R$, k_n is the resonant state's wavenumber, R is the sphere radius, $n_b = \sqrt{\varepsilon_b \mu_b}$ and $n_r = \sqrt{\varepsilon(k_n)\mu(k_n)}$ are the refractive indices of, respectively, the surrounding medium and the sphere, and we define $\beta(r)$ as the square root of the ratio of the permittivity $\varepsilon(r)$ to the permeability $\mu(r)$:

$$\beta(r) = \sqrt{\frac{\varepsilon(r)}{\mu(r)}}\,, \tag{2.55}$$

taking values $\beta = \sqrt{\frac{\varepsilon(k_n)}{\mu(k_n)}}$ inside the sphere and $\beta_b = \sqrt{\frac{\varepsilon_b}{\mu_b}}$ outside the sphere. This ratio becomes important for a later discussion on achieving degenerate modes in non-dispersive spherical systems in Chapter 5.

We now focus on a relatively simple example of a spherical non-magnetic nanoparticle in vacuum with the dispersion described by the Drude model, with noting that the Drude model is a special case of the more general Drude-Lorentz dispersion

given by Eq. (2.35). We highlight again that while all pRSs are degenerate, i.e. $k_m = \Omega$, different pRSs have different refractive indices $n_r = \sqrt{\varepsilon_m}$. To find the values of n_r, the secular equations Eqs. (2.53) and (2.54) need to be solved for n_r while fixing the mode frequency at $k_m = \Omega$. For a spherical Drude nanoparticle in vacuum ($\varepsilon_b = \varepsilon_{b_0} = 1$), Eq. (2.53) leads to

$$n_r J'(n_r z)H(z) = J(n_r z)H'(z) \qquad \text{(TE)} \tag{2.56}$$

for TE polarization, with the eigenvalues $n_r = \sqrt{\varepsilon_m^{\text{TE}}}$, and Eq. (2.54) leads to

$$\frac{1}{n_r} J'(n_r z)H(z) = J(n_r z)H'(z) \qquad \text{(TM)} \tag{2.57}$$

for TM polarization, with the eigenvalues $n_r = \sqrt{\varepsilon_m^{\text{TM}}}$, and $z = \Omega R$ fixed in both equations.

According to Eqs. (2.32) and (2.34), the effective permittivity has the form

$$\tilde{\varepsilon}(k) = \varepsilon(k)\alpha^2 \,, \tag{2.58}$$

where $\alpha = \Gamma = 1/\sqrt{\varepsilon_b}$, and ε_b is the permittivity of the background medium, here assumed for simplicity non-magnetic. The effective permittivity $\tilde{\varepsilon}(k)$ of the effective perturbed system in vacuum therefore has a Drude pole shifted to $k = \tilde{\Omega} = \Omega\sqrt{\varepsilon_b}$. The effective pRSs due to $\tilde{\varepsilon}(k)$ are given (again taking the limit $\sigma \to 0$) by an effective secular equation

$$\tilde{n}_r J'(\tilde{n}_r \tilde{z})H(\tilde{z}) = J(\tilde{n}_r \tilde{z})H'(\tilde{z}) \qquad \text{(TE)} \tag{2.59}$$

with $\tilde{n}_r = \sqrt{\tilde{\varepsilon}_m^{\text{TE}}}$ for TE polarization, and

$$\frac{1}{\tilde{n}_r} J'(\tilde{n}_r \tilde{z})H(\tilde{z}) = J(\tilde{n}_r \tilde{z})H'(\tilde{z}) \qquad \text{(TM)} \tag{2.60}$$

with $\tilde{n}_r = \sqrt{\tilde{\varepsilon}_m^{\text{TM}}}$ for TM polarization. In other words, the new eigenvalues, $\tilde{\varepsilon}_m^{\text{TE}}$ and $\tilde{\varepsilon}_m^{\text{TM}}$, are found by solving Eqs. (2.59) and (2.60) for a fixed value of $\tilde{z} = \tilde{\Omega}R = \sqrt{\varepsilon_b}\Omega R$. Clearly, Eqs. (2.59) and (2.60) have to be solved every time when background permittivity ε_b changes. However, for small $\tilde{z}$ (for example, $\tilde{z}$ is of order of 10^{-3} for a

gold nanosphere of radius $R = 10\,\mathrm{nm}$), one can approximate $H'(z)/H(z) \approx -l/z$ [68], so that Eq. (2.59) simplifies to

$$\tilde{n}_r \tilde{z} J'(\tilde{n}_r \tilde{z}) \approx -l J(\tilde{n}_r \tilde{z}) \qquad (\mathrm{TE})\,, \tag{2.61}$$

which is equivalent, in the same approximation, to Eq. (2.56), provided that $\tilde{n}_r = n_r/\sqrt{\varepsilon_b}$. Therefore,

$$\tilde{\varepsilon}_m^{\mathrm{TE}} \approx \frac{\varepsilon_m^{\mathrm{TE}}}{\varepsilon_b}\,. \tag{2.62}$$

Applying the same approximation to TM polarization, Eq. (2.60) simplifies to

$$\frac{\tilde{z}}{\tilde{n}_r} J'(\tilde{n}_r \tilde{z}) \approx -l J(\tilde{n}_r \tilde{z}) \qquad (\mathrm{TM})\,, \tag{2.63}$$

which does not seem to be equivalent to Eq. (2.57). However, since $|z| \ll 1$ both Eqs. (2.57) and (2.63) are well approximated by

$$j_l(\tilde{n}_r \tilde{z}) \approx j_l(n_r z) \approx 0 \qquad (\mathrm{TE}\ \&\ \mathrm{TM})\,, \tag{2.64}$$

actually working equally well for both polarizations, so that again

$$\tilde{\varepsilon}_m^{\mathrm{TM}} \approx \frac{\varepsilon_m^{\mathrm{TM}}}{\varepsilon_b} \approx \frac{1}{\varepsilon_b}\left(\frac{Z_{l,m}^{\mathrm{Bess}}}{\Omega R}\right)^2 \quad , \tag{2.65}$$

where $Z_{l,m}^{\mathrm{Bess}}$ is the m-th root of the spherical Bessel function $j_l(Z)$. However, the fundamental pRS in TM polarization, $m = 0$, can be treated separately, namely by approximating also $J'(z)/J(z) \approx (l+1)/z$ at small z [68]. This yields

$$\tilde{\varepsilon}_{m=0}^{\mathrm{TM}} \approx \varepsilon_{m=0}^{\mathrm{TM}} \approx -\frac{l+1}{l}\,, \tag{2.66}$$

which is formally the same equation as for the localized surface plasmon in a spherical nanoparticle in the low frequency limit [63]. Clearly, Eq. (2.66) implies that the lowest-order pRS can be taken the same as in the unperturbed system.

To summarize, the approximate basis of pRSs (further called pRSs II) introduced

above is calculated from the unperturbed basis of pRSs, satisfying Eqs. (2.56) and (2.57), by using simple relations between their eigen permittivities Eqs. (2.62) and (2.65), with the exception for the fundamental pRS in TM polarization, which is instead taken the same as in the unperturbed system. The approximate basis of pRSs II is then used to replace the effective basis of pRSs (further called pRSs I) satisfying Eqs. (2.59) and (2.60).

2.5 Summary

We have developed an exact perturbation theory for open systems based on the RSE to treat homogeneous perturbations in the surrounding medium of an optical system with a generalized response. This was accomplished by introducing a transformation matrix that maps Maxwell's equations of the perturbed system into an effective system enclosing the perturbation inside its boundaries, where the resonant states are complete. The effective system is therefore treatable by the RSE which produces exact perturbed modes, provided that all the unperturbed resonant states are included in the basis.

Additionally, we have distinguished two single-mode approximations resulting from our theory: the diagonal approximation and a simplified version of the diagonal approximation. The former was obtained by neglecting the off-diagonal elements of the RSE matrix, and the latter, the simple-diagonal approximation, was obtained by neglecting all the matrix elements entirely. We have also extracted the first-order contributions from the diagonal approximation.

In the case of dispersion, for a system described by the generalized Drude–Lorentz model, the transformation scales the poles of dispersion, and therefore the infinitesimal-dispersive RSE has to be applied. The infinitesimal-dispersive RSE requires adding the scaled pRSs (pRSs I) to the RSE basis. Since the pRSs I are frequency-dependent, they have to be recalculated repeatedly whenever the perturbation changes. This complication can be avoided by introducing a transformation of the original pRSs of the basis system to generate an alternative set of pRSs (pRSs II) fixed for all perturbations. We have demonstrated the idea with a simple example of a spherical non-magnetic

nanoparticle in vacuum with dispersion described by the Drude model. For dispersive environments, the transformation becomes state dependent, and thus the proposed theory may not be applicable.

In the next chapter, we will illustrate the proposed theory and its approximations using practically relevant systems, including both plasmonic particles and microresonators.

Chapter 3

Application of the RSE to refractive-index sensing

In this chapter, we calculate the spectral changes of experimentally relevant systems due to changing their surrounding medium, focusing on highly responsive modes: localized surface plasmon modes and whispering gallery modes of a wide class of resonators different in size and shape. We use the RSE approach based on the transformation introduced in Chapter 2 as well as its asymptotics, namely, the diagonal and the simple diagonal approximations. Since our illustrations are non-magnetic, we use the transformation for non-magnetic systems Eqs. (2.33) and (2.34) in the RSE equation, diagonal, and simple diagonal approximations, given by Eqs. (2.23), (2.37), and (2.38), respectively. We evaluate the accuracy of the presented theories by comparing the obtained results to exact values obtained either analytically or numerically. We further employ the high accuracy found in the diagonal approximation in plasmonic systems to propose an approach for calculating the integral of their fields, resulting in an accurate evaluation of the matrix element of the arbitrary-shaped systems.

3.1 Plasmonic nonoparticles

We classify applications on plasmonic particles into two groups: nanospheres and arbitrarily shaped geometries or configurations of more than one particle. The method employed to calculate the matrix elements of arbitrary-shaped systems is discussed in Sec. 3.1.3.

3.1.1 Nanospheres

To apply the RSE-based theory, we considered a gold nanosphere of radius $R = 200\,\text{nm}$ in vacuum ($\varepsilon_{b_0} = 1$) as a basis system. The permittivity of the sphere was taken in the Drude model, $\varepsilon(k) = \varepsilon_\infty - \sigma\gamma/[k(k + i\gamma)]$, with $\varepsilon_\infty = 4$, $\hbar c\sigma = 957\,\text{eV}$, and $\hbar c\gamma = 0.084\,\text{eV}$, the same parameters of dispersion as well as the size used in Chapter 1. Figure 3.1 shows the complex energy ($E = \hbar ck$) of the TM unperturbed resonant states of the sphere with $l = 1$, used to calculate the TM resonant states of the same sphere surrounded by a dielectric with $\varepsilon_b = 2$. This was achieved by mapping the perturbed system into an effective system surrounded by vacuum using the transformation for non-magnetic medium Eqs. (2.33) and (2.34). The internal perturbation in the effective system was treated by the RSE. Since the transformation shifts the unperturbed Drude pole of the permittivity at $\Omega = -i\gamma$ to an effective pole at $\tilde{\Omega} = -i\gamma\sqrt{\varepsilon_b}$, we used the infinitesimal dispersive RSE. The latter requires adding both the DRSs and the pRSs of the effective pole (pRSs I) to the basis. The accumulation of the DRSs as well as the effective pole generating the pRSs I are presented in Fig. 3.1. The modes of the perturbed system $k_\nu = \frac{1}{\sqrt{\varepsilon_b}}\tilde{k}$ are displayed in Fig. 3.1, showing a visual agreement of the RSE-based results and the modes calculated analytically from the secular equation.

Using the same sphere in vacuum as a basis system, the surface plasmon mode, indicated as SP in the mode spectrum in Fig. 3.1, was further investigated in Fig. 3.2, varying the background permittivity ε_b from vacuum to $\varepsilon_b = 3.9$. Figure 3.2(a) and (b) show the real energy Re(E) and the linewidth (-2Im(E)), calculated exactly and approximately using, respectively, the secular equation and the diagonal and first-order

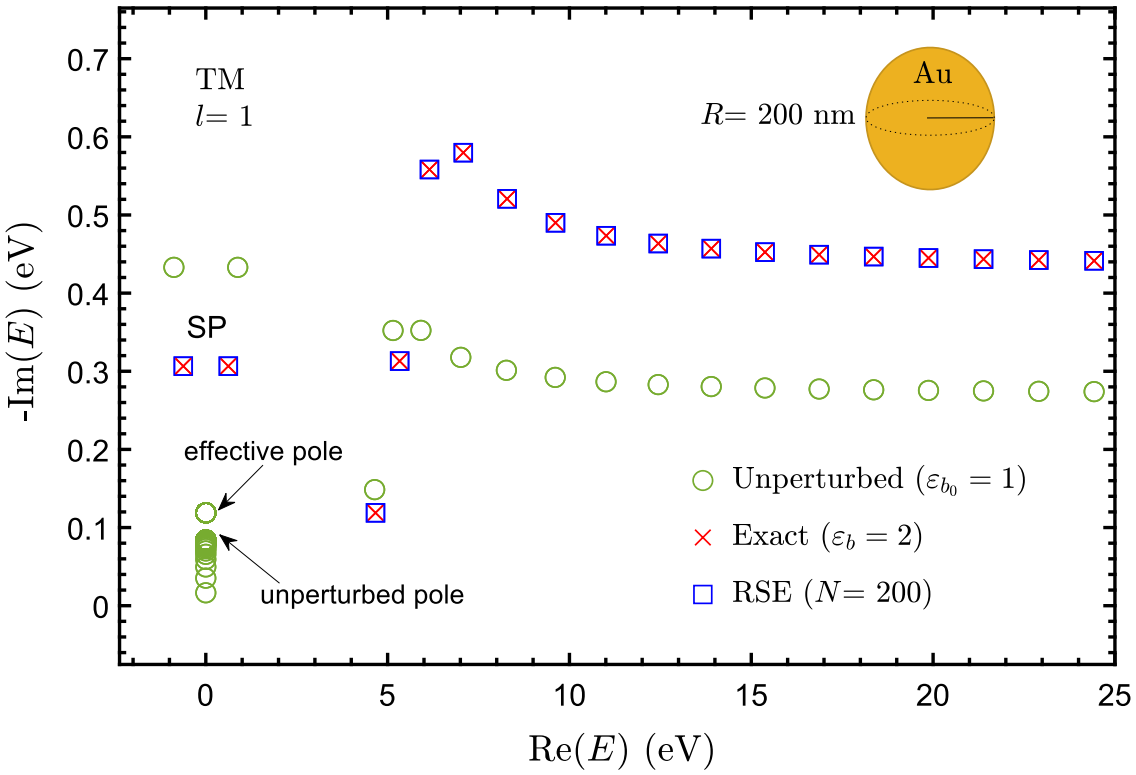

Figure 3.1. Complex energies $E = \hbar ck$ of the resonant states of a gold nanosphere of radius $R = 200\,\text{nm}$, surrounded by vacuum (open circles) and by a dielectric with $\varepsilon_b = 2$, calculated by the RSE (squares) and obtained exactly using the secular equation Eq. (2.54) (×), for TM polarization and $l = 1$. The inset shows accumulation of the basis resonant states around the unperturbed Drude pole, as well as the effective Drude pole generating pRSs I.

approximations as functions of the background permittivity ε_b. The error relative to the exact values are shown in Fig. 3.2(c) for the approximations, including the simple diagonal, and the RSE-based method using different basis size N. The basis size N is the only numerical parameter in the RSE calculation which is determined by the cut-off frequency k_c, such that all resonant states with k_n within the circle $|k_n\sqrt{\varepsilon(k_n)}| < k_c$ in the complex wave number plane are kept in the basis. Figure 3.2(c) shows the error of the RSE-based results scaling with the basis size as $1/N^3$, as expected from the standard RSE [13, 14]. The diagonal approximation turns out to be extremely accurate for the surface plasmon mode. Furthermore, it shows at least an order of

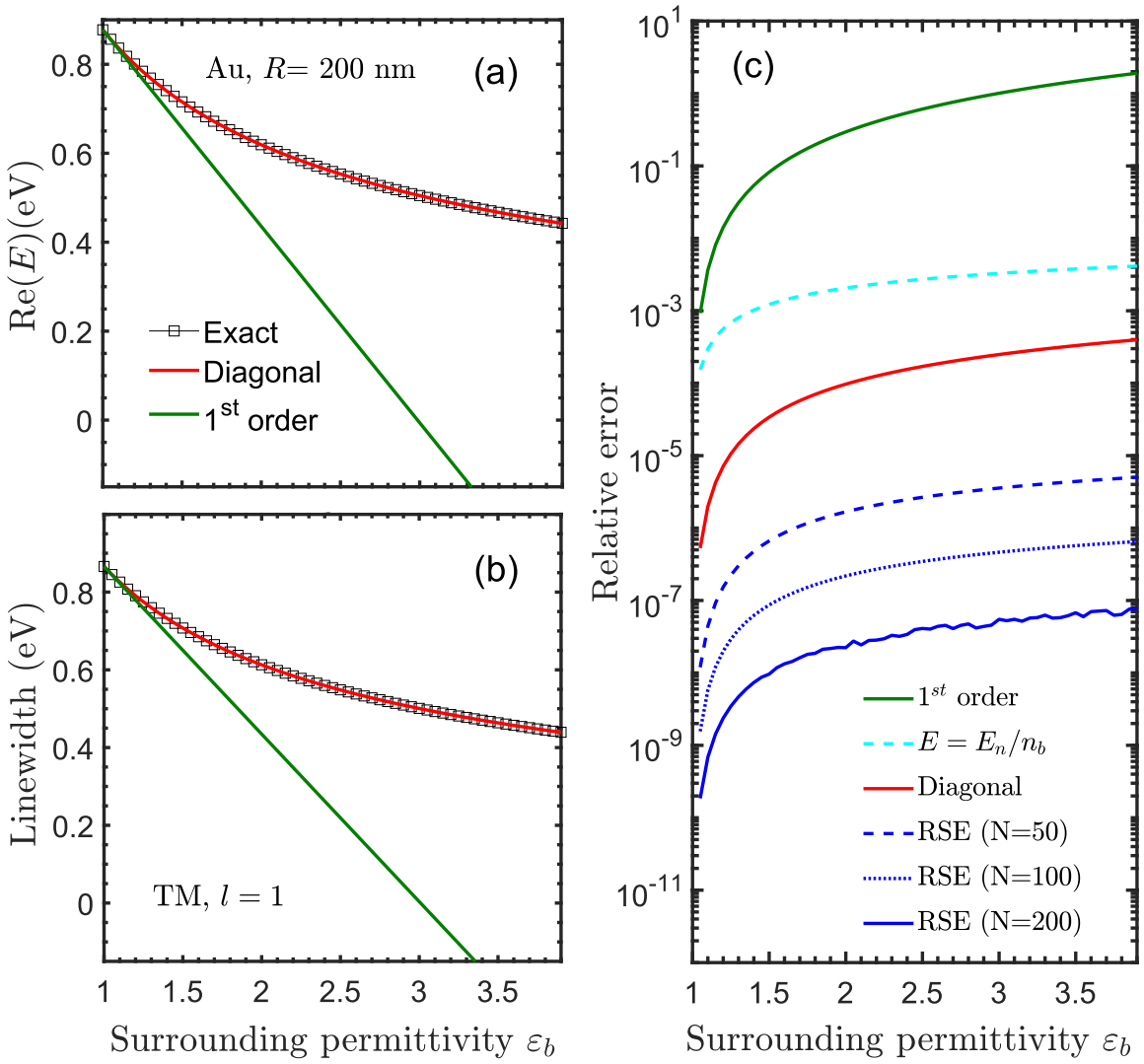

Figure 3.2. (a) Resonance energy (Re E), (b) linewidth (-2Im E), and (c) relative error of the complex energy E of the fundamental surface plasmon mode of a gold nanosphere ($R = 200$ nm) as functions of the background permittivity ε_b, calculated analytically (thin black lines with open squares), using the diagonal dispersive RSE (red lines) and first-order approximation (green lines). (c) Relative error of the first-order (green), simple diagonal (cyan), and diagonal approximation (solid red line), as well as of the full RSE with $N = 50$ (dashed blue), 100 (dotted blue) and 200 (solid blue line).

magnitude reduction of the error compared to the simple approximation. The first-order approximation instead fails when ε_b has moderate or even small deviation from ε_{b_0}, as evident from Fig. 3.2.

Furthermore, the surface plasmon mode was investigated, varying the sphere

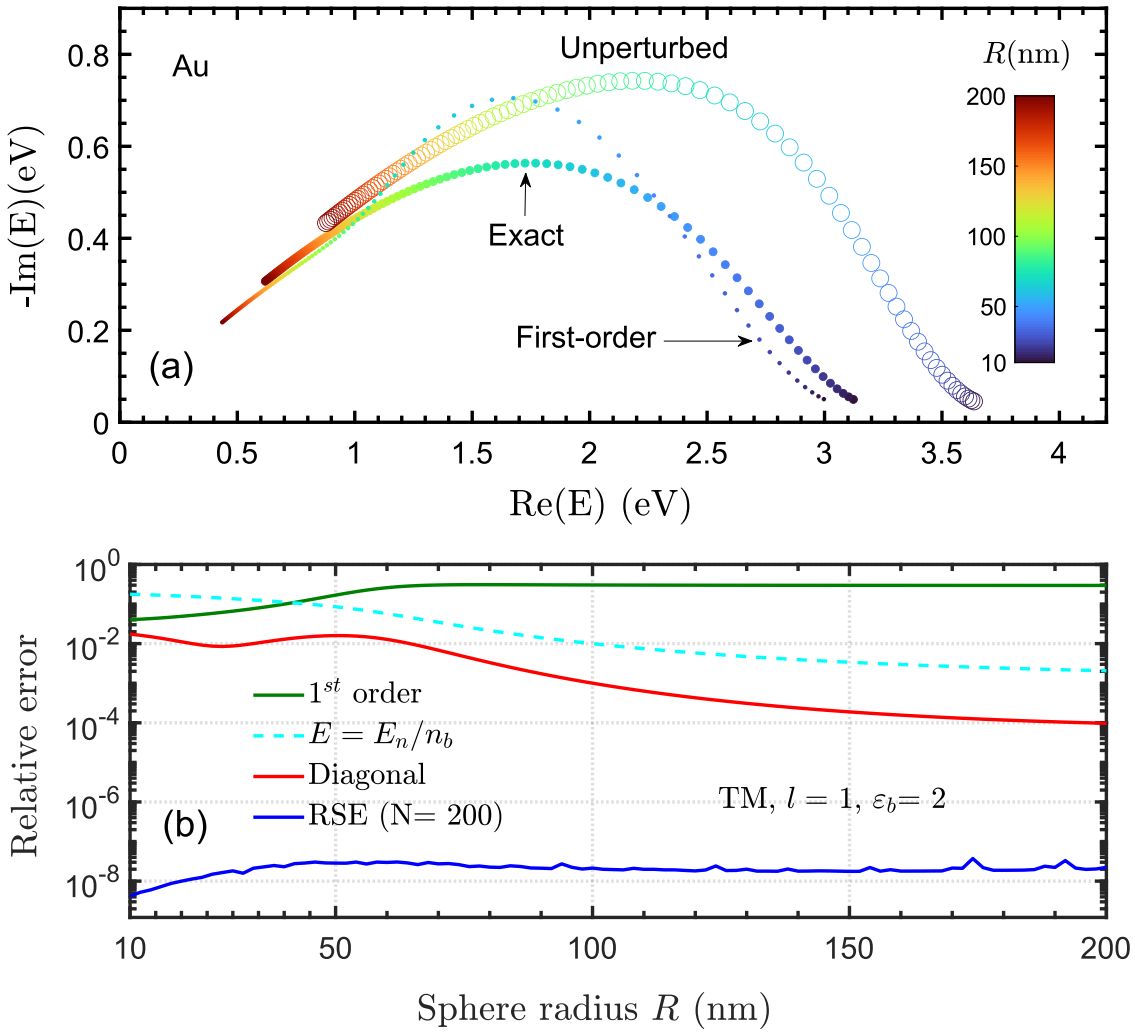

Figure 3.3. (a) Complex energy of the fundamental surface plasmon mode of a gold nanosphere surrounded by vacuum (unperturbed) and by a dielectric with $\varepsilon_b = 2$ (exact and first-order) as functions of the sphere radius R given by the color code. (b) Relative error of first-order (green), simple diagonal (cyan), and diagonal approximation (red), as well as of the full RSE (blue line), as functions of R.

radius R, taking values between 10 nm and 200 nm – a similar size range of plasmonic nanoparticles is used in experiments [72]. The evolution of the surface plasmon mode in the complex plane is shown in Fig. 3.3(a) for the gold sphere in vacuum and the gold sphere embedded in a medium with $\varepsilon_b = 2$, representing the unperturbed and the exact modes, respectively. Since both the basis size N and the perturbation are fixed, the RSE results maintain the same level of accuracy across the whole range of R as shown

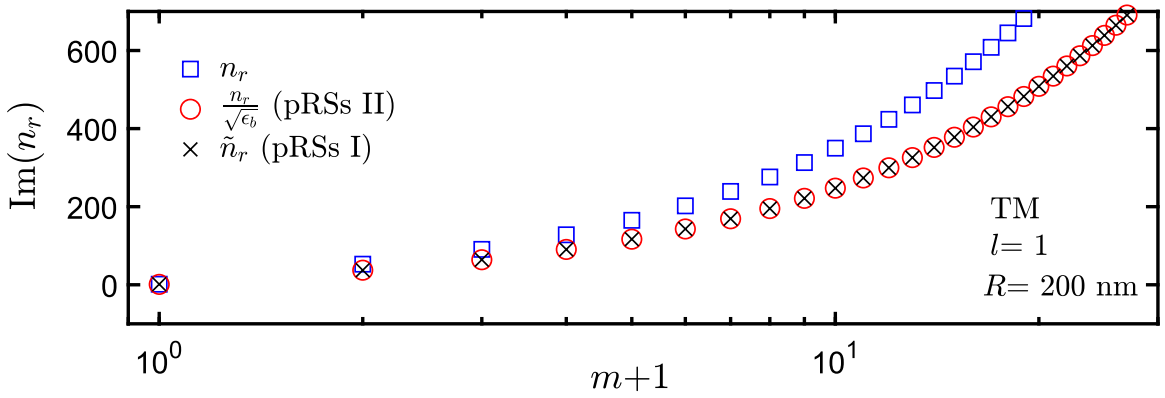

Figure 3.4. Values of the imaginary parts of the refractive index n_r (blue squares), $\frac{n_r}{\sqrt{\varepsilon_b}}$ (red circles), and $\tilde{n}_r$ of the pRSs as function of the mode number m. The $\frac{n_r}{\sqrt{\varepsilon_b}}$ and $\tilde{n}_r$ generate the pRSs II and pRSs I, respectively.

in Fig. 3.3(b). The diagonal approximation also maintains a good level of accuracy, with about one order of magnitude reduction compared to the simple diagonal, even for small radii. The error of the diagonal approximation is about 10^{-3} at $R = 40\,\text{nm}$, for example. The deviation of the surface plasmon mode calculated in the first order is visible in the evolution of the mode in the complex plane and demonstrated in the error Fig. 3.3(a,b).

Effective pole resonant states

The pRSs I of the effective pole are perturbation-dependent which makes the whole calculation rather inefficient. We illustrate here the approximation of the pRSs I to pRSs II using the same gold sphere. We also compare using the pRSs II with pRSs I in the convergence of the RSE-based theory for the calculation of the surface plasmon mode.

The pRSs I are generated from the refractive index of the effective system $\tilde{n}_r$ while the approximation pRSs II are generated from $\frac{n_r}{\sqrt{\varepsilon_b}}$, where n_r is the refractive index of the unperturbed system. Figure 3.4 shows the refractive index of the pRSs generated from n_r, $\frac{n_r}{\sqrt{\varepsilon_b}}$, and $\tilde{n}_r$, and demonstrates a visual agreement between $\tilde{n}_r$ and $\frac{n_r}{\sqrt{\varepsilon_b}}$, and thus pRSs I and pRSs II.

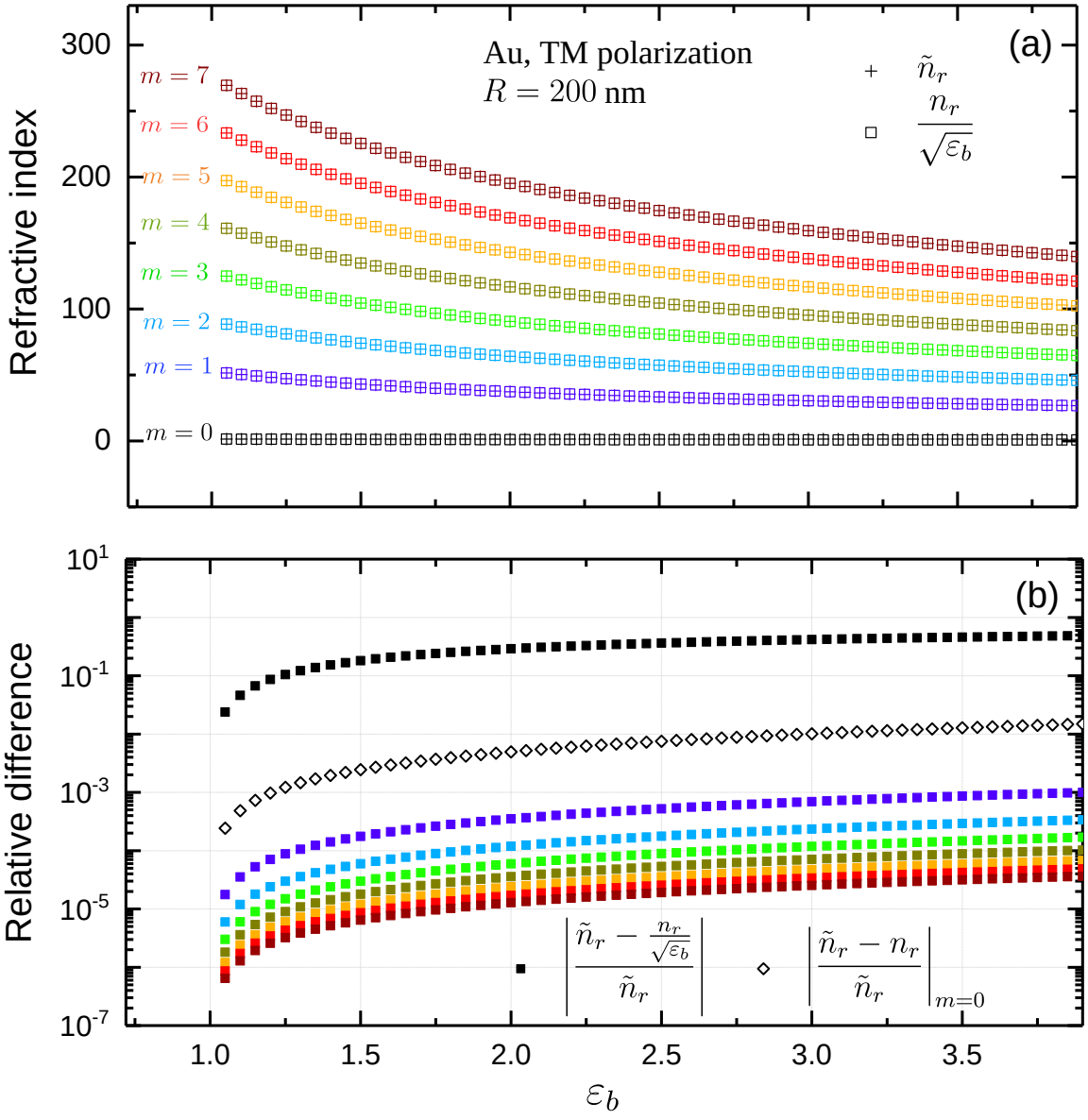

Figure 3.5. (a) The imaginary part of refractive index of the first few pRSs in TM polarization of a gold nanosphere of radius $R = 200\,\text{nm}$ described by the Drude model as functions of the permittivity of the surrounding medium ε_b, generated by the effective refractive index $\tilde{n}_r$ (crosses), and by using the approximation $\frac{n_r}{\sqrt{\varepsilon_b}}$ (open squares) (b) The relative error for the approximation (full squares) and the unperturbed lowest-order pRS (open diamonds).

We also provide in Figs. 3.5 and 3.6 a detailed comparison of the pRSs I and II. One can see that the values of the refractive index $\tilde{n}_r$ of the pRSs I (crosses) are in good visual agreement with those of the approximate pRSs II generated from $\frac{n_r}{\sqrt{\varepsilon_b}}$

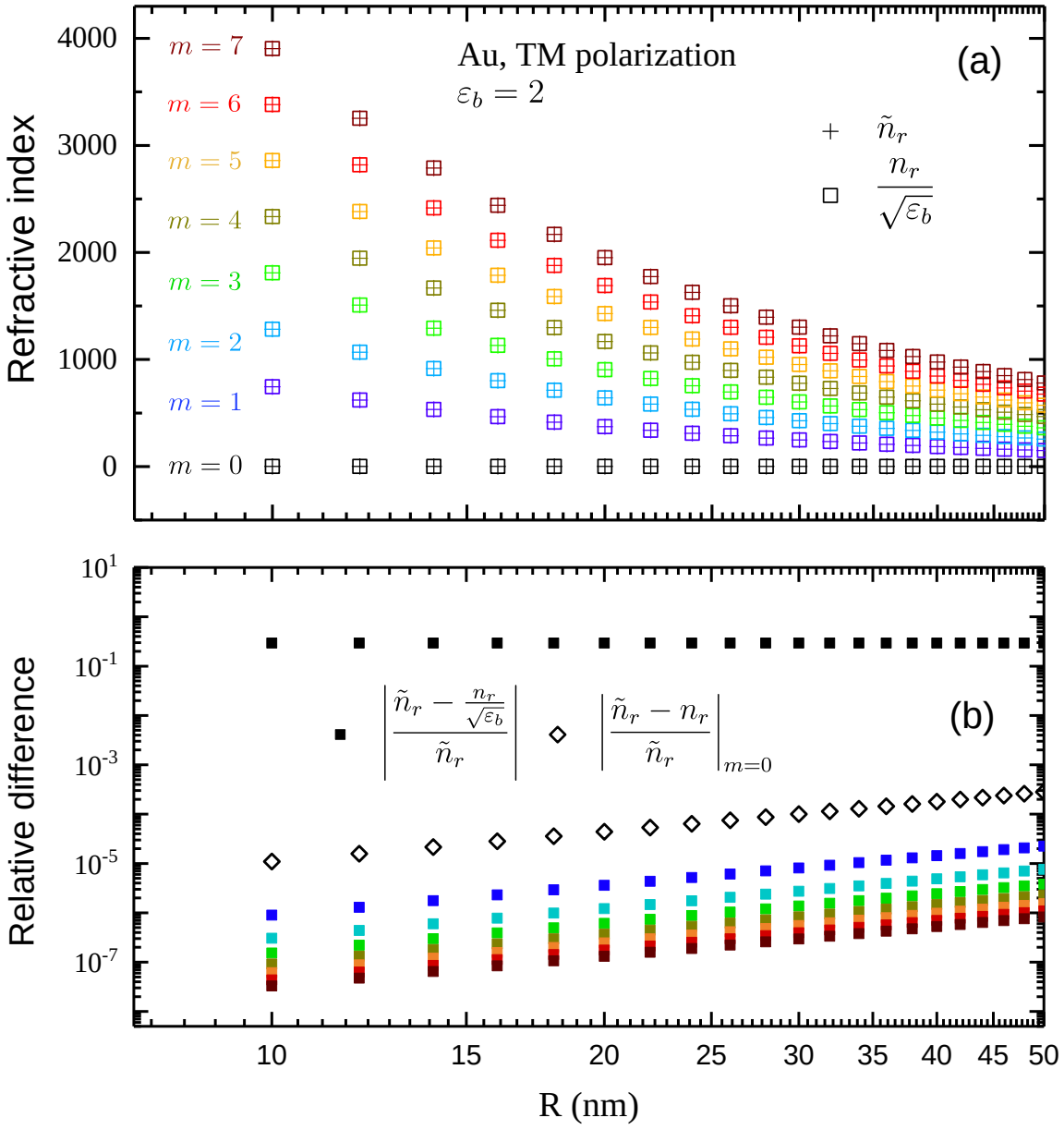

Figure 3.6. As Fig. 3.5 but for the dependence on the sphere radius R, for $\varepsilon_b = 2$.

(squares), for a wide range of values of the medium permittivity ε_b and sphere radius R, as exemplifies in Figs. 3.5(a) and 3.6(a), for the first eight pRSs. The relative error for the approximate modes presented in Figs. 3.5(b) and 3.6(b) shows, however, the weakness of this approximation for the fundamental ($m = 0$) mode. This approximation is then refined by using the unperturbed mode instead, compare the full black squares and diamonds in Figs. 3.5(b) and 3.6(b). Note that the error for all modes grows with

radius [see Fig. 3.6(b)], in accordance with the approximation $|\tilde{\Omega}R| \ll 1$ used.

We now compare including the perturbation-independent set (pRSs II) with pRSs I in the convergence of the RSE-based theory. We use the modes of the gold sphere in vacuum to calculate the surface plasmon mode as before, varying both the surrounding permittivity ε_b and the sphere radius R. The basis with approximation pRSs II is working so well that the $1/N^3$ convergence to the exact solution is almost unaffected, as demonstrated by Fig. 3.7(a,b). Without pRSs, the error for $N = 50$ basis RSs, also shown in Fig. 3.7(a,b), is almost the same as for the diagonal approximation ($N = 1$), i.e. keeping only the unperturbed surface plasmon mode in the basis. We thus note that even though the pRSs II are found with a limited accuracy, more important is the completeness of the full set of basis functions used in the RSE, supplemented with either pRSs I or pRSs II, both providing a quick convergence to the exact solution.

Lastly, since the pRSs II can also be generated from the roots of Bessel functions for TE and TM polarizations, in accordance with Eqs. (2.64) and (2.65). We produce in Appendix C.1 two figures as in Figs. 3.5 and 3.6, but for the pRSs II generated by the roots of Bessel function, with the exception of the lowest-order pRS, being generated by Eq. (2.66). The relative errors of the approximated pRSs II, either in Figs. 3.5 and 3.6 or in Appendix C.1, validate the suggested approximations.

3.1.2 Arbitrarily shaped particles

Focusing on the diagonal approximations as well as the first-order approximation, we further demonstrate that the quality of these approximations is almost independent of the shape and even the material of the resonator.

The basis modes for systems with arbitrary shapes were calculated using QNMEig, an open-source software accessible through the Modal Analysis of Nanoresonators (MAN-7.1) [53, 74, 75]. QNMEig is designed to accurately compute resonant states of dispersive optical resonators based on the eigenvalue solver in COMSOL Multiphysics [53, 75]. In COMSOL's eigenvalue solver, any non-linearity in the material properties is approximated up to second-order via Taylor expansion. The

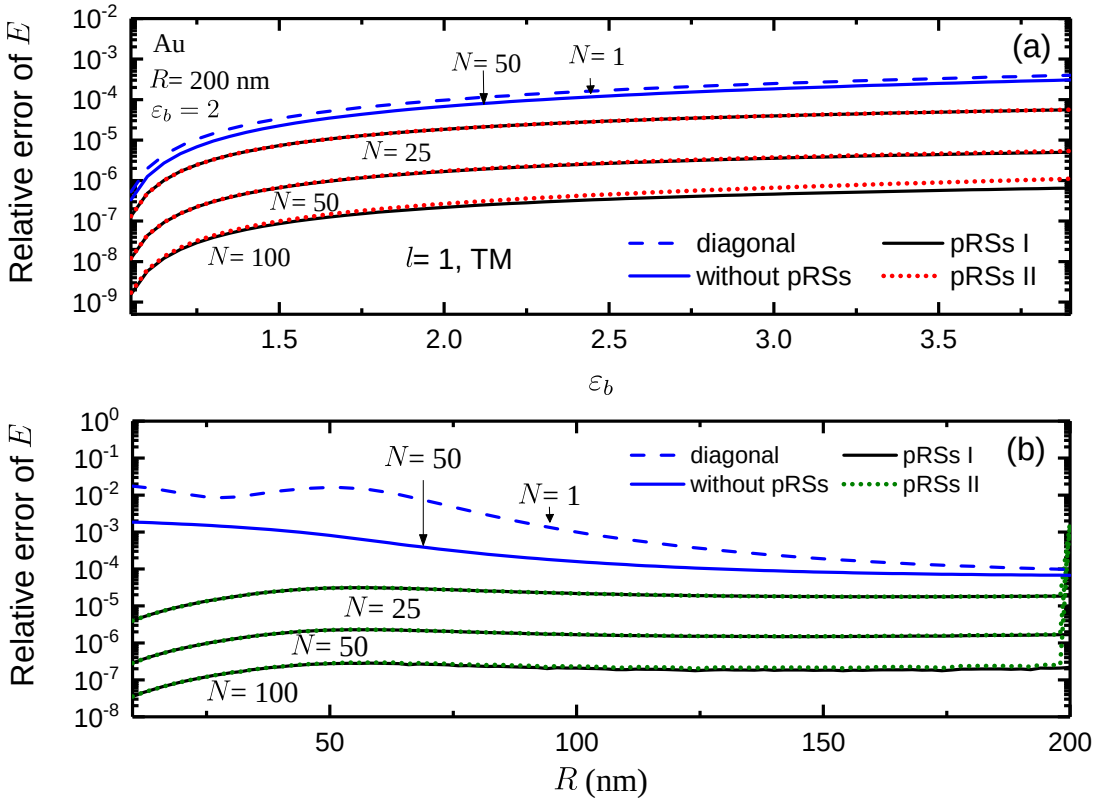

Figure 3.7. Relative error for the wave numbers of the fundamental (dipolar, $l = 1$) plasmonic mode of a gold nanosphere as function of the permittivity ε_b of the surrounding medium, calculated by the RSE with pRSs I (black solid lines) and pRSs II (red and green dotted lines) for $N = 50$, 100 and 200, as well as without pRSs ($N = 50$, solid blue lines) and in the diagonal approximation ($N = 1$, dashed blue lines).

solver then linearizes Maxwell's equations around a user-defined linearization point, iteratively updating this point to search for the eigenvalues [76]. However, convergence becomes problematic for highly dispersive systems, such as Drude-Lorentz metals [53]. QNMEig considers dispersion precisely by introducing auxiliary fields into Maxwell's equations and reformulating them into integral forms solvable by COMSOL's eigenvalue solver [75]. This method is optimized for several plasmonic nanoparticles within QNMEig [73]. In such systems, several eigenmodes are well-identified and analyzed, and they demonstrate good agreement with an earlier freeware that calculates the eigenmodes based on scattered field analysis [75]. Thus, we used such modes as basis modes in our illustrations of the diagonal and first-order approximations for arbitrarily shaped particles. QNMEig was also employed to compute the values of the modes in

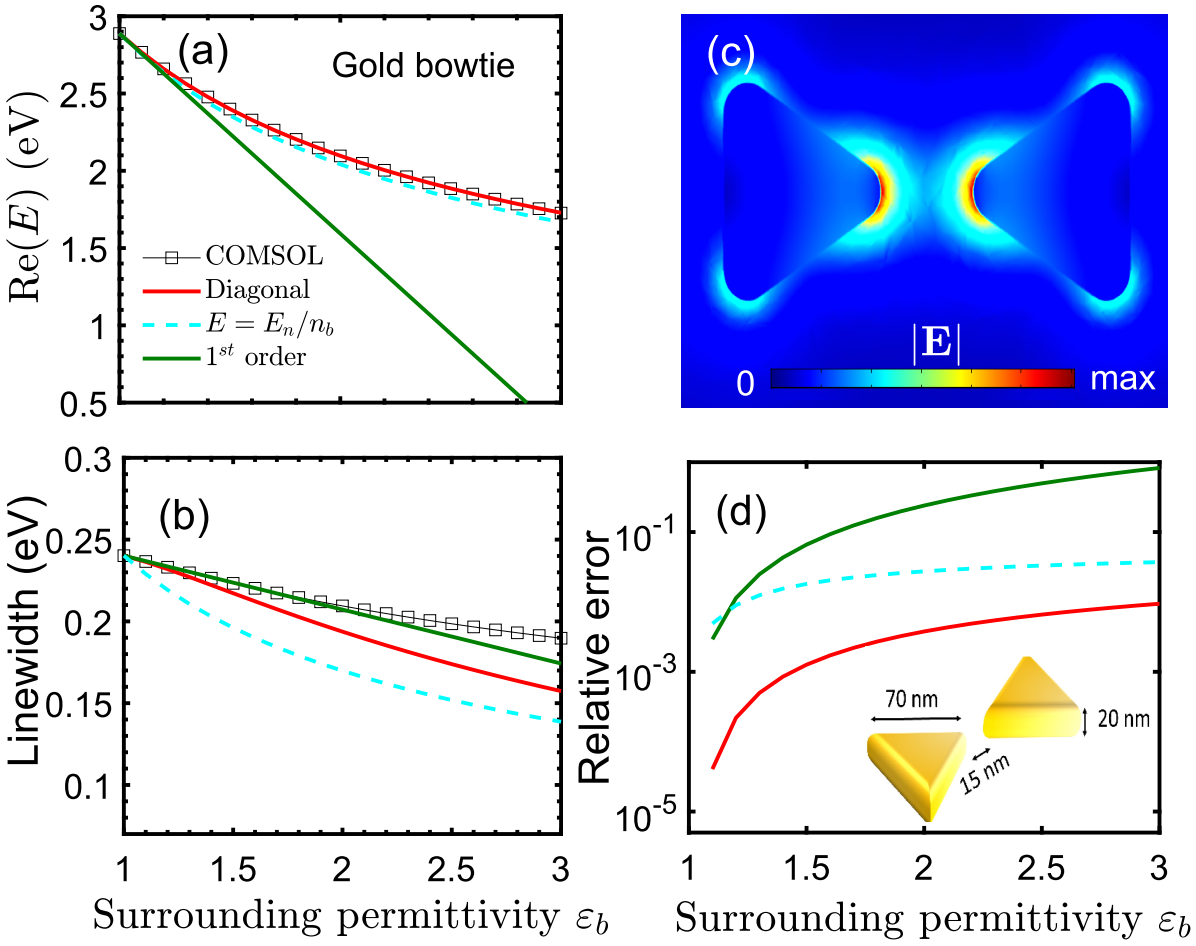

Figure 3.8. (a) Resonance energy (Re E) and (b) linewidth of a selected mode of a gold bow-tie antenna as functions of the permittivity of the surrounding medium ε_b, calculated using COMSOL [73] (black squares), diagonal (red), simple diagonal (cyan), and the first-order approximations (green). (c) Electric field of the unperturbed mode. (d) Error of the diagonal (red), simple diagonal (cyan), and first-order approximation (green) relative to COMSOL data. The inset shows schematics and dimensions of the system, with corners rounded to arcs with a radius of 8 nm.

different surrounding media as reference points for calculating the relative errors. To prevent any confusion with other modes, we tracked the evolution of the basis mode by slightly increasing ε_b. We also ensured that the PML thickness remained greater than two wavelengths, and the modes remained independent of the mesh or PML thickness for each calculation.

An example provided in Fig. 3.8 is a gold bow-tie antenna having dimensions shown in the inset [75]. The Drude parameters of gold were again generated by [66], giving

$\varepsilon_\infty = 1$, $\hbar c\sigma = 801.6\,\text{eV}$, and $\hbar c\gamma = 0.085\,\text{eV}$. The unperturbed mode of the bow-tie antenna in vacuum, having the electric field shown in Fig. 3.8(c), calculated by COMSOL (PML thickness is 80 nm and mesh minimum element size is 2.7 nm), was used as a basis state for the diagonal and first-order approximations. The diagonal, simple diagonal, and first-order approximations were used to calculate the real energy $\text{Re}(E)$ and linewidth of the bow-tie surrounded by different dielectrics with ε_b, as shown in Fig. 3.8(a,b). The open-source solver was used for calculating the values of the mode in different surrounding media having ε_b. Such values were used for visual comparison in Fig. 3.8(a,b) and error evaluation in Fig. 3.8(d). The relative errors are qualitatively similar to those of a gold sphere in Figs. 3.2(c) and 3.3(b).

We apply the same method used for the gold bow-tie to calculation of perturbed resonant state wavenumbers for different non-spherical systems and different materials, such as a silver dolmen (PML thickness is 300 nm and mesh minimum element size is 3.3 nm) [75, 77, 78] and silver bow-tie antenna (PML thickness is 80 nm and mesh minimum element size is 2.7 nm) [53, 75]. In the considered examples, the following parameters were used. The width of the top rod in the dolmen structure is 128 nm and the length is 50 nm. The vertical rods are 100 nm long, 30 nm wide, and 20 nm thick. The silver bow-tie antenna has a side length of 70 nm, a thickness of 20 nm, and a 15 nm gap, the same parameters used for the gold bow-tie antenna. The silver parameters generated by the program in [66] are $\varepsilon_\infty = 1$, $\hbar c\sigma = 4157\,\text{eV}$, and $\hbar c\gamma = 0.018\,\text{eV}$. The electric field of the basis modes in vacuum are shown in Fig. 3.9(a,b) for the silver dolmen and bow-tie, respectively. The real energy and linewidth calculated using COMSOL, diagonal, first-order, and simple diagonal approximations as functions of ε_b are shown in Fig. 3.9(d,g) for the silver dolmen and in Fig. 3.9(e,h) for the silver bow-tie. All approximations show a similar level of accuracy across the systems treated, as shown in the error in Fig. 3.9(j,k).

The main message of the RSE-based theory is for treating homogeneous changes in the unbounded space surrounding the system accurately. Nevertheless, we show that the diagonal approximation works well also for a resonator placed on a substrate. We consider an example of a silver cube on a gold substrate (PML thickness is 100 nm and

mesh minimum element size in the cube is 4 nm) [52, 53, 75]. The cube has a side of 65 nm, with corners rounded to arcs with a radius of 4 nm and the substrate has 80 nm thickness separated by 8 nm wide polymer. The Drude parameters of the gold cube are the same as those for the gold bow-tie, $\varepsilon_\infty = 1$, $\hbar c\sigma = 801.6\,\text{eV}$, and $\hbar c\gamma = 0.085\,\text{eV}$. The polymer beneath the cube has the permittivity of $\varepsilon = 2.25$. Interestingly, the diagonal and first order approximations maintain the same level of performance with a slight improvement in the first-order while the simple diagonal fails and deviates from other approximations for both the energy and linewidth in Fig. 3.9(f,i,l).

We observe, in particular, that the diagonal approximation works in the same way for nanoparticles of different shapes and materials. Furthermore, we note that not only does the diagonal approximation predict the slope but also the curvature using only a single mode, computed once either analytically or numerically. On the other hand, utilising any of Maxwell's solvers to replicate the sensing curve, as in Fig. 3.8(a,b) for example, typically requires iterative calculations and optimisation of the computational parameters, such as the initial guess or PML thickness for each data point. Insufficient calculations of the data points may result in confusion between the desired mode and higher-order modes, PML modes, or adjacent modes if they are around (a very close mode appears in the spectrum of the dolmen example [77], for instance). Additionally, a single data point for a simple model, such as the sphere or the bow-tie in Fig. 3.8 requires approximately one to two minutes. Any increase in the complexity of the geometry or in the dimensions would significantly add to the computational time. The computational time for each data point also depends on the number of computed modes, level of tolerance in the eigenmode solver, and number of poles in the Drude-Lorentz model. Hence, computing the basis mode only once and employing it in the diagonal RSE produces the sensing curve reliably and reduces computational time substantially.

To develop a clear understanding of the accuracy of the diagonal approximation, a more comprehensive study may be needed. Our present understanding suggests that the examined modes are more isolated from other modes in the complex plane of the wavenumber. We show in Sec. 3.2 when the modes are more adjacent to each other, the

diagonal approximation may not produce optimal results.

To evaluate the matrix elements of the perturbation for the resonant states in these examples, the resonant states calculated numerically have to be normalized correctly. Instead of calculating the normalization constants explicitly, we exploited the accuracy of the diagonal approximation to calculate the overlap integrals of the normalized fields from known wavenumbers. We elaborate on this method in Sec. 3.1.3.

3.1.3 Normalization and matrix elements for resonant states calculated numerically

To apply the diagonal approximation or the first-order to a numerically calculated basis RS, we need to evaluate the matrix element of the perturbation, given by

$$V_{nm}(k) = \int \vec{\mathbb{F}}_n(\mathbf{r}) \cdot \Delta\hat{\mathbb{P}}(k, \mathbf{r})\vec{\mathbb{F}}_m(\mathbf{r})d\mathbf{r}\,, \tag{3.1}$$

for $n = m$, which is proportional to an integral over the system volume of the square of the electric and/or magnetics fields. Both have to be correctly normalized, which also involves calculating volume and surface integrals of the field squared, according to [16]. Numerical evaluations of the analytical form of the normalization integral, however, may generate significant inaccuracies due to the evaluation of the derivatives in the surface term, which introduces an error even for a simple spherically symmetric system, such as the sphere [9]. Such inaccuracy grows with more complex geometries due to field uncertainty around the edges of such geometries. Alternatively, one could employ the PML normalization introduced in [10], which requires an optimization of the PML parameters as discussed in Sec. 1.3.3. We therefore deploy the high accuracy of the diagonal approximation to introduce a practical method for evaluating these integrals. In this method, the problem is reversed and instead of calculating the perturbed modes from the diagonal approximation, we use the numerical values of the unperturbed mode and a slightly perturbed mode in the diagonal approximation to solve for the overlap integral in Eq. (3.1). For a system consisting of more than one material, additional

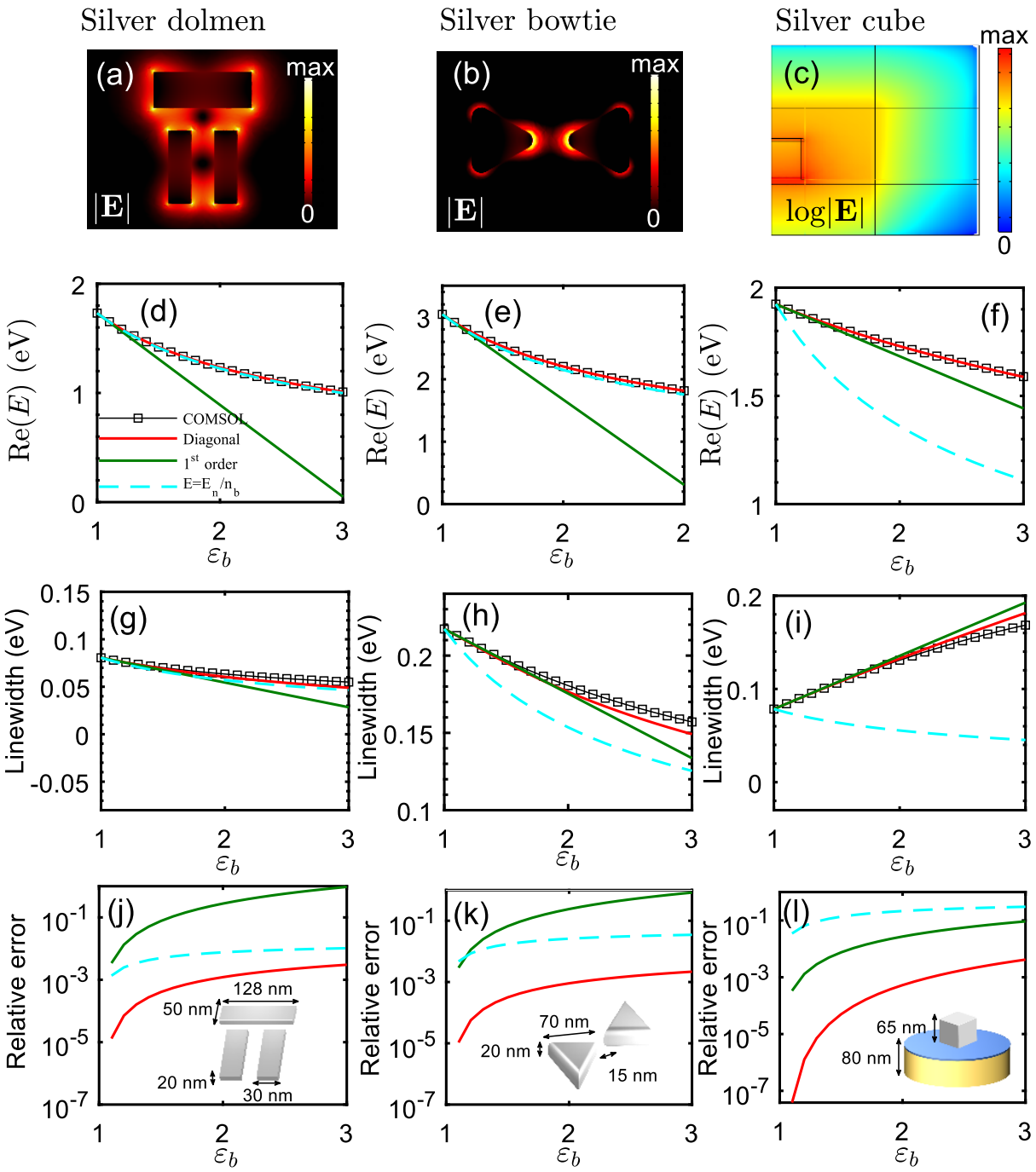

Figure 3.9. Electric field of the unperturbed mode of (a) silver dolmen, (b) silver bow-tie and (c) silver cube on a gold substrate in vacuum. (d,e,f) Energy and (g,h,i) linewidth of the mode of, respectively, silver dolmen, silver bow-tie, and cube resonators calculated using COMSOL (thin lines with squares), the diagonal (red line), first order (green line) and the simple approximation $E = E_n/n_b$ (dashed cyan line). (j,k,l) Error of each approximation relative to COMSOL, with insets showing the structure of the resonator in each case.

perturbed modes should be calculated numerically to construct a system of linear equations to solve for the unknown integrals. To illustrate the idea, let us consider for simplicity a non-magnetic, non-chiral but dispersive system which can be split into J pieces, each piece described by a homogeneous isotropic permittivity $\varepsilon_j(k)$. Then the diagonal approximation can be written as

$$1-\chi_\nu=\sum_{j=1}^{J} I_j\left[(\chi_\nu-1)\Delta\varepsilon_j(\infty)+\Delta\varepsilon_j(k_n)\right], \tag{3.2}$$

where

$$I_j=\int_{\mathcal{V}_j}\mathbf{E}_n^2(\mathbf{r})d\mathbf{r} \tag{3.3}$$

is the integral of the square of the electric field of the unperturbed resonant state (with the wave number k_n) over the volume $\mathcal{V}_j$ of the j-th part of the system,

$$\chi_\nu=\frac{k_\nu}{\Gamma k_n}, \tag{3.4}$$

and

$$\Delta\varepsilon_j(k)=\alpha^2\varepsilon_j(\Gamma k)-\varepsilon_j(k). \tag{3.5}$$

The unknown J integrals I_j can then be determined from solving J linear simultaneous equations, for which one can provide J different values of the perturbed wave number k_ν and one unperturbed wave number k_n, in this way performing $J+1$ calculations for different values of the surrounding permittivity ε_b. After all I_j are determined, stronger perturbations of the environment are accurately calculated via Eq. (3.2).

We verified this approach on an exactly solvable system, a silver nanosphere of radius $R=40\,\text{nm}$, located in vacuum. The Drude parameters of the silver sphere were taken as those for the silver bow-tie example ($\varepsilon_\infty=1$, $\hbar c\sigma=4157\,\text{eV}$, and $\hbar c\gamma=0.018\,\text{eV}$). To apply the proposed method, we calculated numerically the surface plasmon mode for the sphere in vacuum, as a basis mode, using the same freeware (PML thickness is 80 nm and mesh minimum element size is 6.7 nm [53, 75]). We also calculated numerically a slightly perturbed mode by a small deviations of ε_b from ε_{b_0}, i.e., 0.005%, and used the calculated modes in Eq. (3.2) to solve for the overlap

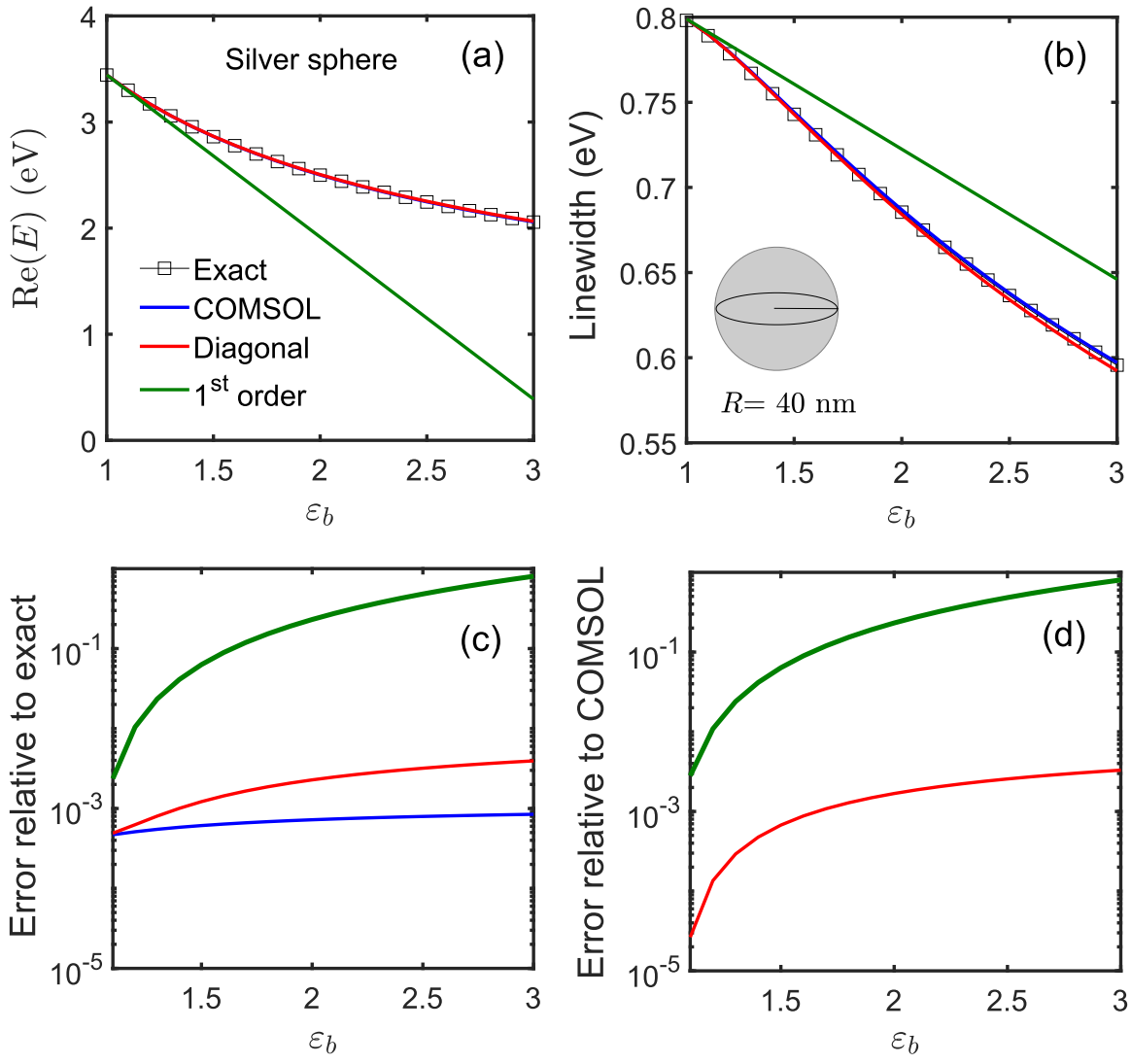

Figure 3.10. Resonance energy ReE (a) and linewidth (-2Im(E)) (b) calculated by using the exact analytic secular equation (squares), COMSOL (blue line), diagonal RSE (red line), and first-order approximation (green line) for the $l = 1$ TM fundamental surface plasmon mode of a silver sphere of $R = 40$ nm for varying permittivity of the surrounding medium ε_b, with the error of each method shown relative (c) to the exact and (d) to the COMSOL data. (c) also includes the COMSOL error relative to the exact solution (blue line).

integral I_1. We used then the calculated integral I_1 and the numerically calculated basis mode in the diagonal approximation in Eq. (3.2) and in the first order approximation to find the perturbed modes due to bigger perturbations in the surrounding medium. Now, we compare the accuracy of these perturbed modes, calculated by the diagonal approximation to the modes calculated entirely by COMSOL and to the exact solution

calculated by the secular equation for TM polarization and $l = 1$. Figure 3.10(a,b) show both the exact and COMSOL calculations of the energy and linewidth of the localized surface plasmon mode of the silver sphere as functions of the permittivity of the surrounding medium ε_b, along with the diagonal and first-order approximations based on the suggested method. We also show in Fig. 3.10(c,d) the error of both approximations relative, respectively, to the exact solution and to the COMSOL data. The accuracy of the diagonal approximation reflects the accurate evaluation of the overlap integral I_1 in the matrix element by the proposed method.

The above method also resulted in accurate evaluation of the matrix elements of the perturbation as demonstrated by examples of arbitrary shapes in Sec. 3.1.2. For the cube on a substrate, the method was implemented by including the system and its substrate in the effective system and mapping the external perturbation into the whole configuration, consisting of the system and the substrate. Most interestingly, despite the inhomogeneity introduced by the infinite substrate in this example, which cannot be treated by the RSE, the matrix elements produced by this method were also accurately evaluated as demonstrated in Fig. 3.9(f,i,l). Although we do not have a rigorous explanation for the substrate case, employing such an inverse approach, where the overlap integral is determined from a finite change in the resonant state wavenumber, might suggest a form of regularization for the overlap integral over the infinite volume occupied by the substrate. Evaluating the overlap integral using the proposed approach overcomes the difficulty of normalizing resonant states of complicated shapes since it relies only on determining of $J + 1$ eigen wavenumbers, which can be obtained numerically. We finally note that calculating the wavenumbers numerically for small changes in the environment does not necessarily require repetitive optimization of the simulation parameters, such as changing the initial guess or the PML thickness.

3.2 Microresonators

Another experimentally relevant example we show here is high-angular momentum ($l = 450$) whispering gallery modes of a silica micro-sphere of radius $R = 39.5\,\mu$m [79,

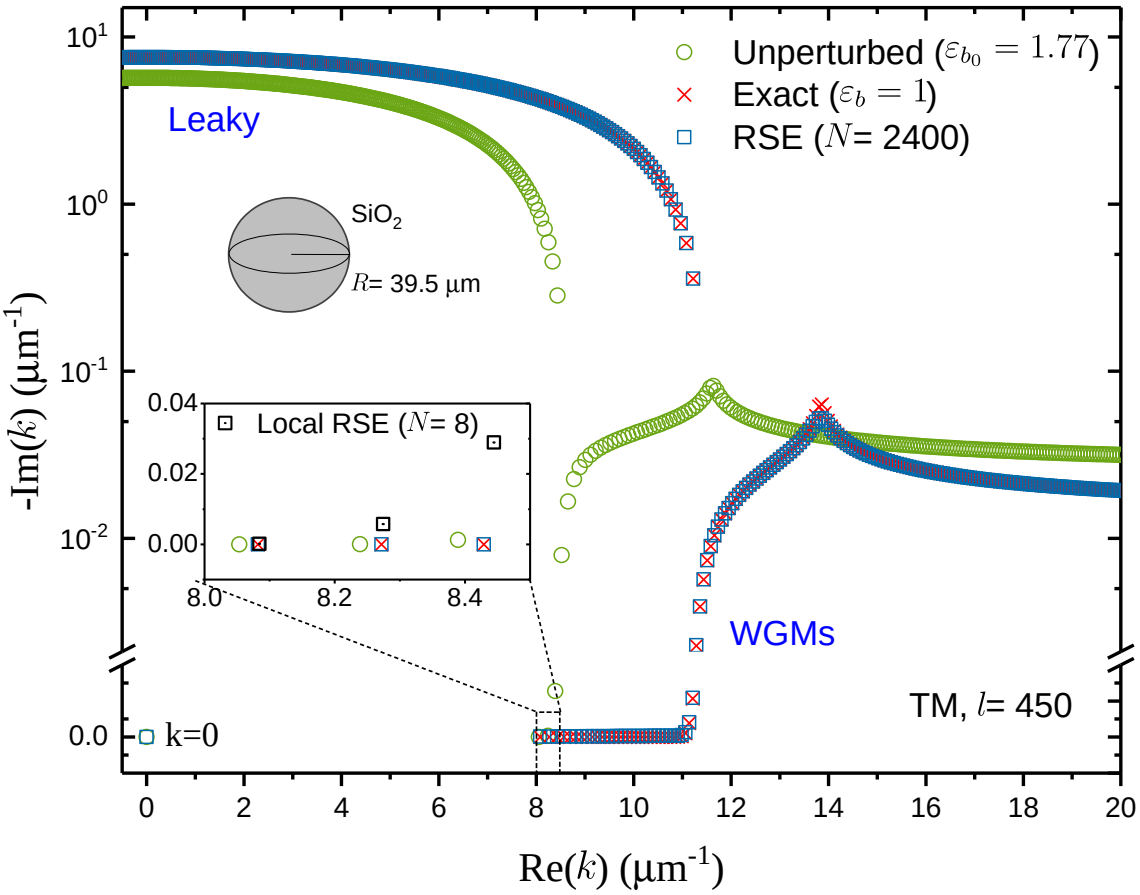

Figure 3.11. Complex wave numbers k of the resonant states of a silica microsphere of radius $R = 39.5\,\mu$m in water with $\varepsilon_{b_0} = 1.77$ (green open circles) and in vacuum, calculated with the RSE (blue squares) and analytically (red crosses), for TM polarization and $l = 450$. Inset: Local RSE (black squares with dots) with only whispering gallery modes included in the basis.

80]. For silica, the permittivity was calculated using Sellmeier formula [80] at wavelength $\lambda = 780\,$nm, giving $\varepsilon = 2.114$. Figure 3.11 shows the spectra of the resonant states of the silica sphere in water ($\varepsilon_{b_0} = 1.77$) and in vacuum ($\varepsilon_b = 1$) playing the role of, respectively, the basis and perturbed systems. The perturbed system has a large number of whispering gallery modes which are all well reproduced by the RSE-based theory even though the basis system has only four pairs of them.

Figure 3.12 show the real part of wavenumber of the fundamental whispering gallery mode and the relative error for its calculation by the RSE, diagonal, and first-order approximation as functions of the permittivity ε_b of the surrounding material changing

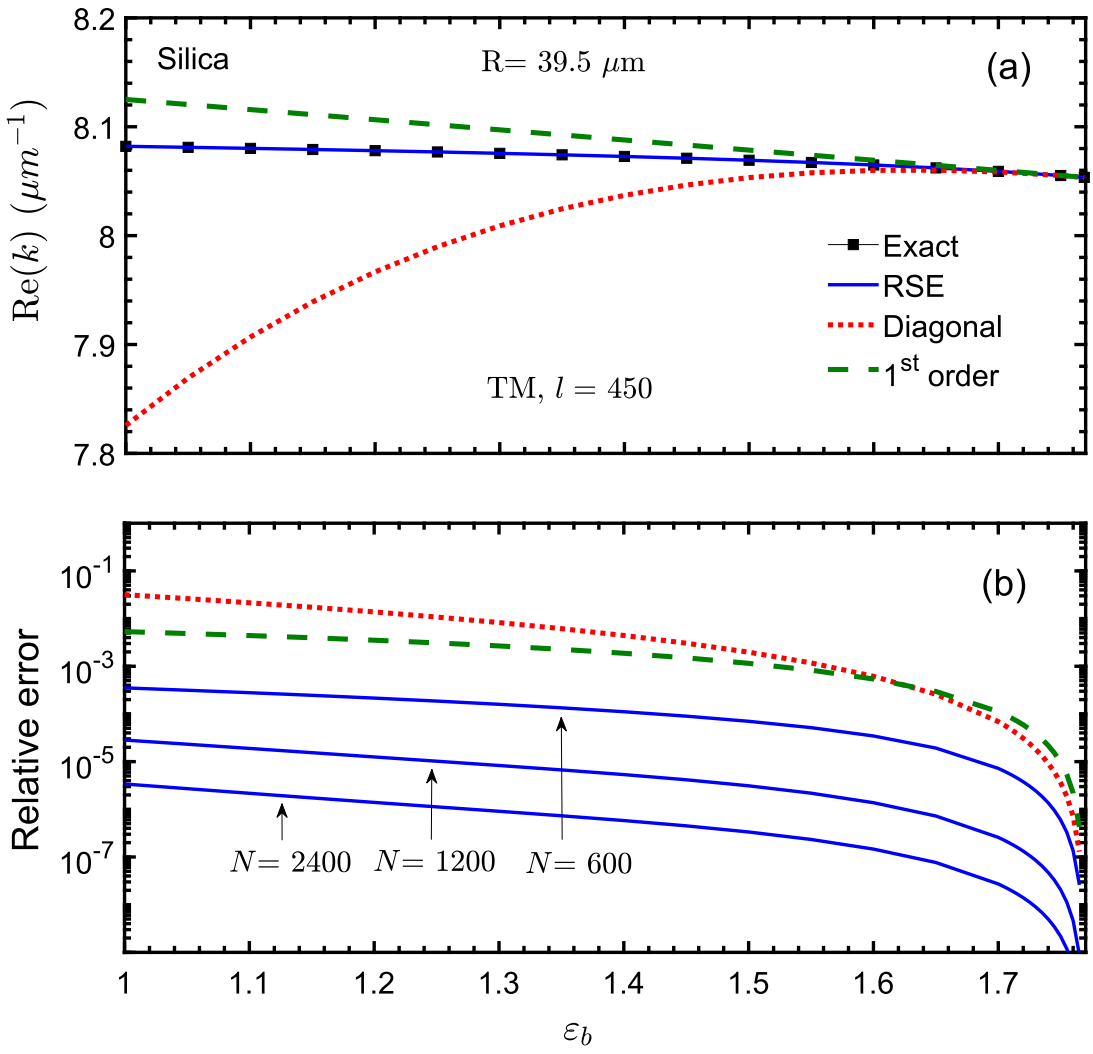

Figure 3.12. (a) Real part and (b) relative error of the wave number k of the $l = 450$ TM fundamental whispering gallery mode of a silica microsphere as functions of the background permittivity ε_b, calculated exactly (black line with squares), using the full RSE with different basis sizes N as given, using the diagonal ($N = 1$) RSE (dotted red lines), and first-order (green lines) approximations.

between water ($\varepsilon_b = \varepsilon_{b_0} = 1.77$, unperturbed) and vacuum ($\varepsilon_b = 1$). The diagonal and first-order approximations fail in this case, as it is clear from Fig. 3.12(a) and the error in Fig. 3.12(b). The relative error shown in Fig. 3.12(b) demonstrates a quick convergence of the RSE to the exact solution. In fact, the relative error scales with the basis size N approximately as $1/N^3$, which is the same behaviour as in all other systems treated by the RSE. However, the errors in Fig. 3.12(b) have larger magnitude

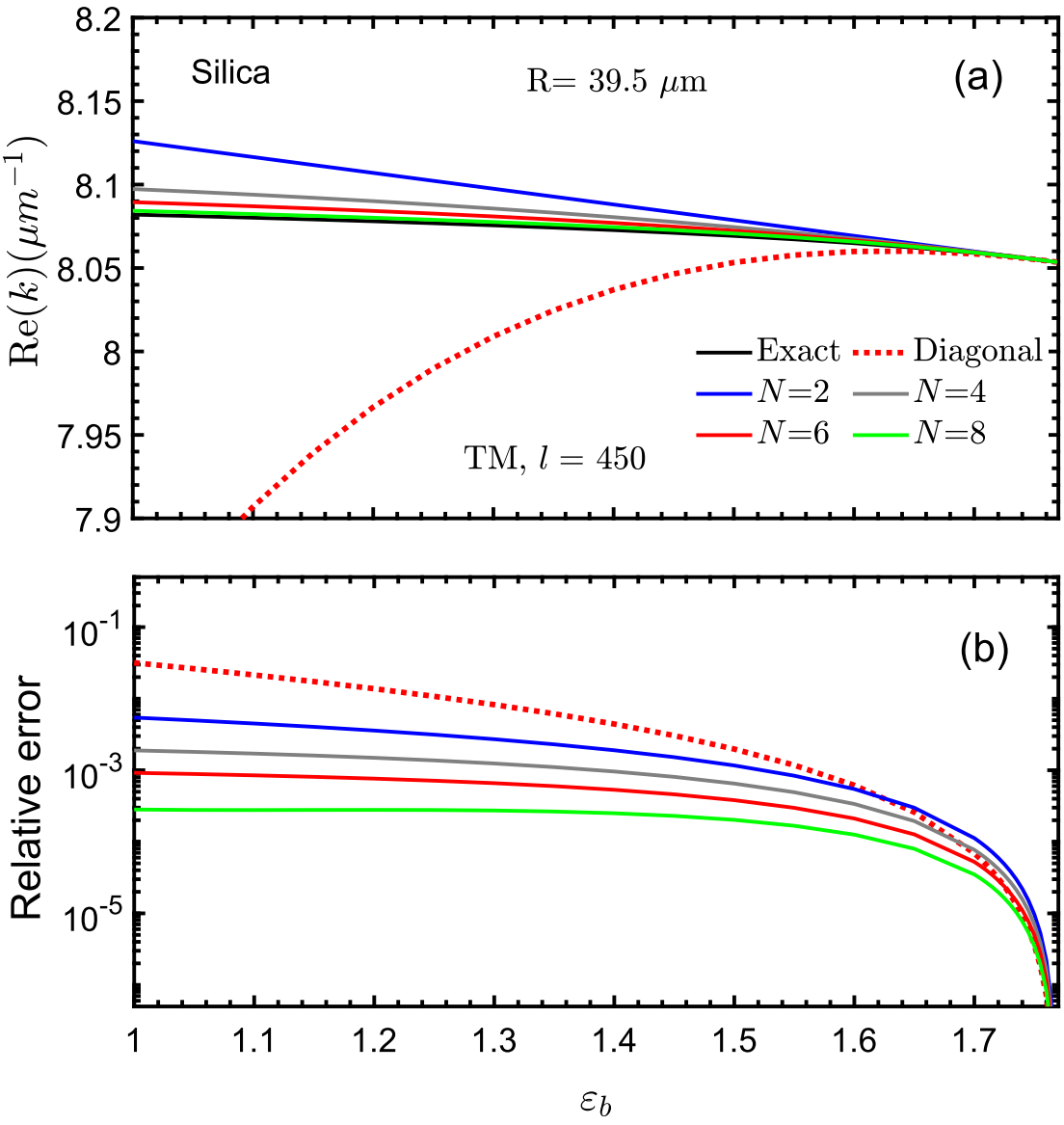

Figure 3.13. As Fig. 3.12 but with the exact solution (black line) compared with diagonal RSE ($N = 1$, dotted red lines), and local RSE with $N = 2$ (blue lines), $N = 4$ (gray lines), $N = 6$ (red solid lines), and $N = 8$ (green lines).

for the same basis size compared to other examples. To reach relative error of 10^{-5} or below, one needs to keep $N = 2400$ states in the basis. This may be attributed to the very low permittivity contrast in the unperturbed system which makes the resonances described by the basis resonant states less pronounced. Decreasing ε_b, this permittivity contrast rapidly increases which in turn makes the basis and perturbed

states very different. This would also contribute in explaining why the single-mode (i.e. diagonal and first-order) approximations so poorly reproduce the exact result, as we see in Fig. 3.12.

The poor quality of the approximations presented in Fig. 3.12 can be significantly improved by using the local RSE, introduced in [14]. In the local RSE, only the resonant states that are close in frequency to the state of interest or have the biggest overlap matrix elements with this state are kept in the basis. This was controlled in [14] by introducing weights $W = |V_{nm}^2/(k_n - k_m)|$ proportional to the second-order correction to the inverse wave number, in accordance with the Rayleigh-Schrödinger perturbation theory [8]. These weights quantify the effective contribution of the basis states (m) to the perturbed state of interest (n). The criterion for keeping state m in the basis is that the weight W is larger than a chosen threshold. While this method normally works very well, in the present case the above criterion would require to take into account many leaky and Fabry-Perot modes which in reality do not help much to reduce the error. We have therefore modified this criterion by simply taking into account only the whispering gallery modes of the basis system, i.e. all the resonant states with $|k| < \frac{l}{n_{b_0} R}$, in accordance with the condition for total internal reflection [37].

We reproduced Fig. 3.12(a,b) but for the real part of the wavenumber of the fundamental whispering gallery mode calculated by the local whispering gallery modes as shown in Fig. 3.13. The results are demonstrated for one, two, three, and all four pairs of whispering gallery modes positioned symmetrically with respect to the imaginary k-axis ($N = 2$, 4, 6, and 8, respectively). It shows a vast improvement compared to the diagonal approximation ($N = 1$). Interestingly, adding to the basis only the conjugated mode on the other side of the spectrum ($N = 2$) already improves the result significantly. Taking all four whispering gallery modes and their counterparts ($N = 8$) provides nearly a full visual agreement with the exact solution, seen in Fig. 3.13(a) and in the inset to Fig. 3.11. Adding to this basis more modes increases the error, unless a really large number of basis states is included.

3.3 Summary

We have implemented the RSE-based method and its approximations, namely the simple diagonal and diagonal approximations, with the extracted first-order approximation taken into account. The objective of this application was to calculate perturbed modes caused by changes in the surrounding medium. Systems that are experimentally relevant have been taken into consideration, including dielectric microresonators and plasmonic nanoparticles. We have compared the accuracy of our results to exact values obtained analytically or numerically.

For a nanosphere, the error relative to the exact values of the RSE-based theory with a basis size N scales as $1/N^3$, as in the standard RSE. By replacing the pole resonant states (pRSsI) with the perturbation-independent pole resonant states (pRSs II) in the basis of the infinitesimal RSE, the $1/N^3$ convergence to the exact solution is almost maintained. Both the diagonal approximations exhibited accuracy beyond the first order. The diagonal approximation demonstrates a reduction of at least one order of magnitude when compared to the simple diagonal. We have employed such an accuracy to propose a method for finding the integral of the normalized fields. This method was used in our calculations of both the diagonal and first-order approximations for the arbitrary-shaped systems. All approximations present qualitatively a similar accuracy across a broad class of plasmonic nanoparticles described by Drude model, including an example of a system on a substrate.

The diagonal and first-order approximations fail to accurately predict the change of the WGM of our micro-resonator example. They were replaced by a local basis of whispering gallery modes, achieving considerable accuracy with only a few whispering gallery modes in the RSE basis.

In the following chapter, we will attempt to develop an alternative basis based on regularization to directly treat changes in the surrounding medium of the system, without a transformation as an intermediate step.

Chapter 4

Regularization-based approaches

In this chapter, we introduce an alternative approach to the calculation of perturbations of the resonant states of an optical system due to changes in the surrounding medium [71]. This approach is based on regularization of the wavefunctions of resonant states.

To regularize them, Zeldovich proposed to multiply all the wavefunctions of the resonant states with a Gaussian factor $e^{-\alpha r^2}$ and take the limit $\alpha \to +0$ after integration [81]. This allows one to extend the integration in the volume term of the analytic normalization to the entire space and drop the vanishing surface term. This yields exactly the same normalization as the analytic rigorous normalization, as has been recently demonstrated in [57] for the resonant states of a homogeneous dielectric sphere. Alternatives to this regularization are the complex coordinate transformation [54] and use of PML [10, 51], ideally leading to the same result for the resonant state's norm.

Applying any valid regularization to the resonant state's field, such as a Gaussian regularization introduced by Zeldovich [81], or using the PML [10], one can see that both the resonant state's normalization and orthogonality then take the form of a scalar product, similar to those of a Hermitian system [75]. However, a completeness of such regularized resonant states in the full space is not achievable, as demonstrated in Sec. 4.2.

The idea of regularizing the resonant states allows us to develop an alternative, valuable approximation in Sec. 4.3, similar to the full diagonal approximation, but it is not as accurate as the diagonal approximation, as we demonstrate. We also prove in Sec. 4.4 that the developed regularized diagonal approximation is equivalent to the perturbation theory [26] in the first order.

4.1 Orthonormality and Poynting's theorem for regularized resonant states

Let us start by assuming isotropic response of the environment with or without perturbation. We also assume, for simplicity of the derivation, a non-chiral environment ($\kappa_{b_0} = \kappa_b = 0$) surrounding an arbitrary anisotropic system, i.e., $\hat{\boldsymbol{\zeta}} = \hat{\boldsymbol{\xi}} = \hat{\mathbf{0}}$. The general analytic normalization of the (unperturbed) resonant states has the form [16]:

$$\int_{\mathcal{V}} \vec{\mathbb{F}}_n(\mathbf{r}) \cdot \left[k\hat{\mathbb{P}}_0(k,\mathbf{r})\right]' \vec{\mathbb{F}}_n(\mathbf{r}) d\mathbf{r} + \frac{i}{k_n} \oint_{\mathcal{S}} (\mathbf{E}_n \times \mathbf{H}'_n - \mathbf{E}'_n \times \mathbf{H}_n) \cdot d\mathbf{S} = 1\,, \tag{4.1}$$

using the 6×6 compact form, where $\mathcal{V}$ is an arbitrary volume including all inhomogeneities of the generalized permittivity $\hat{\mathbb{P}}_0(k,\mathbf{r})$, $\mathcal{S}$ is the outer boundary of $\mathcal{V}$, the prime means the derivative with respect to k taken at $k = k_n$, and $\mathbf{E}'_n$ and $\mathbf{H}'_n$ are the derivatives of an analytic continuation of the resonant states' fields in the complex k-plane.

The orthogonality of the resonant states has a similar form [13, 61]:

$$\int_{\mathcal{V}} \vec{\mathbb{F}}_n(\mathbf{r}) \cdot \left[k_n\hat{\mathbb{P}}_0(k_n,\mathbf{r}) - k_m\hat{\mathbb{P}}_0(k_m,\mathbf{r})\right] \vec{\mathbb{F}}_m(\mathbf{r}) d\mathbf{r} + i \oint_{\mathcal{S}} (\mathbf{E}_m \times \mathbf{H}_n - \mathbf{E}_n \times \mathbf{H}_m) \cdot d\mathbf{S} = 0 \tag{4.2}$$

for $n \neq m$.

Poynting's theorem for the fields of the resonant states in reciprocal systems takes the following form [16]:

$$\int_{\mathcal{V}} \left[\mathbf{E}_n(\mathbf{r}) \cdot k_n\hat{\boldsymbol{\varepsilon}}(k_n,\mathbf{r})\mathbf{E}_m(\mathbf{r}) + \mathbf{H}_n(\mathbf{r}) \cdot k_m\hat{\boldsymbol{\mu}}(k_m,\mathbf{r})\mathbf{H}_m(\mathbf{r})\right] d\mathbf{r} + i \oint_{\mathcal{S}} \mathbf{E}_m \times \mathbf{H}_n \cdot d\mathbf{S} = 0\,, \tag{4.3}$$

valid for both cases of $n \neq m$ and $n = m$. It is easy to see that subtracting from Eq. (4.3) the same equation in which n and m are swapped results in the resonant state's orthogonality Eq. (4.2).

For regularized resonant states, the volume integration in Eqs. (4.1), (4.2), and (4.3) can be extended to the *entire space*. Then all the surface integrals vanish since the regularized fields tend to zero at infinity. This results in the following form of the normalization condition

$$\int \vec{\mathbb{F}}_n(\mathbf{r}) \cdot \left[k\hat{\mathbb{P}}_0(k,\mathbf{r})\right]' \vec{\mathbb{F}}_n(\mathbf{r}) d\mathbf{r} = 1\,, \tag{4.4}$$

orthogonality

$$k_n \int \vec{\mathbb{F}}_n(\mathbf{r}) \cdot \hat{\mathbb{P}}_0(k_n,\mathbf{r}) \vec{\mathbb{F}}_m(\mathbf{r}) d\mathbf{r} = k_m \int \vec{\mathbb{F}}_n(\mathbf{r}) \cdot \hat{\mathbb{P}}_0(k_m,\mathbf{r}) \vec{\mathbb{F}}_m(\mathbf{r}) d\mathbf{r}\,, \tag{4.5}$$

and Poynting's theorem

$$k_n \int \mathbf{E}_n(\mathbf{r}) \cdot \hat{\boldsymbol{\varepsilon}}(k_n,\mathbf{r}) \mathbf{E}_m(\mathbf{r}) d\mathbf{r} = -k_m \int \mathbf{H}_n(\mathbf{r}) \cdot \hat{\boldsymbol{\mu}}(k_m,\mathbf{r}) \mathbf{H}_m(\mathbf{r}) d\mathbf{r}\,, \tag{4.6}$$

where the integration of the regularized fields is performed over the entire space. Note that a proper regularization of the wavefunctions of the resonant states not only makes the integrals in Eqs. (4.4), (4.5), and (4.6) finite but also the field normalization converging to the exact general normalization given by Eq. (4.1).

For non-dispersive systems and non-dispersive surrounding materials, the orthonormality given by Eqs. (4.4) and (4.5) simplifies to

$$\int \vec{\mathbb{F}}_n(\mathbf{r}) \cdot \hat{\mathbb{P}}_0(\mathbf{r}) \vec{\mathbb{F}}_m(\mathbf{r}) d\mathbf{r} = \delta_{nm}\,, \tag{4.7}$$

where δ_{nm} is the Kronecker delta function. Moreover, with the help of Poynting's theorem Eq. (4.6), the electric and magnetic fields can be separated which results in two

equivalent expressions for the resonant state's orthonormality:

$$2\int \mathbf{E}_n(\mathbf{r})\cdot\hat{\boldsymbol{\varepsilon}}(\mathbf{r})\mathbf{E}_m(\mathbf{r})d\mathbf{r}=\delta_{nm}\,,\qquad 2\int \mathbf{H}_n(\mathbf{r})\cdot\hat{\boldsymbol{\mu}}(\mathbf{r})\mathbf{H}_m(\mathbf{r})d\mathbf{r}=-\delta_{nm}\,. \tag{4.8}$$

Now, going back to dispersive systems and combining the orthonormality Eqs. (4.4) and (4.5) and Poynting's theorem Eq. (4.6), one can express the integrals over the infinite exterior volume,

$$W^E_{nm}=\int_{\mathcal{V}_{\rm out}}\mathbf{E}_n\cdot\mathbf{E}_m d\mathbf{r}\,,\qquad W^H_{nm}=\int_{\mathcal{V}_{\rm out}}\mathbf{H}_n\cdot\mathbf{H}_m d\mathbf{r}\,, \tag{4.9}$$

in terms of those over the system volume $\mathcal{V}_{in}$. In fact, using the integrals defined over the system volume $\mathcal{V}_{\rm in}$,

$$I^E_{nm}=\int_{\mathcal{V}_{\rm in}}\mathbf{E}_n\cdot\hat{\boldsymbol{\varepsilon}}(k_n,\mathbf{r})\mathbf{E}_m d\mathbf{r},\qquad J^E_n=k_n\int_{\mathcal{V}_{\rm in}}\mathbf{E}_n\cdot\hat{\boldsymbol{\varepsilon}}'(k_n,\mathbf{r})\mathbf{E}_n d\mathbf{r}\,, \tag{4.10}$$

$$I^H_{nm}=\int_{\mathcal{V}_{\rm in}}\mathbf{H}_n\cdot\hat{\boldsymbol{\mu}}(k_n,\mathbf{r})\mathbf{H}_m d\mathbf{r},\qquad J^H_n=k_n\int_{\mathcal{V}_{\rm in}}\mathbf{H}_n\cdot\hat{\boldsymbol{\mu}}'(k_n,\mathbf{r})\mathbf{H}_n d\mathbf{r}\,, \tag{4.11}$$

as well as the integral given by Eq. (4.9), the resonant state's normalization Eq. (4.4) can be written as

$$A_n+[k\varepsilon_{b_0}(k)]'W^E_{nn}-[k\mu_{b_0}(k)]'W^H_{nn}=1\,, \tag{4.12}$$

assuming frequency dispersion in the surrounding medium, where again the frequency derivatives are taken at $k=k_n$, and A_n is defined as

$$A_n=I^E_{nn}+J^E_n-I^H_{nn}-J^H_n\,. \tag{4.13}$$

The Poynting theorem Eq. (4.6) in turns takes the form

$$k_n[I^E_{nm}+\varepsilon_{b_0}(k_n)W^E_{nm}]=-k_m[I^H_{mn}+\mu_{b_0}(k_m)W^H_{mn}]\,. \tag{4.14}$$

Using Eq. (4.14) for $n=m$ and combining it with the normalization Eq. (4.12) we

obtain

$$W^E_{nn} = \frac{(1-A_n)\mu_{b_0} - B_n(k\mu_{b_0})'}{(k\varepsilon_{b_0})'\mu_{b_0} + (k\mu_{b_0})'\varepsilon_{b_0}}, \tag{4.15}$$

$$W^H_{nn} = \frac{-(1-A_n)\varepsilon_{b_0} - B_n(k\varepsilon_{b_0})'}{(k\varepsilon_{b_0})'\mu_{b_0} + (k\mu_{b_0})'\varepsilon_{b_0}}, \tag{4.16}$$

where the arguments of $\varepsilon_{b_0}(k)$ and $\mu_{b_0}(k)$ are omitted for brevity, and B_n is defined as

$$B_n = I^E_{nn} + I^H_{nn}. \tag{4.17}$$

For $n \neq m$, we write the orthogonality Eq. (4.5) as

$$k_n[I^E_{nm} - I^H_{nm} + \varepsilon_{b_0}(k_n)W^E_{nm} - \mu_{b_0}(k_n)W^H_{nm}] = k_m[I^E_{mn} - I^H_{mn} + \varepsilon_{b_0}(k_m)W^E_{mn} - \mu_{b_0}(k_m)W^H_{mn}]. \tag{4.18}$$

Using the symmetry $W^{E,H}_{nm} = W^{E,H}_{mn}$ (which does not hold in general for other integrals, i.e., $I^{E,H}_{nm} \neq I^{E,H}_{mn}$), we obtain

$$W^E_{nm} = -\frac{k_n^2\mu_{b_0}(k_n)I^E_{nm} - k_m^2\mu_{b_0}(k_m)I^E_{mn} + k_nk_m[\mu_{b_0}(k_n)I^H_{mn} - \mu_{b_0}(k_m)I^H_{nm}]}{k_n^2\varepsilon_{b_0}(k_n)\mu_{b_0}(k_n) - k_m^2\varepsilon_{b_0}(k_m)\mu_{b_0}(k_m)}, \tag{4.19}$$

$$W^H_{nm} = -\frac{k_n^2\varepsilon_{b_0}(k_n)I^H_{nm} - k_m^2\varepsilon_{b_0}(k_m)I^H_{mn} + k_nk_m[\varepsilon_{b_0}(k_n)I^E_{mn} - \varepsilon_{b_0}(k_m)I^E_{nm}]}{k_n^2\varepsilon_{b_0}(k_n)\mu_{b_0}(k_n) - k_m^2\varepsilon_{b_0}(k_m)\mu_{b_0}(k_m)}. \tag{4.20}$$

Finally, for non-dispersive permittivity and permeability, the orthonormality Eq. (4.8) can be written as

$$I^E_{nm} + \varepsilon_{b_0}W^E_{nm} = \frac{1}{2}\delta_{nm}, \qquad I^H_{nm} + \mu_{b_0}W^H_{nm} = -\frac{1}{2}\delta_{nm}, \tag{4.21}$$

which can also be used as a link between the integrals $W^{E,H}_{nm}$ of the electric and magnetic fields over the infinite volume $\mathcal{V}_{\text{out}}$ of the space surrounding the system and the integrals $I^{E,H}_{nm}$ over the finite volume $\mathcal{V}_{\text{in}}$ containing the system. Clearly, Eq. (4.21) is a special (non-dispersive) case of Eqs. (4.15) and (4.16) for $n = m$ and of Eqs. (4.19) and (4.20) for $n \neq m$.

4.2 Regularized RSE

We here hypothesise that the regularized resonant states presented above are complete not only within the system volume (as the resonant states themselves) but also outside it. Below we test this hypothesis by using the regularized states as a basis for expansion of perturbed regularized resonant states in the region outside the system. We also consider for simplicity the case of both the system and the medium being non-dispersive. Without dispersion, the regularized resonant states satisfy the orthonormality relation Eq. (4.7).

Assuming the regularized resonant states are complete in the entire space, let us expand the fields of a perturbed (regularized) resonant state as

$$\vec{\mathbb{F}}_\nu(\mathbf{r}) = \sum_n \bar{c}_n \vec{\mathbb{F}}_n(\mathbf{r})\,. \tag{4.22}$$

Using Eq. (4.22) and Maxwell's equations for the basis resonant states,

$$\left[k_n \hat{\mathbb{P}}_0(\mathbf{r}) - \hat{\mathbb{D}}(\mathbf{r})\right] \vec{\mathbb{F}}_n(\mathbf{r}) = \vec{\mathbb{0}}\,, \tag{4.23}$$

we solve the perturbed Maxwell's equations

$$\left[k_\nu \hat{\mathbb{P}}_0(\mathbf{r}) + k_\nu \Delta\hat{\mathbb{P}}(\mathbf{r}) - \hat{\mathbb{D}}(\mathbf{r})\right] \vec{\mathbb{F}}_\nu(\mathbf{r}) = \vec{\mathbb{0}}\,, \tag{4.24}$$

where k_ν is the wavenumber of the perturbed state ν and $\Delta\hat{\mathbb{P}}(\mathbf{r})$ is the perturbation of the generalized permittivity. Substituting Eq. (4.22) into Eq. (4.24) and using Eq. (4.23), we find

$$\sum_n \bar{c}_n \left[(k_\nu - k_n)\hat{\mathbb{P}}_0(\mathbf{r}) + k_\nu \Delta\hat{\mathbb{P}}(\mathbf{r})\right] \vec{\mathbb{F}}_n(\mathbf{r}) = \vec{\mathbb{0}}\,. \tag{4.25}$$

Multiplying the last equation Eq. (4.25) with $\vec{\mathbb{F}}_m(\mathbf{r})$, integrating over the entire space, and using the orthonormality Eq. (4.7), we end up with a matrix eigenvalue problem,

$$\bar{c}_n(k_\nu - k_n) + k_\nu \sum_m \bar{V}_{nm}\bar{c}_m = 0\,, \tag{4.26}$$

where

$$\bar{V}_{nm} = \int \vec{\mathbb{F}}_n(\mathbf{r}) \cdot \Delta\hat{\mathbb{P}}(\mathbf{r})\vec{\mathbb{F}}_m(\mathbf{r})d\mathbf{r} \tag{4.27}$$

are the matrix elements of the perturbation.

To verify the regularized matrix equation (4.26) we consider resonant states of TE polarization for a dielectric sphere with permittivity $\varepsilon = 4$, surrounded by vacuum ($\varepsilon_{b_0} = 1$) which is perturbed to a non-magnetic medium with permittivity $\varepsilon_b = 2$. The spectra of the unperturbed and perturbed TE modes with $l = 1$ are compared in Fig. 4.1(a). The perturbed resonant states are calculated exactly and via the regularized Eq. (4.26) truncated to $N = 400$ basis states. Figure 4.1(a) demonstrates an obvious difference between the exact and 'regularized' wavenumbers for this rather large perturbation of the medium ($\Delta\varepsilon = \varepsilon_b - \varepsilon_{b_0} = 1$). Furthermore, the relative error in Fig. 4.1(b) shown for $N = 100$, 200, and 400 clearly demonstrates that the wavenumbers calculated via Eq. (4.26) do not converge to the exact values as N increases. This is a clear evidence that Eq. (4.22) is not valid outside the system. In other words, the resonant states, even when regularized, are not complete outside the system. Interestingly, the diagonal approximation, i.e., the use of Eq. (4.26) with $n = m$ (corresponding to $N = 1$) produces a lot better result than any $N > 1$, see Fig. 4.1.

To see how the RSE-based approach works for the same example, we show in Fig. 4.2 a comparison of the RSE and exact results for the same parameters as in Fig. 4.1, demonstrating a quick convergence to the exact solution, with the relative error scaling as $1/N^3$, typical for the RSE.

The difference between the RSE equation,

$$(\tilde{k} - k_n)c_n = -\tilde{k}\sum_m V_{nm}(\infty)c_m + k_n \sum_m \left[V_{nm}(\infty) - V_{nm}(k_n)\right] c_m \,, \tag{4.28}$$

and regularized Eq. (4.26) can be clearly seen analytically, by bringing both equations to the same form. Let us first transform the matrix elements in Eq. (4.26), expressing them in terms of the field integrals over the system region. Using the perturbation

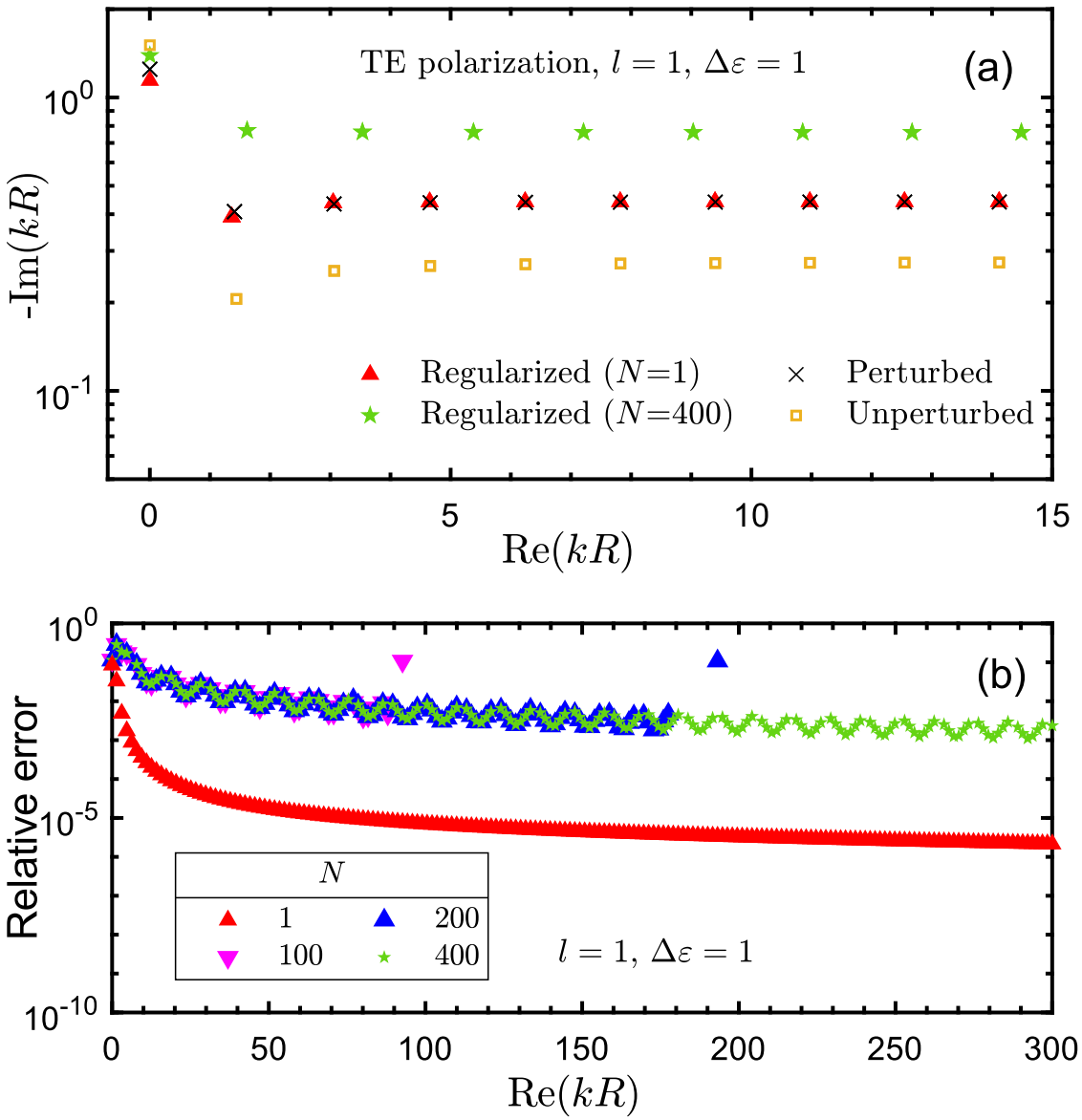

Figure 4.1. (a) Exact unperturbed (squares) and perturbed (crosses) wavenumbers of the resonant states of a dielectric sphere ($\varepsilon = 4$) in vacuum, perturbed to a non-magnetic surrounding medium with $\varepsilon_b = 2$, for TE polarization and $l = 1$. The perturbed wavenumbers are calculated either by solving the exact analytic secular equation for a sphere ($\times$) or by solving the regularized matrix equation (4.26) [equivalent to Eq. (4.30)] with the total number of basis states $N = 400$ (stars) and $N = 1$ (triangles). (b) Relative errors for the wavenumbers calculated via Eq. (4.26) with different N as given.

$\Delta\hat{\mathbb{P}}(\mathbf{r}) = \left[(\varepsilon_b - \varepsilon_{b_0})\,\hat{\mathbf{1}}; (\mu_b - \mu_{b_0})\,\hat{\mathbf{1}}\right]$ for $\mathbf{r} \in \mathcal{V}_{\text{out}}$ and $\Delta\hat{\mathbb{P}}(\mathbf{r}) = \hat{\mathbb{0}}$ for $\mathbf{r} \in \mathcal{V}_{\text{in}}$, we find

$$\bar{V}_{nm} = (\varepsilon_b - \varepsilon_{b_0}) W^E_{nm} - (\mu_b - \mu_{b_0}) W^H_{nm}\,, \tag{4.29}$$

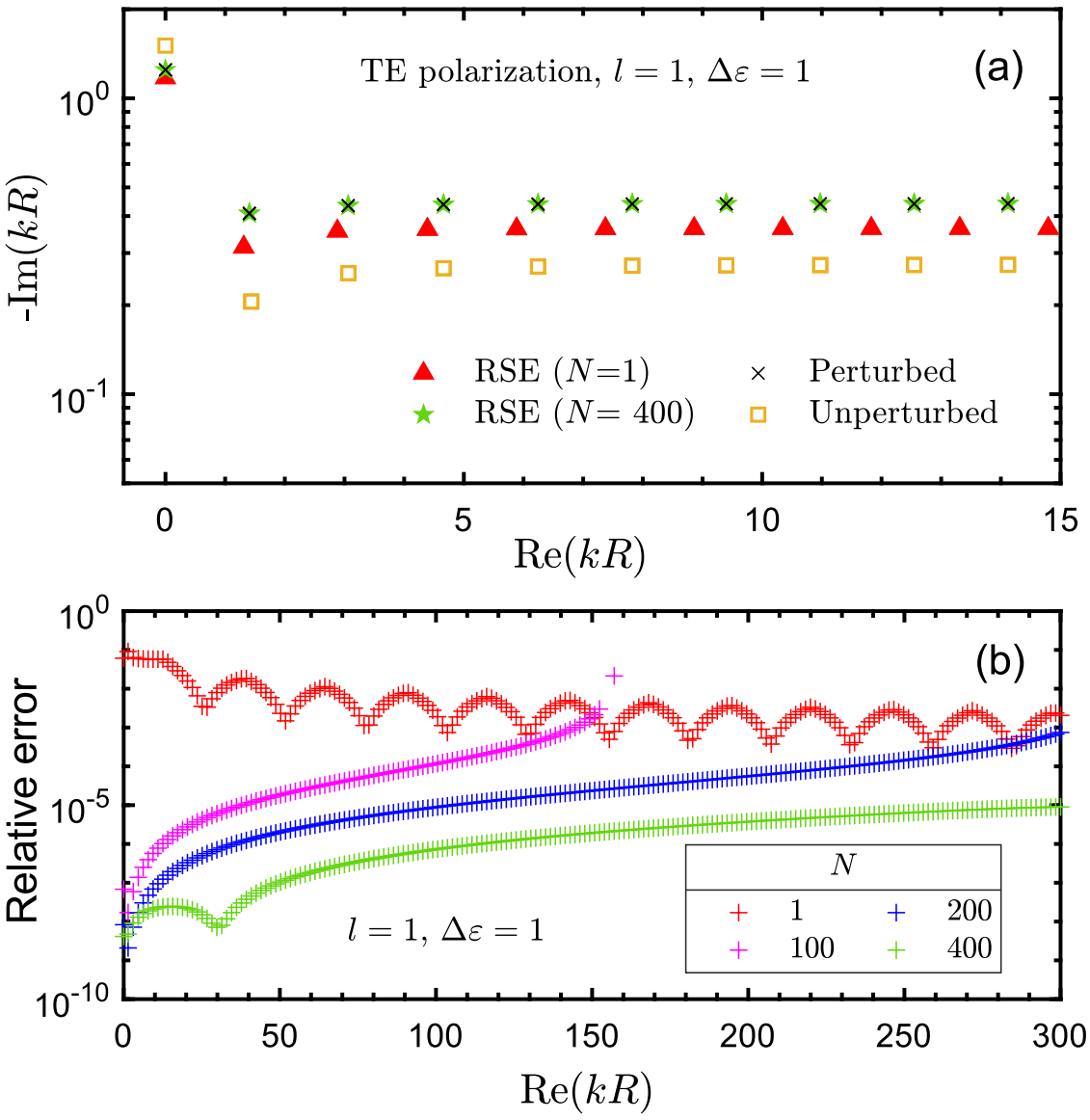

Figure 4.2. As Fig. 4.1 but with the regularized solution replaced with the solution of the RSE equation (4.28) [taking the form of Eq. (4.31) for non-dispersive systems].

where $W_{nm}^{E,H}$ are defined by Eq. (4.9). For non-dispersive permittivity and permeability, they can be expressed, using the orthonormality Eq. (4.21), in terms of the integrals $I_{nm}^{E,H}$ over the system volume, which are defined by Eqs. (4.10) and (4.11). The matrix equation (4.26) then takes the form

$$k_\nu \sum_m \left[\frac{\delta_{nm}}{2} \left(\frac{\varepsilon_b}{\varepsilon_{b_0}} + \frac{\mu_b}{\mu_{b_0}} \right) + \frac{\varepsilon_b}{\varepsilon_{b_0}} \left(\frac{\varepsilon_{b_0}}{\varepsilon_b} - 1 \right) I_{nm}^E - \frac{\mu_{b_0}}{\mu_b} \left(\frac{\mu_b}{\mu_{b_0}} - 1 \right) I_{nm}^H \right] \bar{c}_m = k_n \bar{c}_n \,. \quad (4.30)$$

On the other hand, the RSE equation (4.28) for the same non-dispersive system and an effective perturbation $\Delta\hat{\mathbb{P}}(\mathbf{r}) = [(\varepsilon_{b_0}/\varepsilon_b - 1)\,\hat{\boldsymbol{\varepsilon}}(\mathbf{r}); (\mu_{b_0}/\mu_b - 1)\,\hat{\boldsymbol{\mu}}(\mathbf{r})]$ for $\mathbf{r} \in \mathcal{V}_{\text{in}}$ and $\Delta\hat{\mathbb{P}}(\mathbf{r}) = \hat{\mathbb{0}}$ for $\mathbf{r} \in \mathcal{V}_{\text{out}}$, which describes the same changes of the surrounding material, can be written as

$$k_\nu \sum_m \sqrt{\frac{\varepsilon_b}{\varepsilon_{b_0}}\frac{\mu_b}{\mu_{b_0}}} \left[\delta_{nm} + \left(\frac{\varepsilon_{b_0}}{\varepsilon_b} - 1\right) I^E_{nm} - \left(\frac{\mu_b}{\mu_{b_0}} - 1\right) I^H_{nm}\right] c_m = k_n c_n \,, \tag{4.31}$$

by using the transformation of the perturbed wavenumber Eq. (4.32),

$$k_\nu = \Gamma\tilde{k} \,, \tag{4.32}$$

and the matrix elements of the effective perturbation,

$$V_{nm} = \left(\frac{\varepsilon_{b_0}}{\varepsilon_b} - 1\right) I^E_{nm} - \left(\frac{\mu_b}{\mu_{b_0}} - 1\right) I^H_{nm} \,. \tag{4.33}$$

There is an obvious difference between Eqs. (4.30) and (4.31), even in the diagonal approximation. However, it can be easily seen that they agree in first order, which is also observed in the numerics.

4.3 Regularized diagonal approximation

Following the success achieved by the diagonal approximation of the regularized RSE presented in the last section, we now derive a diagonal-like approximation for perturbations of the regularized resonant states caused by small changes in the surrounding medium. Here, we allow the unperturbed medium to have a frequency dispersion.

The Maxwell equations for the unperturbed resonant states are

$$\left[k_n \hat{\mathbb{P}}_0(k_n, \mathbf{r}) - \hat{\mathbb{D}}(\mathbf{r})\right] \vec{\mathbb{F}}_n(\mathbf{r}) = \vec{\mathbb{0}} \,, \tag{4.34}$$

Now, $\hat{\mathbb{P}}_0(k_n, \mathbf{r})$ includes arbitrary homogeneous isotropic and frequency dispersive

permittivity $\varepsilon_{b_0}(k)$ and permeability $\mu_{b_0}(k)$ of the surrounding medium. Perturbed resonant states satisfy

$$\left[k_\nu \hat{\mathbb{P}}_0(k_\nu, \mathbf{r}) + k_\nu \delta\hat{\mathbb{P}}(k_\nu, \mathbf{r}) - \hat{\mathbb{D}}(\mathbf{r})\right] \vec{\mathbb{F}}_\nu(\mathbf{r}) = \vec{\mathbb{0}}\,, \tag{4.35}$$

where the perturbation $\delta\hat{\mathbb{P}}(k, \mathbf{r})$ consists of only changes of the permittivity and permeability of the surrounding medium, given, respectively, by $\varepsilon_b(k) - \varepsilon_{b_0}(k) = \varepsilon_{b_0}(k)\delta_\varepsilon$ and $\mu_b(k) - \mu_{b_0}(k) = \mu_{b_0}(k)\delta_\mu$. Now using the diagonal approximation for the wave function, $\vec{\mathbb{F}}_\nu(\mathbf{r}) \approx \vec{\mathbb{F}}_n(\mathbf{r})$, Eq. (4.35) becomes

$$\left[k_\nu \hat{\mathbb{P}}_0(k_\nu, \mathbf{r}) - k_n \hat{\mathbb{P}}_0(k_n, \mathbf{r}) + k_\nu \delta\hat{\mathbb{P}}(k_\nu, \mathbf{r})\right] \vec{\mathbb{F}}_n(\mathbf{r}) \approx \vec{\mathbb{0}}\,, \tag{4.36}$$

in which the term $\hat{\mathbb{D}}(\mathbf{r})\vec{\mathbb{F}}_n(\mathbf{r})$ was excluded with the help of Eq. (4.34). For small changes of the wavenumbers, $|k_\nu - k_n| \ll |k_n|$, one can Taylor expand the generalized permittivity in Eq. (4.36) as

$$k_\nu \hat{\mathbb{P}}_0(k_\nu, \mathbf{r}) \approx k_n \hat{\mathbb{P}}_0(k_n, \mathbf{r}) + (k_\nu - k_n)\left[k\hat{\mathbb{P}}_0(k, \mathbf{r})\right]'\,, \tag{4.37}$$

so that Eq. (4.36) becomes

$$\left[(k_\nu - k_n)\left[k\hat{\mathbb{P}}_0(k, \mathbf{r})\right]' + k_\nu \delta\hat{\mathbb{P}}(k_\nu, \mathbf{r})\right] \vec{\mathbb{F}}_n(\mathbf{r}) \approx \vec{\mathbb{0}}\,. \tag{4.38}$$

Multiplying it with $\vec{\mathbb{F}}_n(\mathbf{r})$ and integrating over the entire space, we obtain

$$(k_\nu - k_n) + k_\nu \int \vec{\mathbb{F}}_n(\mathbf{r}) \cdot \delta\hat{\mathbb{P}}(k_\nu, \mathbf{r}) \vec{\mathbb{F}}_n(\mathbf{r}) d\mathbf{r} \approx 0\,, \tag{4.39}$$

where we have used the normalization condition Eq. (4.4). Finally, neglecting the difference between k_ν and k_n in the perturbation $\delta\hat{\mathbb{P}}$, results in the following explicit expression for the perturbed wavenumbers of the resonant states

$$\frac{k_n}{k_\nu} \approx 1 + W^E_{nn}\varepsilon_{b_0}(k_n)\delta_\varepsilon - W^H_{nn}\mu_{b_0}(k_n)\delta_\mu\,, \tag{4.40}$$

which is identical to the diagonal approximation, i.e., ($n = m$) of Eq. (4.26) for non-dispersive systems in non-dispersive environments.

4.4 First-order approximation and comparison with Both and Weiss

To compare with the best available approach in literature by Both and Weiss [26], we extract the first order approximation from the regularized diagonal approximation. In fact, the first-order approximation follows immediately from Eq. (4.40):

$$\frac{k_n - k_\nu}{k_n} \approx W^E_{nn}\varepsilon_{b_0}(k_n)\delta_\varepsilon - W^H_{nn}\mu_{b_0}(k_n)\delta_\mu\,. \tag{4.41}$$

For a non-dispersive surrounding medium, both ε_{b_0} and μ_{b_0} have no dispersion, Eqs. (4.15) and (4.16) simplify to

$$W^E_{nn} = \frac{1 - A_n - B_n}{2\varepsilon_{b_0}}\,, \qquad W^H_{nn} = \frac{-1 + A_n - B_n}{2\mu_{b_0}}\,, \tag{4.42}$$

which coincides with the RSE in first order Eq. (2.52) and Eq. (4.21). For a dispersive surrounding medium, Eq. (4.41) can be written more explicitly, using Eqs. (4.15) and (4.16), as

$$\frac{k_n - k_\nu}{k_n} \approx \frac{(1 - A_n)\varepsilon_{b_0}\mu_{b_0}(\delta_\varepsilon + \delta_\mu) - B_n\left[(k\mu_{b_0})'\varepsilon_{b_0}\delta_\varepsilon - (k\varepsilon_{b_0})'\mu_{b_0}\delta_\mu\right]}{(k\varepsilon_{b_0})'\mu_{b_0} + (k\mu_{b_0})'\varepsilon_{b_0}}\,, \tag{4.43}$$

where again all values are taken at $k = k_n$.

Let us now compare Eq. (4.43) with the first-order results presented in [26]. The latter is given by

$$k_\nu \approx k_n - \frac{k_n\left\langle \mathbb{F}_n \middle| \delta\hat{\mathbb{P}}\,(k_n) \middle| \mathbb{F}_n \right\rangle + S}{\left\langle \mathbb{F}_n \middle| (k\hat{\mathbb{P}})' \middle| \mathbb{F}_n \right\rangle + [\mathbb{F}_n \mid \mathbb{F}'_n]} \tag{4.44}$$

where

$$\left\langle \mathbb{F}_n \middle| (k\hat{\mathbb{P}})' \middle| \mathbb{F}_n \right\rangle = \int_{\mathcal{V}_{in}} \left[\mathbf{E}_n(\mathbf{r}) \cdot (k\hat{\boldsymbol{\varepsilon}})'\,\mathbf{E}_n(\mathbf{r}) - \mathbf{H}_n(\mathbf{r}) \cdot (k\hat{\boldsymbol{\mu}})'\,\mathbf{H}_n(\mathbf{r})\right] d\mathbf{r} \tag{4.45}$$

and

$$[\mathbb{F}_n \mid \mathbb{F}'_n] = \frac{i}{k_n} \oint_{\mathcal{S}_{in}} (\mathbf{E}_n \times \mathbf{H}'_n - \mathbf{E}'_n \times \mathbf{H}_n) \cdot d\mathbf{S}\,, \tag{4.46}$$

with $\mathcal{S}_{in}$ being the outer surface of $\mathcal{V}_{in}$.

The first term in the numerator of Eq. (4.44) vanishes as there is no perturbation within the system, while the second term S represents the perturbation in the region outside it. According to [26], it is given by

$$S = \bar{\eta}\frac{k_n}{2}(\delta_\varepsilon + \delta_\mu)\,[\mathbb{F}_n \mid \mathbb{F}'_n] + \frac{i}{2}\bar{\eta}\left[\frac{(k\mu_{b_0})'}{\mu_{b_0}}\delta_\varepsilon - \frac{(k\varepsilon_{b_0})'}{\varepsilon_{b_0}}\delta_\mu\right] \oint_{\mathcal{S}_{in}} (\mathbf{E}_n \times \mathbf{H}_n) \cdot d\mathbf{S} \tag{4.47}$$

with

$$\bar{\eta} = \frac{\sqrt{\varepsilon_{b_0}\mu_{b_0}}}{(k\sqrt{\varepsilon_{b_0}\mu_{b_0}})'} = \frac{2\varepsilon_{b_0}\mu_{b_0}}{(k\varepsilon_{b_0})'\mu_{b_0} + (k\mu_{b_0})'\varepsilon_{b_0}}\,. \tag{4.48}$$

Using the resonant state's normalization Eq. (4.1), the first surface integral in Eq. (4.47) can be expressed as

$$[\mathbb{F}_n \mid \mathbb{F}'_n] = 1 - \left\langle \mathbb{F}_n \middle| (k\hat{\mathbb{P}})' \middle| \mathbb{F}_n \right\rangle = 1 - A_n\,. \tag{4.49}$$

This also entirely removes from Eq. (4.44) the denominator, since the latter is equal to 1. The second surface integral in Eq. (4.47) can, in turn, be expressed as

$$\frac{i}{k_n} \oint_{\mathcal{S}_{in}} \cdot (\mathbf{E}_n \times \mathbf{H}_n)\, d\mathbf{S} = -\int_{\mathcal{V}in} [\mathbf{E}_n(\mathbf{r}) \cdot \hat{\boldsymbol{\varepsilon}}\mathbf{E}_n(\mathbf{r}) + \mathbf{H}_n(\mathbf{r}) \cdot \hat{\boldsymbol{\mu}}\mathbf{H}_n(\mathbf{r})]\, d\mathbf{r} = -B_n\,, \tag{4.50}$$

using the Poyting theorem Eq. (4.3) for $n = m$ [see Eqs. (4.13) and (4.17) for the definition of A_n and B_n]. This makes Eq. (4.44) identical to the first-order result Eq. (4.43) obtained for regularized resonant states.

The energy and the linewidth of the fundamental plasmonic dipolar ($l = 1$) and quadrupolar ($l = 2$) modes of a gold nanosphere of radius $R = 200\,\text{nm}$ surrounded by a dielectric medium with varying permittivity ε_b are shown in Figs. 4.3(a,b), respectively. The unperturbed system has $\varepsilon_{b_0} = 2$ of the surrounding material. This is exactly the same system as used for illustration of the first-order theory presented in [26]. Figure 4.3 compares the exact solution with the first-order result, identical to [26], with

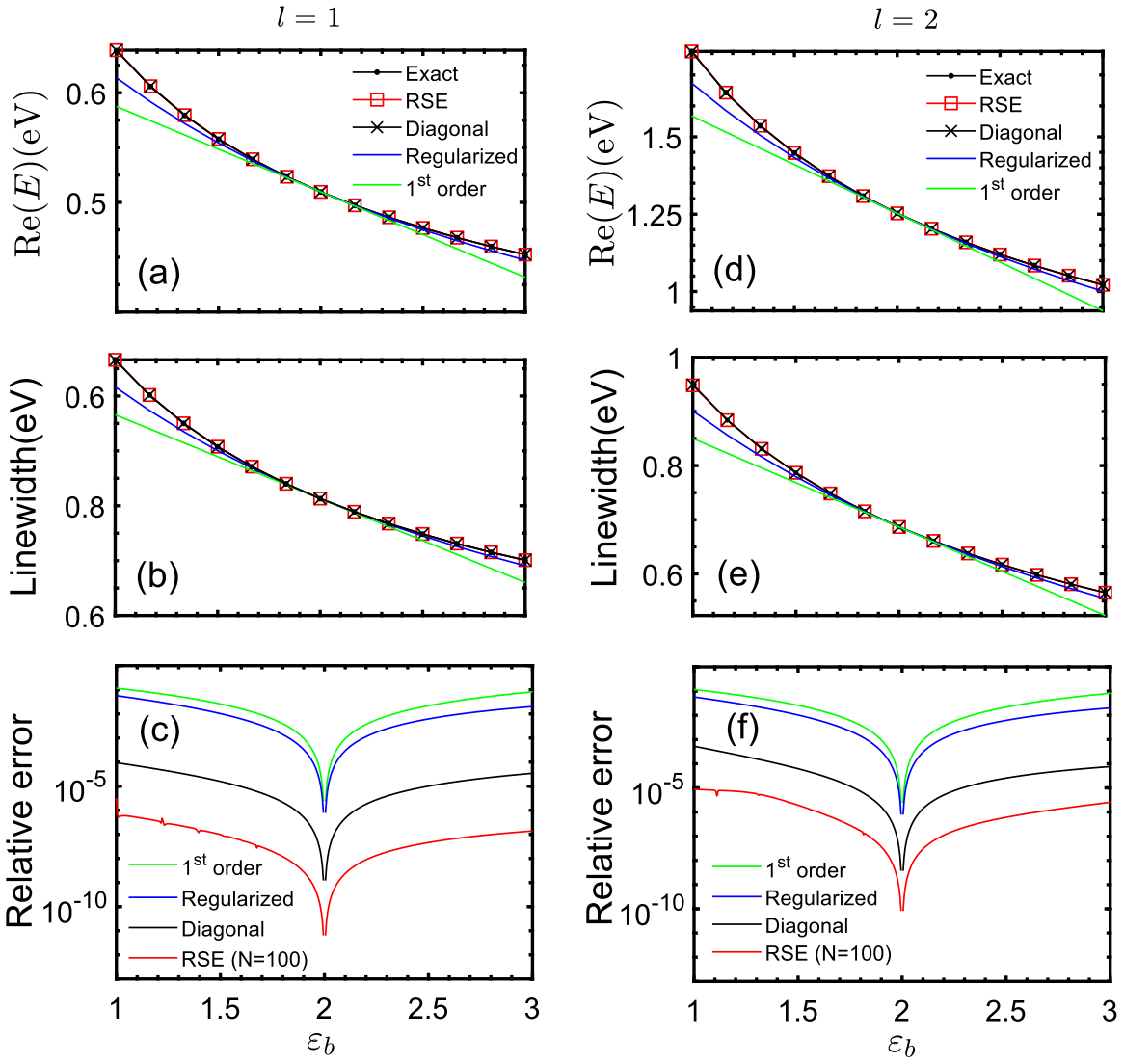

Figure 4.3. Energy (a,d) and linewidth (b,d) of the fundamental plasmonic dipolar (left) and quadrupolar mode (right) of the gold nanosphere of radius $R = 200\,\text{nm}$ as functions of the permittivity ε_b of the material surrounding the sphere, calculated using the full RSE with $N = 100$ basis states (red lines with squares), diagonal RSE (black lines with crosses), regularized theory (blue lines), and first-order approximation (green lines). The unperturbed system has the surrounding permittivity of $\varepsilon_{b_0} = 2$. The Drude model is using $\varepsilon_\infty = 4$ with the other parameters fitted to the Johnson and Christy data [67] via the fit programme provided in [66]. (c) and (f) show the corresponding relative errors compared to the exact solutions.

the full and diagonal RSE, as well as with the regularized diagonal approximation. We see that for the chosen parameters of the unperturbed system, namely for the value of $\varepsilon_{b_0} = 2$ lying in the middle of the selected range $1 \leqslant \varepsilon_b \leqslant 3$, the first-order results

are in a much better agreement with the exact solution in this range than in a similar Fig. 2 of Chapter 3 where the unperturbed system has $\varepsilon_{b_0} = 1$. Nevertheless, as it is clear from Figs. 4.3(c,f), the diagonal RSE shows a lot better agreement with the exact solution, while the full RSE is quickly converging to it with increasing the basis size. For further comparison, Figs. 3.2 and 3.3, for the gold nano-sphere, and Figs. 3.8 and 3.12, for the gold bow-tie and silica microsphere, respectively, from the previous chapter were reproduced in Appendix C.2 with the regularized diagonal approximation. The regularized diagonal approximation provides improved accuracy in comparison to the first-order but lower than the accuracy achieved by the diagonal approximations in dispersive systems. We note that for arbitrary shapes, the integral over the system volume of the square of the electric field of the unperturbed resonant state (with the wavenumber k_n) was calculated using the method proposed in Sec. 3.1.3 of Chapter 3.

4.5 Summary

We have presented in this chapter an alternative method for calculating the perturbed resonant states of an optical system due to homogeneous changes in its surrounding medium based on regularization. Regularization involves multiplying all the wavefunctions of the resonant states with a Gaussian factor $e^{-\alpha r^2}$ and taking the limit $\alpha \to 0$ after integration. Assuming the resonant states exist under regularization, the surface terms in the orthonormality conditions are eliminated, and the volume integral can be extended to the entire space. Thus, the normalization, orthogonality, and Poynting's theorem adopt the forms typically observed in Hermitian systems. Using such conditions for the regularized resonant states, we expressed the integrals of the regularized resonant states over the infinite volume outside the system in terms of the integrals over the system volume. Having this expression of the integrals over the infinite volume outside the system is useful to develop a perturbation theory to treat perturbations in the surrounding medium. We therefore attempted to formulate a perturbation theory akin to the RSE, but with using the regularized resonant states as a basis to treat perturbations both inside and outside the system. The results obtained

from the regularized RSE for perturbations outside the system failed to converge to the exact solution, demonstrating the lack of completeness of such resonant states outside the system. We have, however, succeeded in formulating a regularized diagonal approximation using a single mode only to treat small changes in the surrounding medium. We have proved that the first-order of this approximation is identical to the first-order perturbation theory [26]. We have also shown that they both coincide with the RSE-based theory in first order for non-dispersive surrounding mediums. Lastly, we have illustrated the regularized diagonal approximation with the RSE-based theory and other approximations: diagonal and first order approximations, using the same illustrations in [26]. The regularized diagonal approximation demonstrates a better agrrement with the exact values in comparison to the first-order approximation; however, it does not provide the same level of accuracy as the diagonal approximation. This approximation becomes particularly useful in our treatment of chirality perturbation in Chapter 6.

Chapter 5

Achieving degeneracy in spherical systems

Achieving degeneracy in electric and magnetic modes has already been reported in literature. This was achieved using periodic structures [29, 82] or even in a dielectric sphere with graded index [37] or subjected to an external magnetic field [83]. Degenerate electric and magnetic modes become of a special interest in developing new sensing schemes, particularly those intended for chirality sensing.

Introducing chirality to an optical system couples the electric and magnetic fields. The impact of such chirality-induced coupling on mode shift depends on the value of κ and the overlap integral of the electric and magnetic fields of the same mode and all other resonances of the system ($n \neq m$) [84]. Having degenerate modes converts the impact of chirality on the mode shift to first order. This idea is the key ingredient of enhancing chirality sensing in this thesis, which will be derived rigorously in Chapter 6.

In this chapter, we aim to find degenerate resonant states of single spherically symmetric systems by modifying its material's properties only. In our discussion, we focus on an arbitrary sphere and a core-shell system, consisting of a sphere coated by a layer of another material [85, 86]. Both systems have constant permittivity (or permeability) profiles. We discuss the possibility of achieving degeneracy in TE and TM modes by fully solving the system analytically and providing its secular equation, determining the wavenumbers of the resonant states. Since we consider spherically symmetric systems, we adapt the derivation of resonant states of a spherical system in

vacuum, reported in [61], and present the fields in vector spherical harmonics (VSHs) to have compact forms.

Lastly, we present the resonant states of the sphere, considering chirality both inside and outside the sphere. We also find the secular equation of the system, which determines the exact modes when chirality is introduced to the system.

5.1 General solution

By starting with an arbitrary system and environment with assuming an isotropic response inside and outside the system, we aim to solve Maxwell's equations

$$\left[k\hat{\mathbb{P}}(k,\mathbf{r}) - \hat{\mathbb{D}}(\mathbf{r})\right]\vec{\mathbb{F}}(\mathbf{r}) = \vec{\mathbb{0}}\,, \tag{5.1}$$

having a permittivity tensor

$$\hat{\mathbb{P}}(\mathbf{r}) = \begin{pmatrix} \varepsilon(r)\hat{\mathbf{1}} & -\kappa(r)\hat{\mathbf{1}} \\ -\kappa(r)\hat{\mathbf{1}} & \mu(r)\hat{\mathbf{1}}\,, \end{pmatrix} \tag{5.2}$$

with noting here that rather than defining a permittivity tensor $\hat{\mathbb{P}}(\mathbf{r})$ for each sub-volume, the material's properties $\varepsilon(r)$, $\mu(r)$, and $\kappa(r)$ have the spacial dependence. For spherically symmetric systems, the angular dependence can be absorbed from expressions by spanning the fields into VSH's as [61]

$$\mathbf{E}(\boldsymbol{r}) = \sum_{jlm} E_{jlm}(r)\boldsymbol{Y}_{jlm}(\Omega), \quad i\mathbf{H}(\boldsymbol{r}) = \sum_{jlm} iH_{jlm}(r)\boldsymbol{Y}_{jlm}(\Omega)\,, \quad j = 1,2,3 \tag{5.3}$$

where $\alpha_l = \sqrt{l(l+1)}$. and VHS's are given by [87]

$$\boldsymbol{Y}_{1lm}(\Omega) = \frac{\boldsymbol{r}}{\alpha_l} \times \nabla Y_{lm}(\Omega)\,, \qquad \boldsymbol{Y}_{2lm}(\Omega) = \frac{r}{\alpha_l}\nabla Y_{lm}(\Omega)\,, \qquad \boldsymbol{Y}_{3lm}(\Omega) = \frac{\boldsymbol{r}}{r}Y_{lm}(\Omega)\,, \tag{5.4}$$

with the angular dependence $\Omega = (\theta, \varphi)$, taken in the ranges $0 \leq \theta \leq 2\pi$ and $-\pi \leq \varphi \leq \pi$, and $Y_{lm}(\Omega)$ is a scalar spherical harmonic

$$Y_{lm}(\Omega) = \sqrt{\frac{2l+1}{2}\frac{(l-|m|)!}{(l+|m|)!}} P_l^{|m|}(\cos\theta)\chi_m(\varphi)\,, \tag{5.5}$$

where $P_l^{|m|}$ is the associated Legendre polynomial, and the azimuthal dependence is given by [8]

$$\chi_m(\varphi) = \begin{cases} \pi^{-1/2}\sin(m\varphi) & \text{for} \quad m < 0, \\ (2\pi)^{-1/2} & \text{for} \quad m = 0, \\ \pi^{-1/2}\cos(m\varphi) & \text{for} \quad m > 0\,. \end{cases} \tag{5.6}$$

It follows from Eq. (5.4) that the first two vector harmonics point in a direction contained in the angular plane while the third one points to the radial direction. This becomes useful for the derivation of the secular equation of the resonant states since the tangential components of the electric and magnetic fields, corresponding to the first and second components in VSHs, are continuous across the boundaries. We also note that the VSHs are orthonormal and their orthonormality are [61]

$$\int \boldsymbol{Y}_{1lm}(\Omega)\cdot\boldsymbol{Y}_{1lm}(\Omega)\,d\Omega = \delta_{ll'}\delta_{mm'}\,, \tag{5.7}$$

$$\int \boldsymbol{Y}_{2lm}(\Omega)\cdot\boldsymbol{Y}_{2lm}(\Omega)\,d\Omega = \delta_{ll'}\delta_{mm'}\,, \tag{5.8}$$

$$\int \boldsymbol{Y}_{3lm}(\Omega)\cdot\boldsymbol{Y}_{3lm}(\Omega)\,d\Omega = \delta_{ll'}\delta_{mm'}\,. \tag{5.9}$$

Using the expansions of $\mathbf{E}(\mathbf{r})$ and $\mathbf{H}(\mathbf{r})$ given by Eq. (5.3) in Maxwell's equations with utilizing the properties of the VSHs [11, 61] and then equating the components at the

same $\boldsymbol{Y}_{jlm}$, we obtain

$$\begin{aligned}
\frac{(rE_{2lm})'}{r} - \frac{\alpha E_{3lm}}{r} &= ik[\mu(r)H_{1lm} + i\kappa(r)E_{1lm}]\,, && (5.10)\\
\frac{(rH_{2lm})'}{r} - \frac{\alpha H_{3lm}}{r} &= -ik[\varepsilon(r)E_{1lm} - i\kappa(r)H_{1lm}]\,, && (5.11)\\
-\frac{(rE_{1lm})'}{r} &= ik[\mu(r)H_{2lm} + i\kappa(r)E_{2lm}]\,, && (5.12)\\
-\frac{(rH_{1lm})'}{r} &= -ik[\varepsilon(r)E_{2lm} - i\kappa(r)H_{2lm}]\,, && (5.13)\\
-\frac{\alpha E_{1lm}}{r} &= ik[\mu(r)H_{3lm} + i\kappa(r)E_{3lm}]\,, && (5.14)\\
-\frac{\alpha H_{1lm}}{r} &= -ik[\varepsilon(r)E_{3lm} - i\kappa(r)H_{3lm}]\,, && (5.15)
\end{aligned}$$

where the r dependence is dropped from the components of the fields for brevity, and the derivatives are taken with respect to r. We assume for now that $\kappa(r) = 0$ since we look for degeneracy in non-chiral systems. Eliminating chirality decouples the second and third components of the electric field, $E_{2lm}(r)$ and $E_{3lm}(r)$, respectively, with the first component of the magnetic field $H_{1lm}(r)$ from other components. The other components are $E_{1lm}(r)$, $H_{2lm}(r)$ and $H_{3lm}(r)$. This results in splitting the six equations above into two independent sets for TE and TM polarizations as follows: [61]

$$\left.\begin{aligned}
\frac{(riH_{2lm})'}{r} - \frac{\alpha}{r}iH_{3lm} &= k\varepsilon(r)E_{1lm}\,,\\
-\frac{(rE_{1lm})'}{r} &= k\mu(r)iH_{2lm}\,,\\
-\frac{\alpha}{r}E_{1lm} &= k\mu(r)iH_{3lm}\,,
\end{aligned}\right\}\ \text{for TE,}\qquad
\left.\begin{aligned}
\frac{(rE_{2lm})'}{r} - \frac{\alpha}{r}E_{3lm} &= ik\mu(r)H_{1lm}\,,\\
-\frac{(riH_{1lm})'}{r} &= k\varepsilon(r)E_{2lm}\,,\\
-\frac{\alpha}{r}iH_{1lm} &= k\varepsilon(r)E_{3lm}\,.
\end{aligned}\right\}\ \text{for TM} \qquad (5.16)$$

with a separate secular equation for each set. For more compact forms in presentation, as also suggested in [61], we define a radial function $\boldsymbol{\mathcal{F}}(\mathbf{r}) = r\vec{\mathbb{F}}(\mathbf{r})$, where $\mathcal{E}_{jlm}(r) = rE_{jlm}(r)$ and $\mathcal{H}_{jlm}(r) = riH_{jlm}(r)$. The two sets of equations of TE and TM then

become [61]

$$\left.\begin{aligned} \frac{d}{dr}\mathcal{H}_{2lm} - \frac{\alpha}{r}\mathcal{H}_{3lm} &= k\varepsilon(r)\mathcal{E}_{1lm}\,, \\ -\frac{d}{dr}\mathcal{E}_{1lm} &= k\mu(r)\mathcal{H}_{2lm}\,, \\ -\frac{\alpha}{r}\mathcal{E}_{1lm} &= k\mu(r)\mathcal{H}_{3lm}\,, \end{aligned}\right\} \text{for TE,} \qquad \left.\begin{aligned} \frac{d}{dr}\mathcal{E}_{2lm} - \frac{\alpha}{r}\mathcal{E}_{3lm} &= k\mu(r)\mathcal{H}_{1lm}\,, \\ -\frac{d}{dr}\mathcal{H}_{1lm} &= k\varepsilon(r)\mathcal{E}_{2lm}\,, \\ -\frac{\alpha}{r}\mathcal{H}_{1lm} &= k\varepsilon(r)\mathcal{E}_{3lm}\,. \end{aligned}\right\} \text{for TM} \tag{5.17}$$

Now, we can write the 6×1 vector $\boldsymbol{\mathcal{F}}(\mathbf{r})$ in a reduced 3×1 form in VSHs for each polarization. Solving for TE components yields [61],

$$\boldsymbol{\mathcal{F}}^{\text{TE}}(\mathbf{r}) = \begin{pmatrix} \mathcal{E}_{1lm} \\ \mathcal{H}_{2lm} \\ \mathcal{H}_{3lm} \end{pmatrix} = \begin{pmatrix} \psi(r) \\ -\beta(r)\psi'(r) \\ -\alpha_l\beta(r)\frac{\psi(r)}{r} \end{pmatrix}, \tag{5.18}$$

and solving for TM polarization gives,

$$\boldsymbol{\mathcal{F}}^{\text{TM}}(\mathbf{r}) = \begin{pmatrix} \mathcal{H}_{1lm} \\ \mathcal{E}_{2lm} \\ \mathcal{E}_{3lm} \end{pmatrix} = \begin{pmatrix} \psi(r) \\ -\frac{\psi'(r)}{\beta(r)} \\ -\alpha_l\frac{\psi(r)}{\beta(r)r} \end{pmatrix}, \tag{5.19}$$

where $\beta(r) = \sqrt{\frac{\varepsilon(r)}{\mu(r)}}$, and the wavefunction $\psi(r)$ satisfies the spherical Bessel's equation [14, 61],

$$\psi''(r) - \frac{\alpha^2}{r^2}\psi(r) = -k^2n^2(r)\psi(r)\,. \tag{5.20}$$

with $\psi'(r)$ and $\psi''(r)$ being the first and second derivative respectively with respect to r. Note that in TE polarization, the electric field $\mathcal{E}_{1lm}$ is tangential while the magnetic field has both tangential component $\mathcal{H}_{2lm}$ and normal component $\mathcal{H}_{3lm}$. For TM polarization, the magnetic field $\mathcal{H}_{1lm}$ is tangential while the electric field has the tangential component $\mathcal{E}_{2lm}$ and normal component $\mathcal{E}_{3lm}$. This is the general solution of a non-chiral spherically symmetric system having constant ε and μ profiles. Note that the only difference between TE and TM solutions is the factor $\beta(r)$ in TE and $1/\beta(r)$ in TM. If $\beta(r) = 1$, the two solutions of TE and TM become identical. In the following, we present the resonant states and secular equations of TE and TM polarizations for

both the sphere and the core-shell system, and discuss the possibility of achieving degeneracy.

5.2 An arbitrary magnetic sphere

The system here is a basic sphere of radius R. Both the system and its environment are allowed to have magnetic properties, such that

$$n(r) = \begin{cases} n_r\,, & r \leq R \\ n_b\,, & r \geq R\,, \end{cases} \tag{5.21}$$

where $n(r) = \sqrt{\varepsilon(r)\mu(r)}$. Assuming outgoing boundary conditions outside the sphere for $r > R$, the wavefunction then $\psi_n(r)$ takes the form [17]

$$\psi_n(r) = \begin{cases} A_n^{(p)} J(n_r k_n r)\,, & r \leq R \\ B_n^{(p)} H(n_b k_n r)\,, & r \geq R\,, \end{cases} \tag{5.22}$$

with $\psi_n(r)$ having a Riccati-Bessel's function $J(n_r k_n r)$ regular in the sphere and Riccati-Hankel function of the first kind $H(n_b k_n r)$ outside the system, representing the outgoing waves, where $J(n_r k_n r) = n_r k_n r j(n_r k_n r)$ and $H(n_b k_n r) = n_b k_n r h^{(1)}(n_b k_n r)$ and the functions $j(n_r k_n r)$ and $h^{(1)}(n_b k_n r)$ are the spherical Bessel and Hankel's functions of the first kind [11]. Note that the normalization constants, A_n, B_n are dependent on the polarization, where (p) is for the polarization of light (TE or TM).

Now, by applying Maxwell's boundary conditions on the sphere's boundary, we obtain the secular equation:

$$\frac{\tilde{J}_n(n_r z)}{\tilde{H}_n(n_b z)} = \frac{\beta_b}{\beta}\,, \quad \text{for TE}\,, \qquad \frac{\tilde{J}_n(n_r z)}{\tilde{H}_n(n_b z)} = \frac{\beta}{\beta_b}\,, \quad \text{for TM}\,, \tag{5.23}$$

having $\tilde{J}_n(n_r z) = J_n'(n_r z)/J_n(n_r z)$ and $\tilde{H}_n(n_b z) = H_n'(n_b z)/H_n(n_b z)$ with and $z = k_n R$, and where now $\beta = \sqrt{\frac{\varepsilon}{\mu}}$ and $\beta_b = \sqrt{\frac{\varepsilon_b}{\mu_b}}$ refer to the sphere and the surrounding medium, respectively. This is the same secular equation presented in Chapter 2 for a dispersive

sphere. Here, n_r and β are frequency independent.

In the secular equations of TE and TM polarizations, the same ratio of the functions $\tilde{J}_n$ and $\tilde{H}_n$ is determined by different constants. The different constants, β_b/β for TE and β/β_b for TM, lead to different wavenumbers of TE and TM polarizations of the sphere. In other words, the wavenumber k_n of the resonant states of TE and TM of the sphere can be identical only when $\beta = \beta_b$. This indicates that the ratio of the permittivity to the permeability of the sphere and the surrounding medium have to be equal. Having $\beta = \beta_b = 1$, i.e, $\varepsilon = \mu$ and $\varepsilon_b = \mu_b$ is a very special case since the electric and magnetic fields of both TE and TM modes become identical.

To achieve degeneracy in a non-magnetic system, one may consider introducing a dielectric shell to mitigate the contrast between the permittivity of the core and the external surrounding medium. We elaborate on this in the following section and provide a full analytical solution, secular equation, and normalization of a core-shell system.

5.3 A core-shell system

We consider a core-shell system of an arbitrary isotropic materials, either for the core, shell or surrounding medium. The shell has a thickness $\Delta R = R_2 - R_1$, where R_1 and R_2 are, respectively, the core and the outer radii, and the structure is described by

$$n(r) = \begin{cases} n_1\,, & r \leq R_1 \\ n_2\,, & R_1 \leq r \leq R_2 \\ n_3\,, & r \geq R_2\,, \end{cases} \tag{5.24}$$

where $n(r) = \sqrt{\varepsilon(r)\mu(r)}$ and n_1, n_2 and n_3 are, respectively, the refractive indices of the core, shell, and the surrounding medium. We now have the following solution

$$\psi_n(r) = \begin{cases} A_n^{(p)} J(n_1 k_n r)\,, & r \leq R_1 \\ K_n^{(p)}(n_2 k_n r)\,, & R_1 \leq r \leq R_2 \\ B_n^{(p)} H(n_3 k_n r)\,, & r \geq R_2\,. \end{cases} \tag{5.25}$$

As for the sphere, the core has a solution of a Riccati-Bessel function $J(n_1 k_n r)$, and the outer surrounding medium has a solution of a Bessel-Hankel function $H(n_3 k_n r)$. Within the shell, the solution is a linear combination of two Bessel functions taken as $K_n(n_2 k_n r) = C_n^{(p)} J(n_2 k_n r) + D_n^{(p)} H(n_2 k_n r)$. Note that the normalization constants, $A_n^{(p)}$, $B_n^{(p)}$, $C_n^{(p)}$ and $D_n^{(p)}$ are dependent on the polarization, and they have the superscript TE or TM for the corresponding polarization in the following.

5.3.1 Secular equation

Now, to find the secular equation of the system, the boundary conditions have to be fulfilled across both the core-shell interface and the the shell-environment interface. For TE polarization, this requires that the tangential components $\mathcal{E}_{1lm}$ and $\mathcal{H}_{2lm}$ are continuous across the two boundaries as

$$A_n^{\mathrm{TE}} J_n(n_1 k_n R_1) = C_n^{\mathrm{TE}} J_n(n_2 k_n R_1) + D_n^{\mathrm{TE}} H_n(n_2 k_n R_1)\,, \tag{5.26}$$

$$\beta_1 A_n^{\mathrm{TE}} J_n'(n_1 k_n R_1) = \beta_2 \left[C_n^{\mathrm{TE}} J_n'(n_2 k_n R_1) + D_n^{\mathrm{TE}} H_n'(n_2 k_n R_1) \right]\,, \tag{5.27}$$

$$B_n^{\mathrm{TE}} H_n(n_3 k_n R_2) = C_n^{\mathrm{TE}} J_n(n_2 k_n R_2) + D_n^{\mathrm{TE}} H_n(n_2 k_n R_2)\,, \tag{5.28}$$

$$\beta_3 B_n^{\mathrm{TE}} H_n'(n_3 k_n R_2) = \beta_2 \left[C_n^{\mathrm{TE}} J_n'(n_2 k_n R_2) + D_n^{\mathrm{TE}} H_n'(n_2 k_n R_2) \right]\,, \tag{5.29}$$

where β_1, β_2 and β_3 for the core, shell, and the surrounding medium, respectively. For brevity, we use in the following $\Psi_n(n_i k_n R_j) = \Psi_{ij}$, where $\Psi_n(n_i k_n R_j)$ represents the

solution in any spatial region. The secular equation for TE polarisation is then given by

$$\begin{vmatrix} J_{11} & 0 & -J_{21} & -H_{21} \\ \beta_1 J'_{11} & 0 & -\beta_2 J'_{21} & -\beta_2 H'_{21} \\ 0 & H_{32} & -J_{22} & -H_{22} \\ 0 & \beta_3 H'_{32} & -\beta_2 J'_{22} & -\beta_2 H'_{22} \end{vmatrix} = 0\,. \tag{5.30}$$

Similarly, the secular equation for TM polarization can be obtained from the continuity of the tangential components $\mathcal{H}_{1lm}$ and $\mathcal{E}_{2lm}$ across the shell boundaries:

$$A_n^{\text{TM}} J_{11} = C_n^{\text{TM}} J_{21} + D_n^{\text{TM}} H_{21}\,, \tag{5.31}$$

$$\beta_2 A_n^{\text{TM}} J'_{11} = \beta_1 \left[C_n^{\text{TM}} J'_{21} + D_n^{\text{TM}} H'_{21} \right]\,, \tag{5.32}$$

$$B_n^{\text{TM}} H_{32} = C_n^{\text{TM}} J_{22} + D_n^{\text{TM}} H_{22}\,, \tag{5.33}$$

$$\beta_2 B_n^{\text{TM}} H'_{32} = \beta_3 \left[C_n^{\text{TM}} J'_{22} + D_n^{\text{TM}} H'_{22} \right]\,, \tag{5.34}$$

resulting in the secular equation for TM polarization,

$$\begin{vmatrix} J_{11} & 0 & -J_{21} & -H_{21} \\ \beta_2 J'_{11} & 0 & -\beta_1 J'_{21} & -\beta_1 H'_{21} \\ 0 & H_{32} & -J_{22} & -H_{22} \\ 0 & \beta_2 H'_{32} & -\beta_3 J'_{22} & -\beta_3 H'_{22} \end{vmatrix} = 0. \tag{5.35}$$

We show in Fig. 5.1 the TE and TM modes of a core-shell system with permittivities $\varepsilon_1 = 4$ and $\varepsilon_2 = 2$ of the core and the shell, respectively, located in vacuum, and has a shell thickness $\Delta R/R_2 = 0.1$. The system is non-magnetic, i.e., $\mu = 1$ everywhere. We plotted the TE and TM modes of a sphere with the same permittivity as the core, surrounded by vacuum, in the same figure for comparison. The TE and TM modes of the sphere appear in alternative order [37] while the ones of the core-shell oscillate randomly. The frequencies of both systems are calculated for $l = 5$, and the leaky modes are not shown in this figure.

Now, let us bring the secular equations of TE and TM polarizations of the core-shell

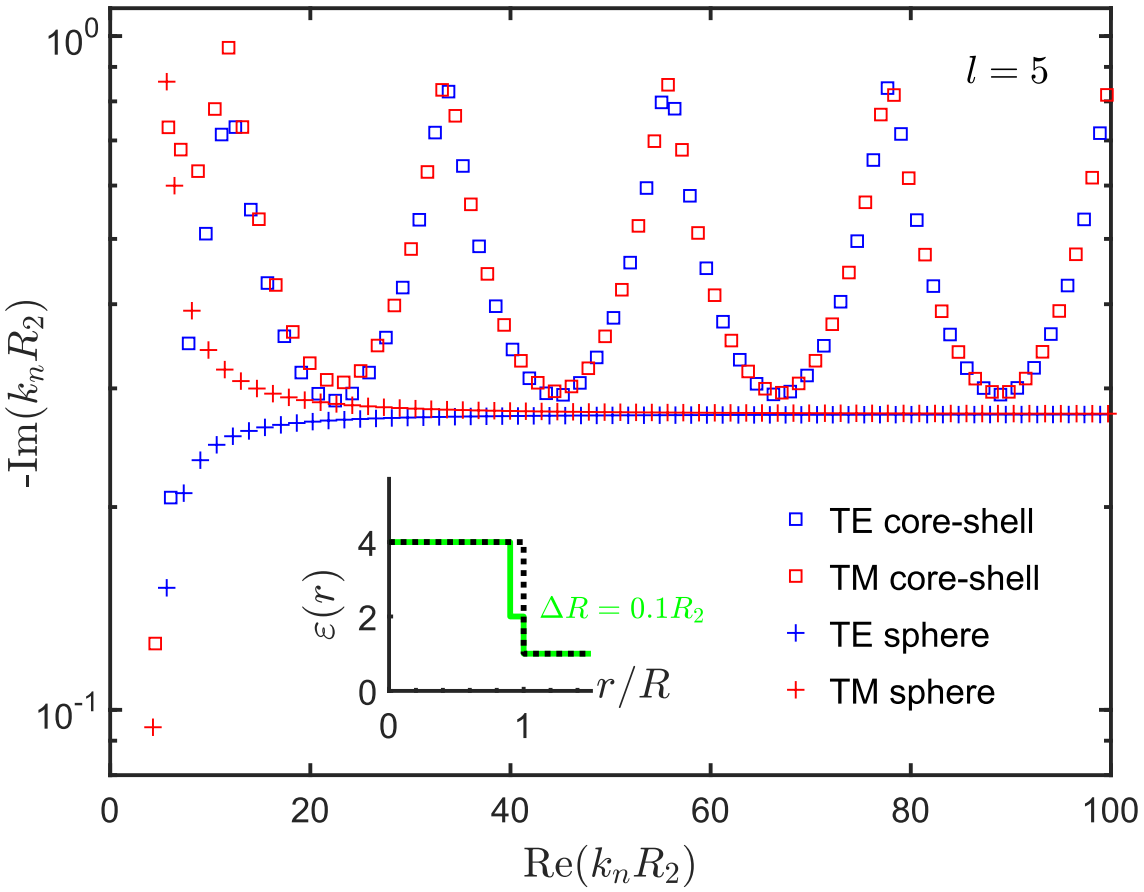

Figure 5.1. The eigen wavenumbers of TE (blue squares) and TM (red squares) modes of a core-shell system with core permittivity $\varepsilon_1 = 4$, shell permittivity $\varepsilon_2 = 2$, and shell thickness $\Delta R/R_2 = 0.1$, are shown in the complex plane. The eigen wavenumbers of TE (blues pluses) and TM (red pluses) of a dielectric sphere of permittivity $\varepsilon = 4$ are also shown. Both system are non-magnetic and located in vacuum.

system, given by Eqs. (5.30) and (5.35), respectively, to analogous forms with those for the sphere in Sec. 5.2. We rearrange the secular equation in the following form

$$\frac{\tilde{J}_{11}}{\tilde{H}_{32}} = \frac{\beta_3}{\beta_1}\frac{\tilde{K}_{21}}{\tilde{K}_{22}} \quad \text{for TE}, \qquad \frac{\tilde{J}_{11}}{\tilde{H}_{32}} = \frac{\beta_1}{\beta_3}\frac{\tilde{K}_{21}}{\tilde{K}_{22}} \quad \text{for TM}\,, \tag{5.36}$$

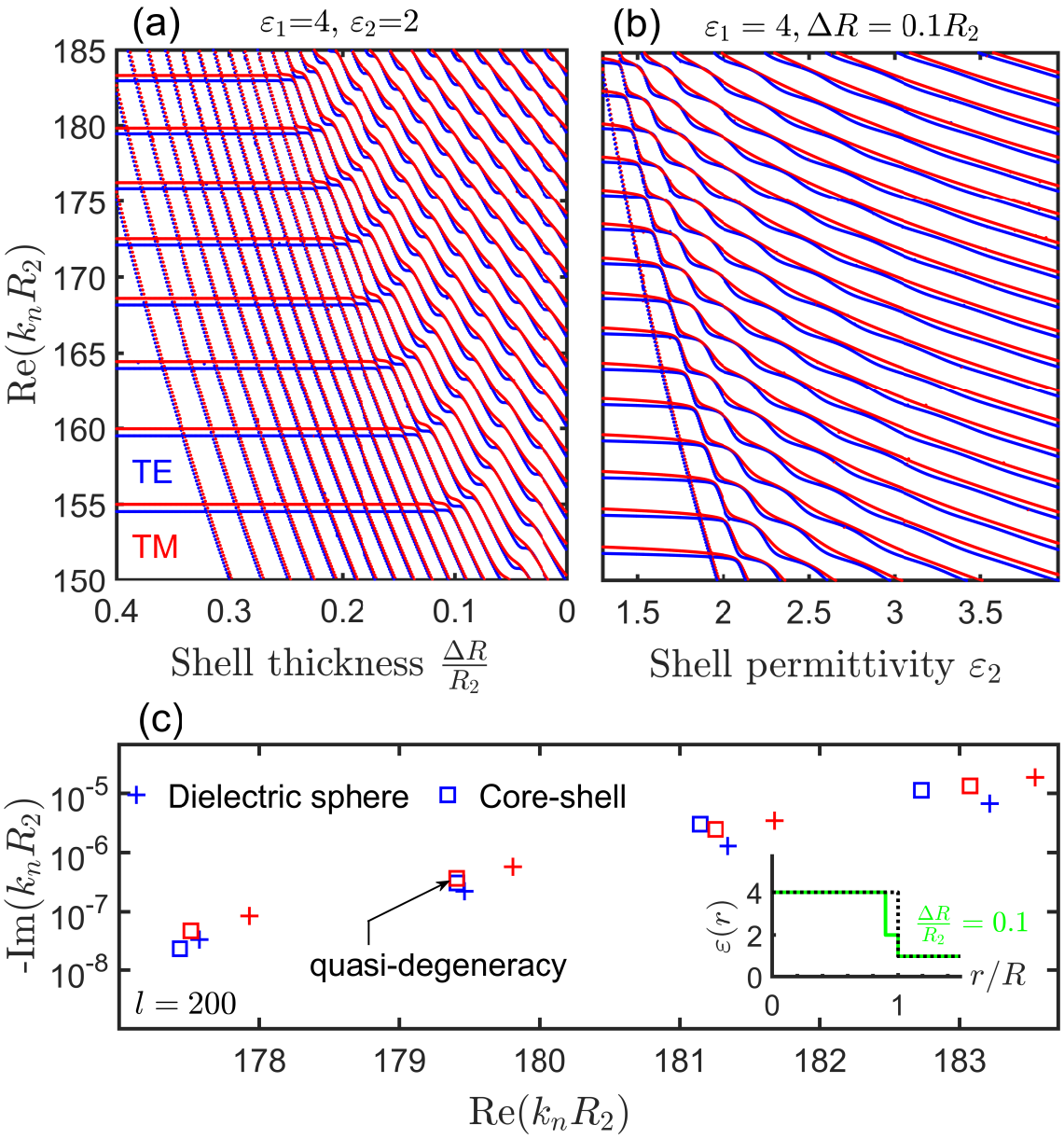

Figure 5.2. (a) The real parts of TE (blue dots) and TM (red dots) wavenumbers of a core-shell system, with core permittivity $\varepsilon_1 = 4$ and shell permittivity $\varepsilon_2 = 2$, versus the shell thickness ΔR. The modes are of order $l = 200$ and quality-factor exceeding 10^2. (b) As in (a) but with $\Delta R/R_2 = 0.1$ fixed and shell permittivity ε_b changing. (c) Selected whispering gallery modes are shown in the complex plane for the same core, with $\varepsilon_2 = 2$ and $\Delta R/R_2 = 0.1$, and for the core without the shell. The system is non magnetic and located in vacuum.

having

$$\tilde{J}_{11} = \frac{J'_{11}}{J_{11}}, \qquad \tilde{K}_{21} = \frac{C_n^{(p)} J'_{21} + D_n^{(p)} H'_{21}}{C_n^{(p)} J_{21} + D_n^{(p)} H_{21}}, \tag{5.37}$$

$$\tilde{H}_{32} = \frac{H'_{32}}{H_{32}}, \qquad \tilde{K}_{22} = \frac{C_n^{(p)} J'_{22} + D_n^{(p)} H'_{22}}{C_n^{(p)} J_{22} + D_n^{(p)} H_{22}}, \tag{5.38}$$

where the constants $C_n^{(p)}$ and $D_n^{(p)}$ refer to the corresponding polarization in Eq. (5.36). For the core-shell, the ratio $\tilde{J}_{11}/\tilde{H}_{32}$ is not only determined by β_1 and β_3 but also by the linearly independent solutions inside the shell. This would allow for the TE and TM modes to be equivalent at some values of R_2 and n_2. The degenerate modes can be described by the equation,

$$\frac{\beta_3}{\beta_1}\left[\frac{\tilde{K}_{21}^{\mathrm{TE}}}{\tilde{K}_{22}^{\mathrm{TE}}}\right] = \frac{\beta_1}{\beta_3}\left[\frac{\tilde{K}_{21}^{\mathrm{TM}}}{\tilde{K}_{22}^{\mathrm{TM}}}\right], \tag{5.39}$$

in which the contrast between β_1 and β_3 is compensated by the shell's contribution inside the brackets. To find degenerate modes, one may find the TE and TM modes from the secular equations for a core and surrounding of interest and change one of the shell's parameters, ε_2, μ_2, or ΔR to locate the degenerate modes. For a non-magnetic structure, one can still change ε_2 or ΔR. Since we are more interested on finding high-quality degenerate whispering gallery modes, we focus on locating degeneracy in the real parts only of the modes.

We consider an example of a non-magnetic core-shell system of $\varepsilon_1 = 4$ and high mode order $l = 200$, located in vacuum. Figure 5.2(a) shows the real parts of TE and TM modes having quality-factor higher than 10^2 versus a range of shell thickness ΔR. The shell thickness is shrinking from 0.4 until the shell vanishes, for a fixed shell permittivity $\varepsilon_2 = 2$. We also see from Fig. 5.2(a) that the likelihood of observing degeneracy (or quasi-degeneracy) is higher in systems characterized by thinner shells, with thicknesses approaching or being less than 20% of the core radius. For a fixed thickness $\Delta R/R_2 = 0.1$, Fig. 5.2(b) shows the real parts of TE and TM modes versus a wide range of shell permittivity ε_2, ranging from 1.3 to 4. We chose this range because the likelihood of achieving degeneracy with higher quality-factors is enhanced when the shell has a smaller permittivity ε_2 than the permittivity of the core ε_1. Additionally, we show in Fig. 5.2(c), a selected quasi-degenerate pair of TE mode at $k_nR_2 = 179.409 - 3.1\times 10^{-7}i$ and TM mode at $k_nR_2 = 179.408 - 3.7\times 10^{-7}i$ in the complex plane. The modes of the core without the shell is also included for comparison. The arbitrary oscillation of the modes of the core-shell system brings some of the TE and TM modes closer to each other in contrast to those in the sphere (core without the shell). The modes of the

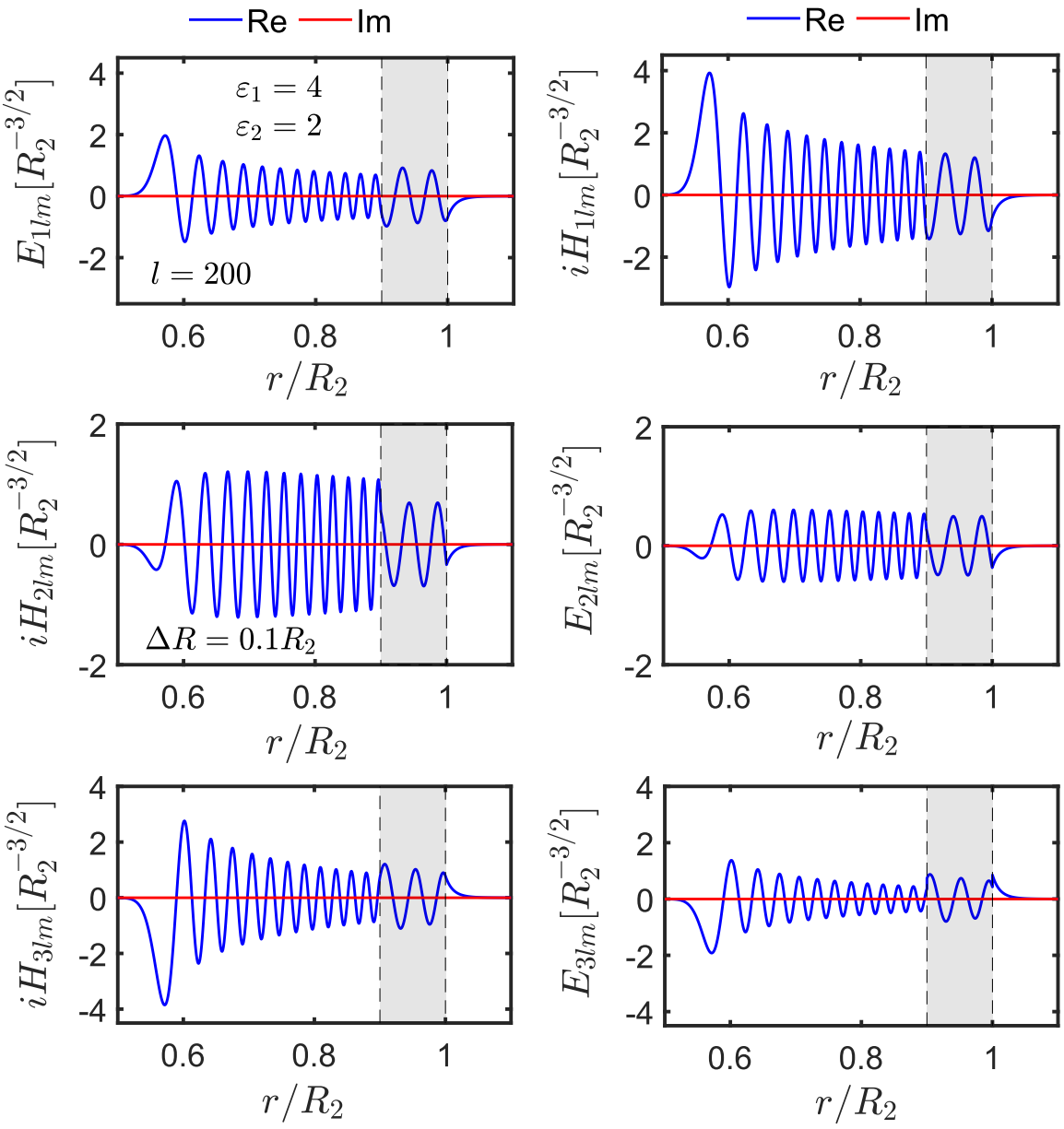

Figure 5.3. The real part (blue) and imaginary part (red) of the radial dependence of the electric and magnetic fields of the TE (left panels) and TM (right panels) polarizations of the quasi-degenerate TE and TM modes, shown in Fig. 5.2(c), of the core-shell system of $\varepsilon_1 = 4$, $\varepsilon_2 = 4$, $\Delta R/R_2 = 0.1$, and mode order $l = 200$. The shaded area represents the shell.

sphere maintain approximately a consistent distance, around 0.4 between the shown modes for high $l = 200$.

5.3.2 Normalization of the core-shell system

The normalization of TE and TM polarizations is given for spherical systems in VSHs in [61]. The TE resonant states of a spherical system are normalised according to

$$\begin{aligned} 1 = \int_0^{R_1} (\varepsilon_1 \mathcal{E}_{1lm}^2 + \mu_1 \mathcal{H}_{2lm}^2 + \mu_1 \mathcal{H}_{3lm}^2) dr + \int_{R_1}^{R_2} (\varepsilon_2 \mathcal{E}_{1lm}^2 + \mu_2 \mathcal{H}_{2lm}^2 + \mu_2 \mathcal{H}_{3lm}^2) dr \\ + \frac{R}{k_n} (\mathcal{H}_{2lm} \mathcal{E}'_{1lm} - \mathcal{E}_{1lm} \mathcal{H}'_{2lm})|_{r=R_+}, \end{aligned} \tag{5.40}$$

where all derivatives are taken with respect to r. Considering a core-shell system in vacuum, Eq. (5.40) yields

$$\begin{aligned} 1 = \left(A_n^{\mathrm{TE}}\right)^2 \Bigg\{ R_1 \left[(\varepsilon_1 - \varepsilon_2) J_{11}^2 + \varepsilon_1 \left(1 - \frac{\mu_2}{\mu_1}\right) J_{11}'^2 - \left(\frac{1}{\mu_1} - \frac{1}{\mu_2}\right) \frac{\alpha^2 J_{11}^2}{(k_n R_1)^2} \right] \\ + \left(\frac{B_n^{\mathrm{TE}}}{A_n^{\mathrm{TE}}}\right)^2 R_2 \left[(\varepsilon_2 - 1) H_{32}^2 + (\mu_2 - 1) H_{32}'^2 - \left(\frac{1}{\mu_2} - 1\right) \frac{\alpha^2 H_{32}^2}{(k_n R_2)^2} \right] \Bigg\}. \end{aligned} \tag{5.41}$$

The normalization condition of TM eigen wavefunctions is given by [61]

$$\begin{aligned} 1 = \int_0^{R_1} (\mu_1 \mathcal{H}_{1lm}^2 + \varepsilon_1 \mathcal{E}_{2lm}^2 + \varepsilon_1 \mathcal{E}_{3lm}^2) dr + \int_{R_1}^{R_2} (\mu_2 \mathcal{H}_{1lm}^2 + \varepsilon_2 \mathcal{E}_{2lm}^2 + \varepsilon_2 \mathcal{E}_{3lm}^2) dr \\ + \frac{R}{k_n} (\mathcal{E}_{2lm} \mathcal{H}'_{1lm} - \mathcal{H}_{1lm} \mathcal{E}'_{2lm})|_{r=R_+}, \end{aligned} \tag{5.42}$$

leading to

$$\begin{aligned} 1 = \left(A_n^{\mathrm{TM}}\right)^2 \Bigg\{ R_1 \left[(\mu_1 - \mu_2) J_{11}^2 + \mu_1 \left(1 - \frac{\varepsilon_2}{\varepsilon_1}\right) J_{11}'^2 - \left(\frac{1}{\varepsilon_1} - \frac{1}{\varepsilon_2}\right) \frac{\alpha^2 J_{11}^2}{(k_n R_1)^2} \right] \\ + \left(\frac{B_n^{\mathrm{TM}}}{A_n^{\mathrm{TM}}}\right)^2 R_2 \left[(\mu_2 - 1) H_{32}^2 + (\varepsilon_2 - 1) H_{32}'^2 - \left(\frac{1}{\varepsilon_2} - 1\right) \frac{\alpha^2 H_{32}^2}{(k_n R_2)^2} \right] \Bigg\}. \end{aligned} \tag{5.43}$$

In the sphere limits, we take $R_1 = R$, $\varepsilon_2 = 1$, and $\mu_2 = 1$. The normalization given by Eq. (5.41) is then reduced to the sphere's normalization,

$$1 = \left(A_n^{\text{TE}}\right)^2 R\left[(\varepsilon-1)J^2(z) + \varepsilon\left(\frac{\mu-1}{\mu}\right)J'^2(z) + \frac{\alpha_l^2 J^2(z)}{(k_n R)^2}\left(\frac{\mu-1}{\mu}\right)\right], \tag{5.44}$$

for TE, and

$$1 = \left(A_n^{\text{TM}}\right)^2 R\left[(\mu-1)J^2(z) + \mu\left(\frac{\varepsilon-1}{\varepsilon}\right)J'^2(z) + \frac{\alpha_l^2 J^2(z)}{(k_n R)^2}\left(\frac{\varepsilon-1}{\varepsilon}\right)\right], \tag{5.45}$$

for TM, where $z = nk_nR$, which is in accordance with the magnetic sphere in vacuum in [61]. We note that to obtain the normalization constants for TM, one can replace each ε with μ and vise versa [61]. Therefore the normalization constants of TE and TM are identical for a magnetic sphere with $\varepsilon = \mu$. For a non-magnetic sphere in vacuum, used in the previous RSE literature [14][61], $\mu_1 = 1$, and the normalization is further reduced to $1 = \left(A_n^{\text{TE}}\right)^2 R(\varepsilon-1)J^2(z)$ for TE, and $1 = \left(A_n^{\text{TM}}\right)^2 R\frac{\varepsilon-1}{\varepsilon}\left[J_n'^2(z) + \frac{\alpha_l^2 J^2(z)}{(k_n R)^2}\right]$ for TM modes. The normalized fields of the quasi-degenerate TE and TM modes, shown in the spectrum in Fig. 5.2 (c), of the core-shell system are plotted in Fig. 5.3, where the TE components are shown in the left panels while the right panels shows the TM components, both in VSHs.

5.4 Introducing chirality to the magnetic sphere: resonant states and secular equation

We now derive a general secular equation for an arbitrary sphere in an arbitrary surrounding medium having constant permittivity, permeability and chirality inside or outside the sphere, described by Eqs. (5.10)-(5.15). Since chirality couples the components of the electric and magnetic fields we combine the same components of the

electric and magnetic field in a column vector and write the equations as [88]

$$\begin{pmatrix} \mathcal{E}'_{2lm} \\ \mathcal{H}'_{2lm} \end{pmatrix} - \frac{\alpha}{r} \begin{pmatrix} \mathcal{E}_{3lm} \\ \mathcal{H}_{3lm} \end{pmatrix} = kM(r) \begin{pmatrix} \mathcal{E}_{1lm} \\ \mathcal{H}_{1lm} \end{pmatrix}, \tag{5.46}$$

$$\begin{pmatrix} \mathcal{E}'_{1lm} \\ \mathcal{H}'_{1lm} \end{pmatrix} = -kM(r) \begin{pmatrix} \mathcal{E}_{2lm} \\ \mathcal{H}_{2lm} \end{pmatrix}, \tag{5.47}$$

$$-\frac{\alpha}{r} \begin{pmatrix} \mathcal{E}_{1lm} \\ \mathcal{H}_{1lm} \end{pmatrix} = kM(r) \begin{pmatrix} \mathcal{E}_{3lm} \\ \mathcal{H}_{3lm} \end{pmatrix}, \tag{5.48}$$

where

$$M(r) = \begin{pmatrix} -\kappa(r) & \mu(r) \\ \varepsilon(r) & -\kappa(r) \end{pmatrix}. \tag{5.49}$$

Using Eqs. (5.46) and (5.48) in the derivative of Eq. (5.47) leads to

$$\begin{pmatrix} \mathcal{E}''_1 \\ \mathcal{H}''_1 \end{pmatrix} - \frac{\alpha^2}{r^2} \begin{pmatrix} \mathcal{E}_{1lm} \\ \mathcal{H}_{1lm} \end{pmatrix} = -k^2 M^2(r) \begin{pmatrix} \mathcal{E}_{1lm} \\ \mathcal{H}_{1lm} \end{pmatrix}. \tag{5.50}$$

The matrix $M(r)$ has the eigenvalues $\lambda = \pm n_\pm(r)$, where $n_\pm(r)$ represents the refractive index of the system as $n_\pm(r) = \sqrt{\varepsilon(r)\mu(r)} \pm \kappa(r)$, and has the corresponding eigenfunctions

$$\begin{pmatrix} \sqrt{\mu}(r) \\ \pm\sqrt{\varepsilon}(r) \end{pmatrix}. \tag{5.51}$$

The the solution then has the form

$$\begin{pmatrix} \mathcal{E}_{1lm} \\ \mathcal{H}_{1lm} \end{pmatrix} = \begin{pmatrix} \sqrt{\mu}(r) \\ \sqrt{\varepsilon}(r) \end{pmatrix} \psi_+(r) + \begin{pmatrix} \sqrt{\mu}(r) \\ -\sqrt{\varepsilon}(r) \end{pmatrix} \psi_-(r). \tag{5.52}$$

Using the last equation in Eq. (5.47), we get

$$\begin{pmatrix} \mathcal{E}_{2lm} \\ \mathcal{H}_{2lm} \end{pmatrix} = -\begin{pmatrix} \sqrt{\mu}(r) \\ \sqrt{\varepsilon}(r) \end{pmatrix} \psi'_+(r) + \begin{pmatrix} \sqrt{\mu}(r) \\ -\sqrt{\varepsilon}(r) \end{pmatrix} \psi'_-(r), \tag{5.53}$$

and

$$\begin{pmatrix} \mathcal{E}_{3lm} \\ \mathcal{H}_{3lm} \end{pmatrix} = \frac{-\alpha}{kr} M^{-1}(r) \left[\begin{pmatrix} \sqrt{\mu}(r) \\ \sqrt{\varepsilon}(r) \end{pmatrix} \psi_+(r) + \begin{pmatrix} \sqrt{\mu}(r) \\ -\sqrt{\varepsilon}(r) \end{pmatrix} \psi_-(r) \right], \tag{5.54}$$

with $\psi_\pm(r)$ satisfying Bessel's equation

$$\psi''_\pm(r) - \frac{\alpha^2}{r^2}\psi_\pm(r) = -k^2 n_\pm^2(r)\psi_\pm(r)\,. \tag{5.55}$$

By considering purely outgoing boundary conditions and defining $n_\pm(r)$ as $q_\pm$ inside the sphere and $p_\pm$ outside the sphere, the resonant state $\psi_{n_\pm(r)}$ takes the form

$$\psi_{n_\pm}(r) = \begin{cases} A_\pm J(q_\pm k_n r)\,, & r \leq R \\ B_\pm H(p_\pm k_n r)\,, & r \geq R\,, \end{cases} \tag{5.56}$$

where $J(q_\pm k_n r) = q_\pm k_n r j_l(q_\pm k_n r)$ and $H(p_\pm k_n r) = p_\pm k_n r h_l^{(1)}(p_\pm k_n r)$, with $q_\pm = \sqrt{\varepsilon\mu} \pm \kappa$ and $p_\pm = \sqrt{\varepsilon_b\mu_b} \pm \kappa_b$. Applying Maxwell's boundary conditions yields

$$\sqrt{\mu}A_+J_+ + \sqrt{\mu}A_-J_- = \sqrt{\mu_b}B_+H_+ + \sqrt{\mu_b}B_-H_-\,, \tag{5.57}$$

$$\sqrt{\varepsilon}A_+J_+ - \sqrt{\varepsilon}A_-J_- = \sqrt{\varepsilon_b}A_+H_+ - \sqrt{\varepsilon_b}A_-H_-\,, \tag{5.58}$$

$$-\sqrt{\mu}A_+J'_+ + \sqrt{\mu}A_-J'_- = -\sqrt{\mu_b}B_+H'_+ + \sqrt{\mu_b}B_-H'_-\,, \tag{5.59}$$

$$\sqrt{\varepsilon}A_+J'_+ + \sqrt{\varepsilon}A_-J'_- = \sqrt{\varepsilon_b}A_+H'_+ + \sqrt{\varepsilon_b}A_-H'_-\,, \tag{5.60}$$

where the arguments are dropped from the functions in the above equations for brevity, and $J_\pm = J(q_\pm k_n R)$ and $H_\pm = H(p_\pm k_n R)$. The set of the above equations results in the following compact secular equation,

$$\begin{aligned} &-4\sqrt{\mu\varepsilon_b\varepsilon\mu_b}(J_+J_-H'_+H'_- + J'_+J'_-H_+H_-) \\ &+(\sqrt{\mu\varepsilon_b} - \sqrt{\varepsilon\mu_b})^2(J_+J'_-H_+H'_- + J'_+J_-H'_+H_-) \\ &+(\sqrt{\mu\varepsilon_b} + \sqrt{\varepsilon\mu_b})^2(J_+J'_-H'_+H_- + J'_+J_-H_+H'_-) = 0\,, \end{aligned} \tag{5.61}$$

for a chiral sphere in a chiral surrounding medium. We use the secular equation Eq. (5.61) to verify our RSE results for treating homogeneous chirality perturbations inside and outside the sphere in Chapter 6.

5.5 Summary

In this chapter, we have provided the analytical solution for non-dispersive spherically symmetric systems: a basic sphere and core-shell system. Both systems are described by constant permittivity and permeability profiles. We have discussed the possibility of achieving degeneracy in TE and TM resonant states by analyzing their secular equations, which determine their wavenumbers. A strict degeneracy can be achieved in a sphere by maintaining an identical ratio of the permittivity to the permeability between the interior and exterior mediums of the sphere. A special case occurs when the permittivity is identical to the permittivity, which makes the electric and magnetic fields of the TE and TM modes are identical. Introducing the shell compensates for the contrast in the ratio of permittivity to permeability between the core and the external surrounding medium. This allows for finding degenerate modes in a non-magnetic core-shell system in vacuum at selective values of thickness and permittivity of the shell. At the end of this chapter, we have derived the secular equation of the sphere, considering isotropic chirality either inside or outside the sphere.

Chapter 6

Employing degenerate modes for chirality sensing

6.1 Motivation

Chirality, or handedness, is a property of objects that cannot be superimposed on their mirror images by any translational or rotational transformations like human hands [89]. Other popular examples include objects with spiral shapes, such as screws and snails' shells. At the molecular scale, the majority of biological molecules, if not all, are chiral [90]. Chiral molecules are known as enantiomers, and the two mirror-images are distinguished as left-handed and right-handed enantiomers. Although enantiomers share identical chemical structure, right-handed and left-handed enantiomers or a mixture of both may interact differently and cause different biological effects [91]. Left-handed Thalidomide, for example, causes severe birth defects, whereas the right-handed Thalidomide is sedative and relieves nausea, and the prescription of a mixture of both handedness leads to severe genetic complications [90, 92]. In another extreme case, one handedness of Penicillamine is a cure for Wilson's disease, an inherited condition results in access of copper in the human body [93], and the other handedness is toxic [94].

Such a significant impact of chirality on life science applications in general and drug development in particular generates a wide interest in understanding and improving

chirality sensing schemes. Sensing chiral molecules essentially relies on the interaction of such materials with light. The rotation angle of a linearly polarized light passing through a chiral medium is known as the optical activity, determined by the real part of chirality κ [89]. The imaginary part of κ, on the other hand, leads to a differential absorption of left and right-handed circularly polarized light, known as circular dichroism (CD) [89]. Opposite handedness has opposite sign of κ and thus different optical activity and CD signal. However, chiral light-matter interaction is rather weak with typical values of chirality $\kappa \approx 10^{-4}$ [29, 84], therefore improving chirality sensing schemes requires boosting the optical response of chiral molecules, as has already been established in nanophotonic systems [95, 96].

The light interaction with chiral systems is rigorously explained as perturbation of resonant states [84]. They reported that the first-order resonance shift due to chirality perturbation is zero for any geometrically achiral resonator, and does not contribute to the CD signal. The case of degenerate modes was not included in their analysis. Recently, Chen *et al.*, reported that strong coupling of quasi bound states in the continuum can be achieved by introducing chirality perturbation to a metasurface structure. This was achieved by utilising a pair of degenerate quasi bound states in the continuum. Degeneracy converts the dependence of their splitting on chirality from second order to first order. Such chirality-induced coupling was shown to enhance chirality sensing (CD signal) by order of magnitudes [29].

In this chapter [97], we use the RSE to rigorously derive the linear splitting of degenerate modes in chirality. We employ the RSE truncated to only two modes in the basis to calculate the perturbed modes resulting from a presence of a chiral medium or chiral molecule. In our analysis, we focus on spherically symmetric systems and demonstrate linear splitting using quasi-degenerate modes of spherical systems presented in Chapter 5. The magnetic sphere of permittivity identical to its permeability plays the role of a proof of principle, and the core-shell system provides an experimentally more relevant example. Although handedness, the sign of κ, is indistinguishable from the proposed analysis, the splitting of degenerate modes is linear with the concentration since κ is proportional to the number of molecules [96].

6.2 Two-mode RSE

In this section, we derive an explicit form of the perturbed mode using the two-mode RSE [27]. The truncation of the RSE to two modes only in the basis is justified by the local RSE [8]. The local basis keeps only the resonant states which are close in frequency to the state of interest or have the biggest overlap matrix elements with this state.

We start by considering a general case of two resonant states used as a basis in the RSE equation, given by Eq. (1.35):

$$k_1 c_1 = k\left[(V_{11}+1)c_1 + V_{12}c_2\right] , \tag{6.1}$$

$$k_2 c_2 = k\left[(V_{21}c_1 + (V_{22}+1)c_2\right] . \tag{6.2}$$

The latter equation can be rearranged as,

$$\frac{1}{\alpha}\begin{pmatrix} \bar{k}_1 & -V_{12}k_2 \\ -V_{21}k_1 & \bar{k}_2 \end{pmatrix}\begin{pmatrix} c_1 \\ c_2 \end{pmatrix} = k\begin{pmatrix} c_1 \\ c_2 \end{pmatrix} , \tag{6.3}$$

where $\alpha = (1+V_{11})(1+V_{22}) - V_{12}V_{21}$, and the diagonal elements $\bar{k}_1$ and $\bar{k}_2$ are given by

$$\bar{k}_1 = [V_{22}+1]\,k_1 , \qquad \bar{k}_2 = [V_{11}+1]\,k_2 . \tag{6.4}$$

We obtain the perturbed modes by diagonalizing the matrix in Eq. (6.3), resulting in the perturbed wavenumbers,

$$k_\pm = \frac{\bar{k}_1 + \bar{k}_2}{2\alpha} \pm \frac{1}{\alpha}\sqrt{\left(\frac{\bar{k}_1 - \bar{k}_2}{2}\right)^2 + k_1 k_2 V_{12}V_{21}} , \tag{6.5}$$

with the generalized RSE matrix elements

$$\begin{aligned} V_{nm}(k,r) = \int_V \left[\mathbf{E}_n \cdot \Delta\hat{\boldsymbol{\varepsilon}}(k,r)\mathbf{E}_m + \mathbf{E}_n \cdot \Delta\hat{\boldsymbol{\xi}}(k,r)\mathbf{H}_m\right] d\mathbf{r} \\ - \int_V \left[\mathbf{H}_n \cdot \Delta\hat{\boldsymbol{\zeta}}(k,r)\mathbf{E}_m + \mathbf{H}_n \cdot \Delta\hat{\boldsymbol{\mu}}(k,r)\mathbf{H}_m\right] d\mathbf{r} . \end{aligned} \tag{6.6}$$

6.2.1 Matrix elements for spherical systems

In the following, we discuss the matrix elements V_{nm} in Eq. (6.6) when two modes of a non-chiral spherical system are used as a basis to calculate the perturbed modes caused by a presence of a chiral perturber. We assume here that the system is isotropic and non-dispersive.

Owing to the orthogonality of the electric and magnetic field of the same polarization of light in spherical systems, the terms containing chirality perturbation never appear in the matrix elements V_{nm} when the two resonant states are of the same polarization, i.e, TE and TE or TM and TM. The matrix elements in this case simply are

$$V_{12} = \int_V \mathbf{E}_1 \cdot \Delta\varepsilon \mathbf{E}_2 \, d\mathbf{r} - \int_V \mathbf{H}_1 \cdot \Delta\mu \mathbf{H}_2 \, d\mathbf{r} \,, \tag{6.7}$$

where the r dependence is dropped for brevity. However, when the modes are of different polarization (TE and TM modes), the chirality terms appear in the matrix elements V_{12} and V_{21} only, and the matrix elements become

$$V_{11} = \int_V \mathbf{E}_1 \cdot \Delta\varepsilon \mathbf{E}_1 \, d\mathbf{r} - \int_V \mathbf{H}_1 \cdot \Delta\mu \mathbf{H}_1 \, d\mathbf{r} \,, \tag{6.8}$$

$$V_{22} = \int_V \mathbf{E}_2 \cdot \Delta\varepsilon \mathbf{E}_2 \, d\mathbf{r} - \int_V \mathbf{H}_2 \cdot \Delta\mu \mathbf{H}_2 \, d\mathbf{r} \,, \tag{6.9}$$

and

$$V_{12} = V_{21} = -i \int_V \left[\mathbf{E}_1 \cdot \kappa \mathbf{H}_2 + \mathbf{H}_1 \cdot \kappa \mathbf{E}_2 \right] d\mathbf{r} \,, \tag{6.10}$$

with V_{12} and V_{21} being symmetric for reciprocal systems in general.

6.3 Chirality contribution in mode splitting

Assuming zero variations in the permittivity and permeability in Eqs. (6.8) and (6.9), the matrix elements V_{11} and V_{22} vanish, and the perturbed wavenumbers Eq. (6.5) take

the following form

$$k_{\pm} = \frac{k_1 + k_2}{2\alpha} \pm \frac{1}{\alpha}\sqrt{\left(\frac{k_1 - k_2}{2}\right)^2 + k_1 k_2 V_{12} V_{21}}\,, \tag{6.11}$$

with $\alpha = 1 - V_{12}V_{21}$. The splitting of the two modes due to chirality perturbation becomes

$$k_+ - k_- = \frac{2}{\alpha}\sqrt{\left(\frac{k_1 - k_2}{2}\right)^2 + k_1 k_2 V_{12} V_{21}}\,. \tag{6.12}$$

It follows from Eq. (6.12) that chirality contribution to the mode splitting is quadratic. In principle, the chirality contribution can be converted to first order in the limit

$$\left|\sqrt{k_1 k_2} V_{12}\right| \gg \left|\frac{k_1 - k_2}{2}\right|\,, \tag{6.13}$$

which results in a linear splitting of the perturbed modes in chirality,

$$k_+ - k_- \approx 2V_{12}k_1\,, \tag{6.14}$$

It follows from Eq. (6.13) that the limit can be achieved by minimising the initial splitting of the mode $k_1 - k_2$ while boosting the matrix element V_{12}. The former is fulfilled for quasi-degenerate modes, and the latter can be obtained by increasing the overlap integral of $\mathbf{E}_1$ with $i\mathbf{H}_2$ and $i\mathbf{H}_1$ with $\mathbf{E}_2$ in accordance with Eq. (6.10)

For a magnetic sphere with $\beta = \beta_b$, i.e, the ratio of the permittivity to permeability of the sphere and the surrounding medium are equal, the TE and TM modes are strictly degenerate, eliminating the initial splitting of the modes. For a magnetic sphere with permittivity identical to its permittivity and located in vacuum ($\beta = \beta_b = 1$), not only the modes of TE and TM are degenerate, but also the electric and magnetic fields of TE and TM are identical, and here we get

$$\mathbf{E}_1 = i\mathbf{H}_2\,, \qquad i\mathbf{H}_1 = \mathbf{E}_2\,. \tag{6.15}$$

Thus, the TE and TM degenerate resonant states of the magnetic sphere, having $\varepsilon = \mu$ and surrounded by vacuum, are ideal basis for achieving the linear limit in Eq. (6.14),

taking into account negligible variations of the permittivity and/or permeability.

While the magnetic sphere plays the role of a test system to our theory, we also consider a non-magnetic core-shell system as a more realistic illustration, in which the degeneracy of TE and TM modes is achievable as we showed in Chapter 5. Further, the shell compensates for the contrast between the permittivity of the core and environment, bringing the wavefunctions of the electric field and magnetic field closer to each other, which ultimately increases the overlap integral in V_{12}.

6.4 Application 1: a magnetic sphere

A magnetic sphere of radius R, surrounded by vacuum, with permeability identical to its permittivity has identical spectra of its TE and TM modes and identical TE and TM fields. The spectrum of the degenerate TE and TM modes of a sphere with $\varepsilon = \mu = 4$, and surrounded by vacuum, is shown in Fig. 6.1 (a) for low angular momentum, $l = 5$. The electric and magnetic fields of TE and TM polarizations are shown for the fundamental mode $k_1R = k_2R = 2.22 - 9.45 \times 10^{-5}i$ on the right inset, demonstrating the exact equivalence of the electric and magnetic fields of TE polarization to the magnetic and electric fields in TM polarization.

The splitting of the degenerate TE and TM fundamental modes due to application of homogeneous chirality perturbation $\kappa = 10^{-3}$ in the core is demonstrated in the left inset. The splitting of the fundamental degenerate modes is plotted versus chirality in Fig. 6.1 (b), for homogeneous chirality perturbations either inside or outside the sphere. The splitting of the modes is linear in chirality in accordance with the RSE analysis Eq. (6.14). The matrix elements of chirality perturbation outside the sphere was treated by regularization. Notably, when chirality perturbation is considered inside the sphere, the splitting is higher due to higher value of the overlap integral inside the sphere. The absolute value of the overlap integral in Eq. (6.10) is 0.23 inside the sphere and 0.06 outside the sphere.

When we slightly altered the permittivity of the sphere, we impose an initial

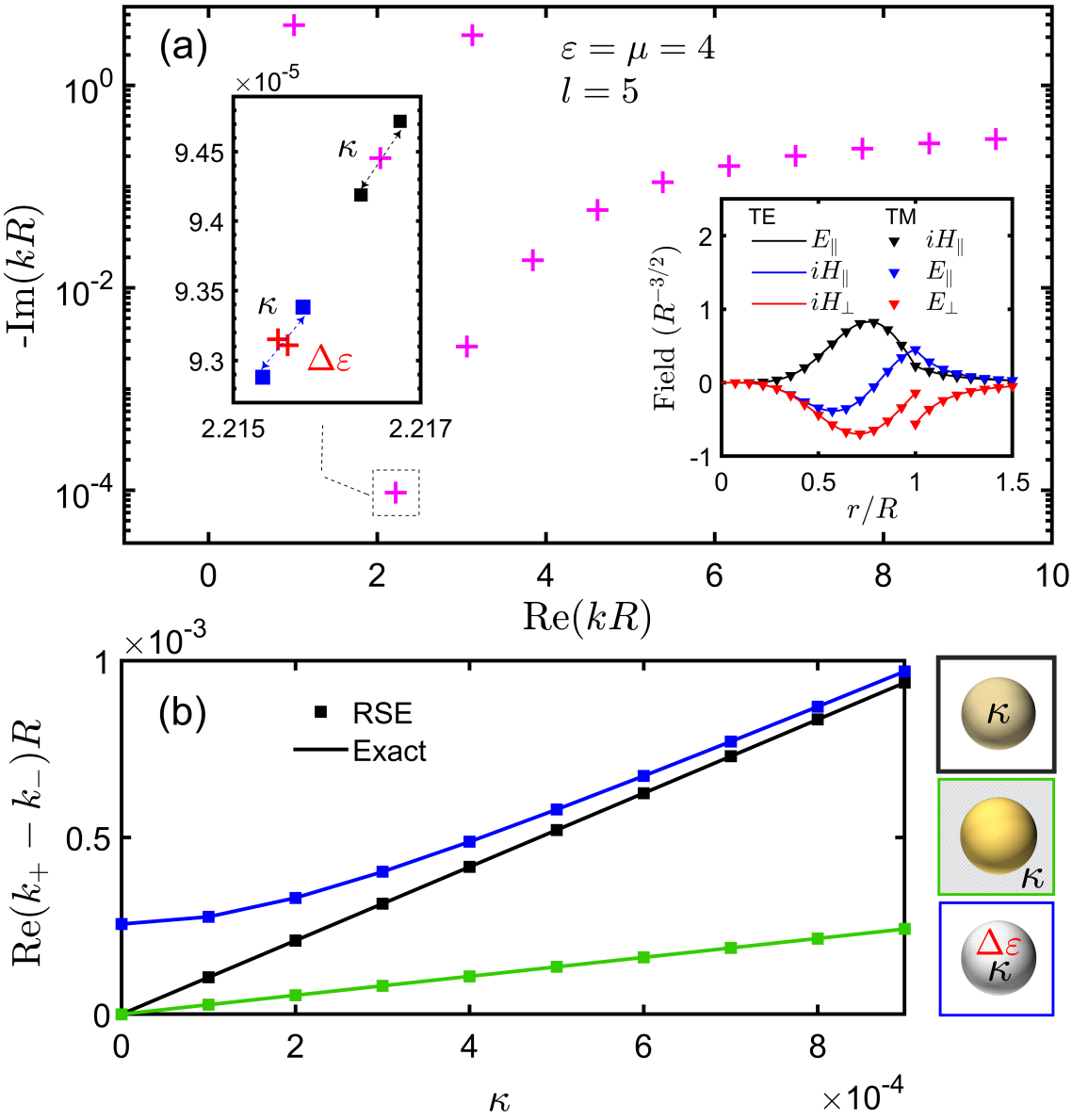

Figure 6.1. (a) Wavenumbers (magenta pluses) of degenerate TE and TM resonant states of a sphere of $\varepsilon = \mu = 4$ and radius R, located in vacuum. The splitting of the fundamental mode (purple plus) is shown in the left inset as two black squares due to $\kappa = 10^{-3}$ inside the sphere. In the same inset, the splitting of non-degenerate TE and TM modes of the sphere due to $\Delta\varepsilon = 0.01$ (red crosses) and due to chirality perturbation applied on top (blue squares). Right inset: radial dependence of tangential ($\parallel$) and normal ($\perp$) components of the normalized electric and magnetic fields of the fundamental WGM of TE (lines) and TM (triangles) resonant states. (b) The splitting of the modes Eq. (6.12), calculated using the RSE (squares) and secular equation (lines) versus chirality considered inside (black) and outside (green) the sphere of $\varepsilon = \mu = 4$, and inside the sphere with a slight change in the permittivtiy $\Delta\varepsilon = 0.01$ (blue). The corresponding schematics are shown in right.

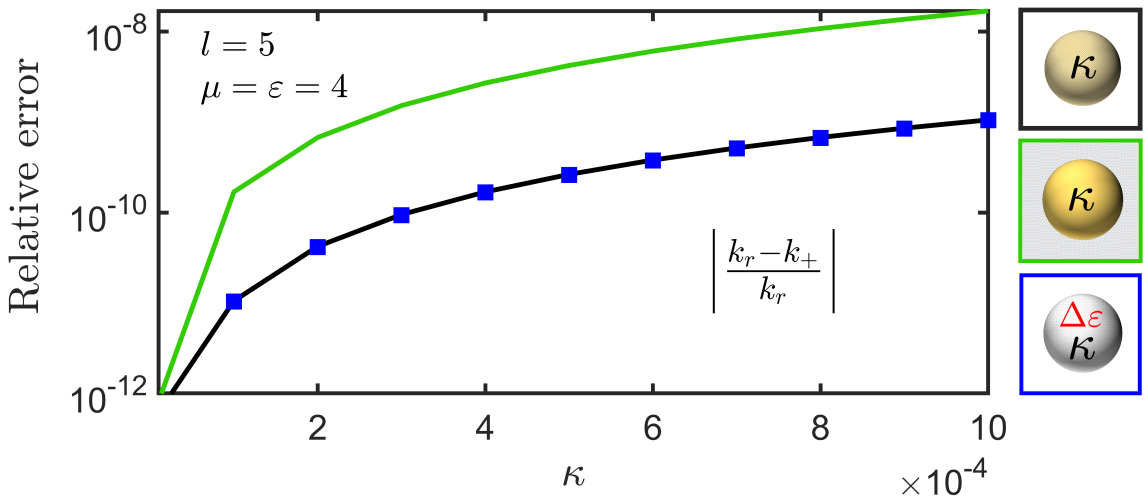

Figure 6.2. The error of the eigen wavenumber k_+, calculated by the RSE for chirality perturbation inside (black line), outside (green line) a sphere of $\varepsilon = \mu$, located in vacuum, and inside a sphere with $\varepsilon = 4.01$ and $\mu = 4$ (blue squares), shown in the schematics in (a), (b), and (c), respectively. The error is relative to the real value k_r, calculated analytically from the secualr equation.

splitting of the modes, given by $\Delta\bar{k} = k_1(V_{22} - V_{11})$, where $\bar{k}$ is the perturbed mode caused by the permittivity perturbation. This initial splitting breaks the strict degeneracy of the modes. In the inset of Fig. 6.1, we show the initial splitting of the fundamental modes k_1 and k_2 in the complex plane due to permittivity perturbation $\Delta\varepsilon = 0.01$. The modes further split when chirality perturbation of $\kappa = 10^{-3}$ is applied inside the sphere, as shown in the same inset. In Fig. 6.1(b), we show the splitting of such non-degenerate fundamental modes, corresponding to $\Delta\varepsilon = 0.01$, due to applying chirality perturbation inside the sphere. The splitting is quadratic in κ when the initial splitting $\Delta\bar{k} = 2.6 \times 10^{-4}$ is larger than κ. For larger values of κ, the quadratic shift transforms to a linear dependence.

The secular equation of an isotropic chiral sphere in a chiral surrounding medium, derived in Chapter 5, is used to calculate the exact values k_r of the wavenumbers. The relative error of the mode k_+, calculated by the RSE, considering chirality perturbation inside and outside the sphere of $\varepsilon = \mu = 4$ and inside the perturbed sphere with $\varepsilon = 4.01$ and $\mu = 4$ is shown in Fig. 6.2 versus κ. The error reflects the good agreement of the RSE results with the exact values for the three cases. Using the regularized

matrix elements for chirality perturbation outside the sphere leads to one order of magnitude rise in the relative error, in comparison to the perturbation inside the sphere. The matrix elements are provided in Appendix B in Sec. B.1 for homogeneous chirality perturbations inside and outside the sphere.

6.5 Application 2: a core-shell system

While the magnetic sphere of $\varepsilon = \mu$ provides a proof of principle to our theory, we tested the theory on a non-magnetic core-shell system located in vacuum as a more realistic system. We employ here the core-shell system of $\varepsilon_1 = 4$ and thickness $\Delta R = 0.1R_2$, and show in Fig. 6.3(a) the real parts of TE and TM modes for a selected range of the permittivity of the shell. The selected range corresponds to modes having high quality factor of $\approx 10^8$. The modes in the centre of Fig. 6.3(a) are shown in Fig. 6.3(b) and used as a basis to calculate the perturbed modes (black lines) due to homogeneous chirality perturbation $\kappa = 10^{-3}$ in the core.

Since chirality couples the electric and magnetic fields of TE and TM polarizations, the perturbed modes are a mixture of both TE and TM resonant states. This is demonstrated in Fig. 6.3(c), showing the absolute square of the expansion coefficients c_1 and c_2 of the lower perturbed mode, where the subscripts 1 and 2 refer to TE and TM, respectively. The expansion coefficients are nearly one half at $\varepsilon_2 = 2$, where the modes are quasi-degenerate, and exactly half of each polarization at the crossings of the modes. The expansion coefficients of the upper perturbed mode (not shown) is the mirror-image of the lower modes. The splitting of the pair of quasi-degenerate modes, $k_1R_2 = 179.409 - 3.08 \times 10^{-7}i$ and $k_2R_2 = 179.408 - 3.69 \times 10^{-7}i$, at $\varepsilon_2 = 2$ are plotted in Fig. 6.3(d) as functions of chirality, considered in the core, shell and surrounding medium. The splitting of the quasi-degenerate modes is linear and falls as one order of magnitude for each case, respectively. The reduction in the splitting for the perturbation in the shell and surrounding medium is again attributed to smaller values of the overlap integral over the perturbed volumes in the matrix element V_{12}. The overlap integral has the values 1.33, 0.1, and 0.007, for the core, shell, and surrounding

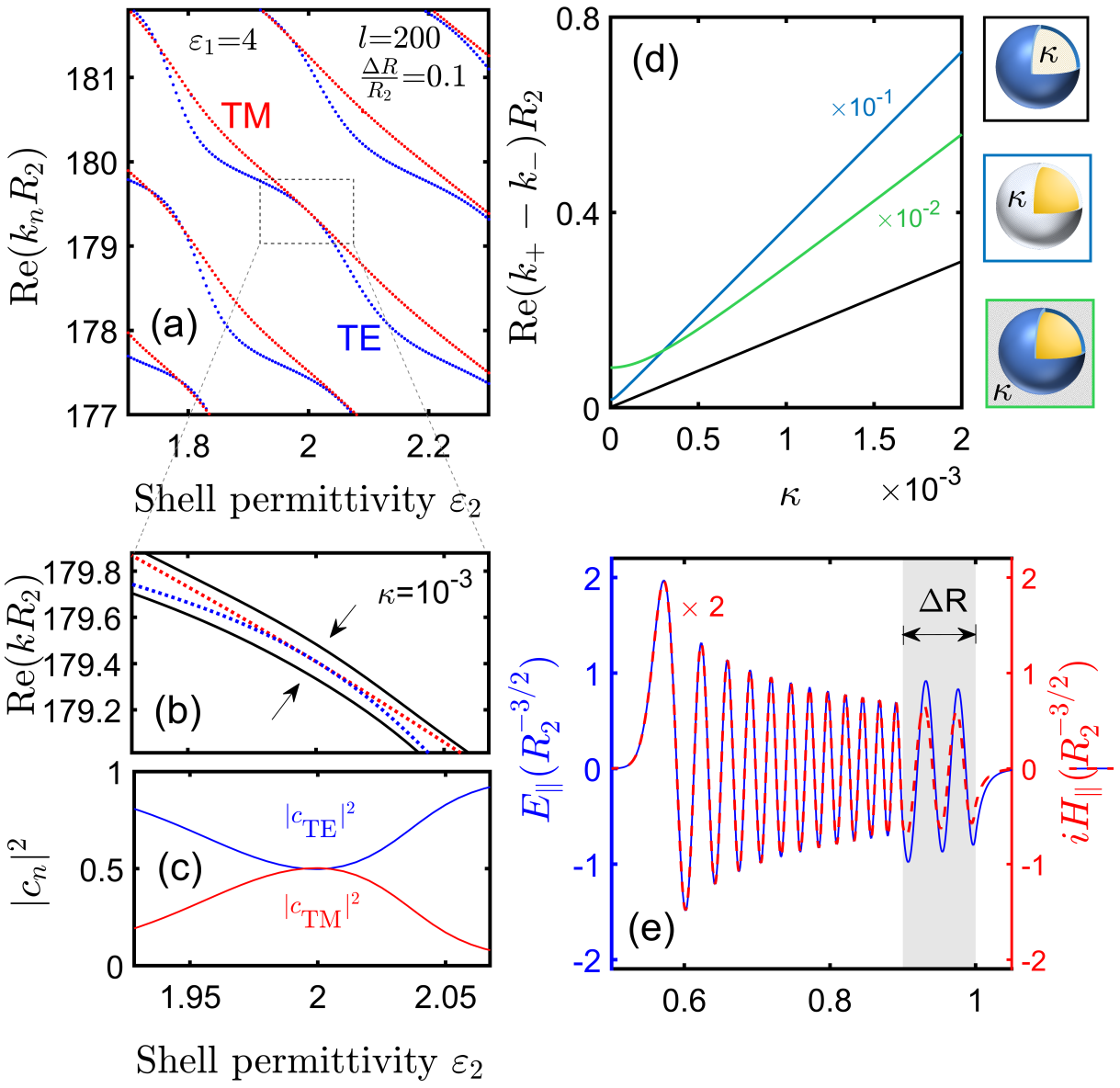

Figure 6.3. Real parts of the wavenumbers of TE (blue dots) and TM (red dots) modes with $l = 200$, of a core-shell system, with $\varepsilon_1 = 4$ in the core, shell thickness $\Delta R = 0.1R_2$ versus the permittivity of the shell ε_2. The quasi-degenerate modes at the centre of (a) are enlarged in (b), showing the split of the modes as chirality perturbation $\kappa = 10^{-3}$ is applied to the core. The expansion coefficients of the lower perturbed mode are shown in (c). The splitting of the two quasi-degenerate modes at $\varepsilon_2 = 2$ ($k_1R_2 = 179.409 - 3.08 \times 10^{-7}i$ and $k_2R_2 = 179.408 - 3.69 \times 10^{-7}i$) as a function of κ is shown in (d), considering chirality in the core (black), shell (blue), and outside the system (green), with the corresponding schematics shown to the right. The tangential components of the electric field of the TE mode (blue) and magnetic field of TM mode (red) are shown in (e). Note that the red curve in panel (e) and the blue and green in (e) are scaled for clarity. The actual results can be obtained by multiplying the curves with the factors of the same color.

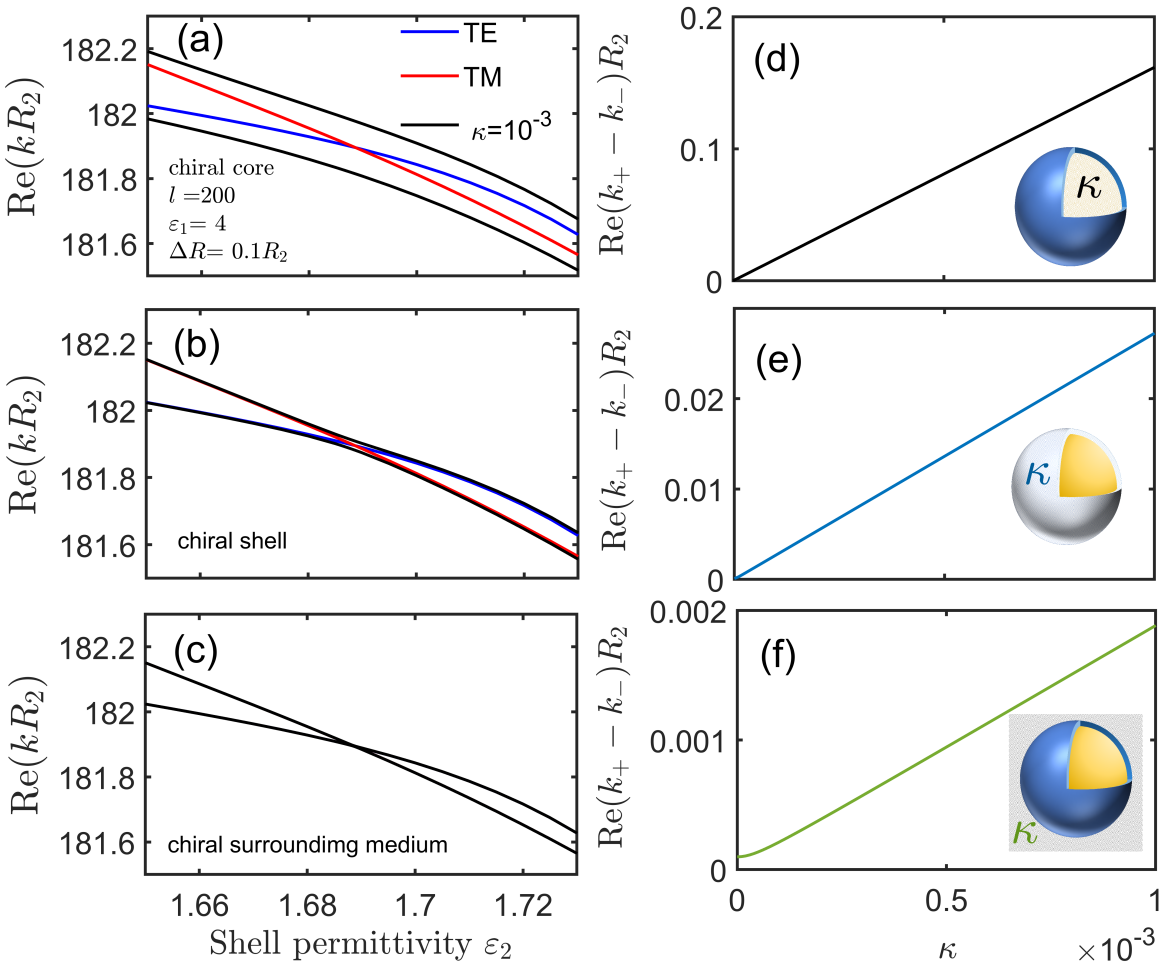

Figure 6.4. The real parts of the unperturbed wavenumbers of TE (blue line) and TM (red lines) modes with $l = 200$, of a core-shell system, having permittivity $\varepsilon_1 = 4$ of the core and thickness of the shell $\Delta R = 0.1$, used to calculate the perturbed modes (black lines) due to applying chirality in the (a) core, (b) shell, (c) surrounding medium, versus the permittivity of the shell ε_2. The splitting of the modes $k_1 R_2 = 181.3804 - 4.01 \times 10^{-6} i$ and $k_2 R_2 = 181.3803 - 2.87 \times 10^{-6} i$ at $\varepsilon_2 = 1.6887$, as a function of chirality strength κ, considering chirality in (d) the core, (e) shell, and (f) surrounding medium. The position of κ in the schematics on the right refers to the corresponding region of perturbation inside or outside the sphere, and the color of κ represents the chirality perturbation in the matching lines.

medium, respectively. For smaller values of κ, the splitting of the modes due to the presence of chirality in the surrounding medium appears quadratic for smaller values of κ below 5×10^{-4}. This is because $k_1 V_{12}$ is comparable to the initial splitting $|k_1 - k_2| \approx 8.2 \times 10^{-4}$, see the inequality Eq. (6.13). Figure 6.3(e) shows comparable values of the tangential components of the electric and the magnetic fields, at least within the core, due to introducing the shell which compensates for the difference between them.

Figure 6.4 shows another area in Fig. 6.3(a) with the real parts of the unperturbed modes and the perturbed due to applying chirality in the core (a), shell (b) and the surrounding medium (c) versus the permittivity of the shell. The quasi-degenerate modes at $\varepsilon_2 = 1.6887$ are $k_1 R_2 = 181.3804 - 4.01 \times 10^{-6} i$ and $k_2 R_2 = 181.3803 - 2.87 \times 10^{-6} i$, have smaller initial splitting $|k_1 - k_2| \approx 10^{-5}$ and quality factor $\approx 10^7$. The smaller initial splitting makes the linear splitting possible for smaller values of κ for the case of chiral surrounding medium. The splitting of the other modes due to chirality perturbation $\kappa = 10^{-3}$ in the core, shell, and surrounding medium can be seen in Fig. 6.5(a,b) as a function of both ε_2 ($\Delta R = 0.1$) and ΔR ($\varepsilon_2 = 2$). The dips represent the points of minimal initial splitting, where the response to chirality perturbations is more pronounced. The expansion coefficients as a function of the shell permittivity displaying both quasi-degenerate modes at $\varepsilon_2 = 2$ and $\varepsilon_2 = 1.6887$ are shown in Fig. 6.6. The crossing of expansion coefficients indicates full exchange of TE and TM resonant states at these positions as also demonstrated in [29]. The matrix elements for homogeneous chirality perturbations within the core, shell and the surrounding medium of the core-shell system are provided in Appendix B in Sec. B.1.

Lastly, we consider applying a point-like chiral perturber, expressed as Dirac delta function $\kappa(\mathbf{r}) = \kappa_p V_p \delta(\mathbf{r} - \mathbf{r}_p)$, where the parameters κ_p and V_p are the effective chirality and volume of the particle, respectively, and $\mathbf{r}_p = (r_p, \theta_p, \varphi_p)$ is the position of the particle. The presence of the chiral particle breaks the spherical symmetry, and the matrix elements in this case have contributions from all the degenerate modes with the magnetic quantum number m for a certain l. This means that the full RSE has to be considered with the matrix elements $V^{12}_{lm,l'm'}$, where the labels lm and $l'm'$ now

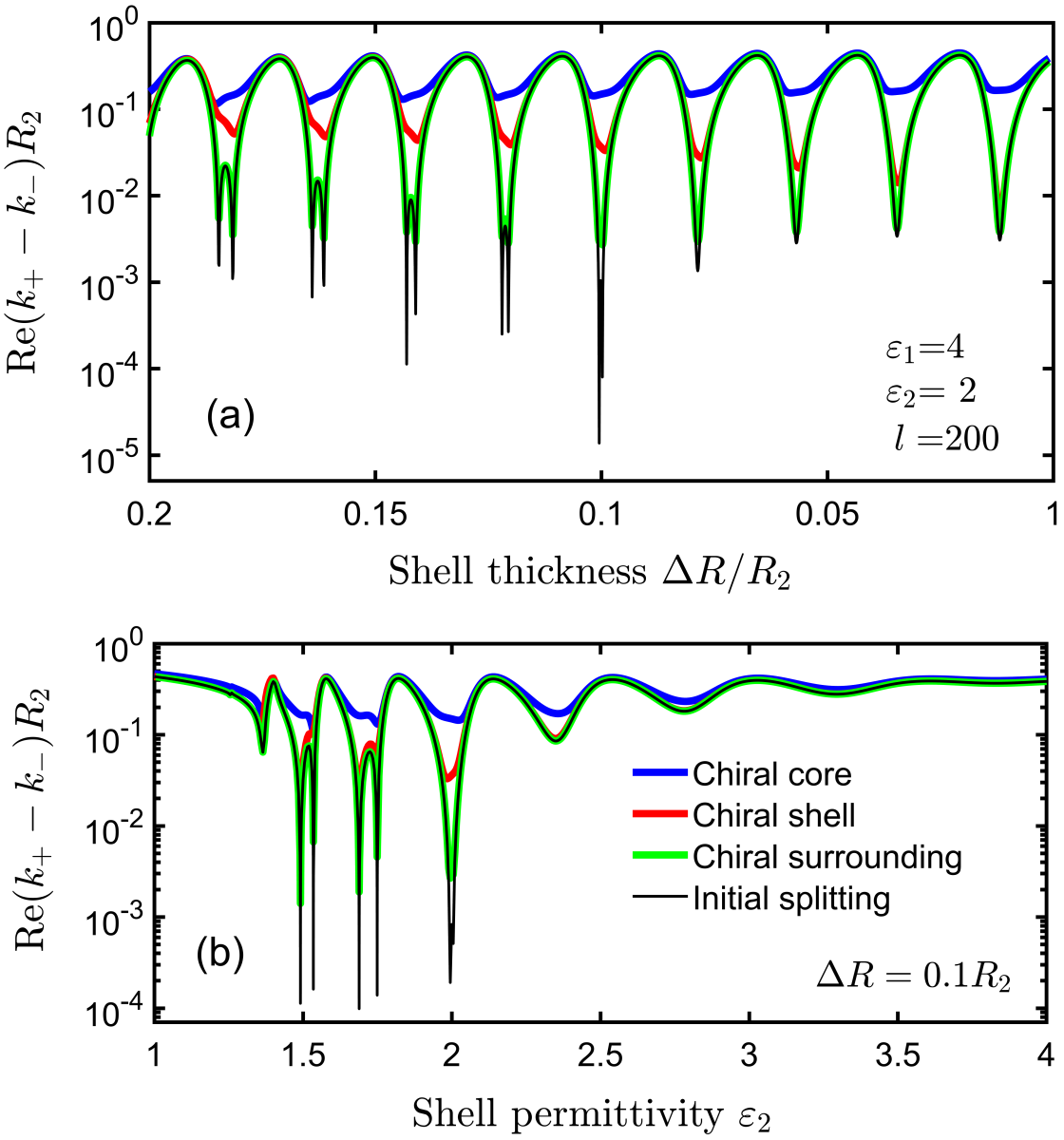

Figure 6.5. The splitting of the modes due to applying chirality perturbation $\kappa = 10^{-3}$ in the core (blue), shell (red), and the surrounding medium (green) versus (a) the shell thickness $\Delta R/R_2$ and (b) the shell permittivity ε_2. The initial splitting (black) when $\kappa = 0$ corresponds to the unperturbed modes used as a basis to calculate the chirality-induced splitting.

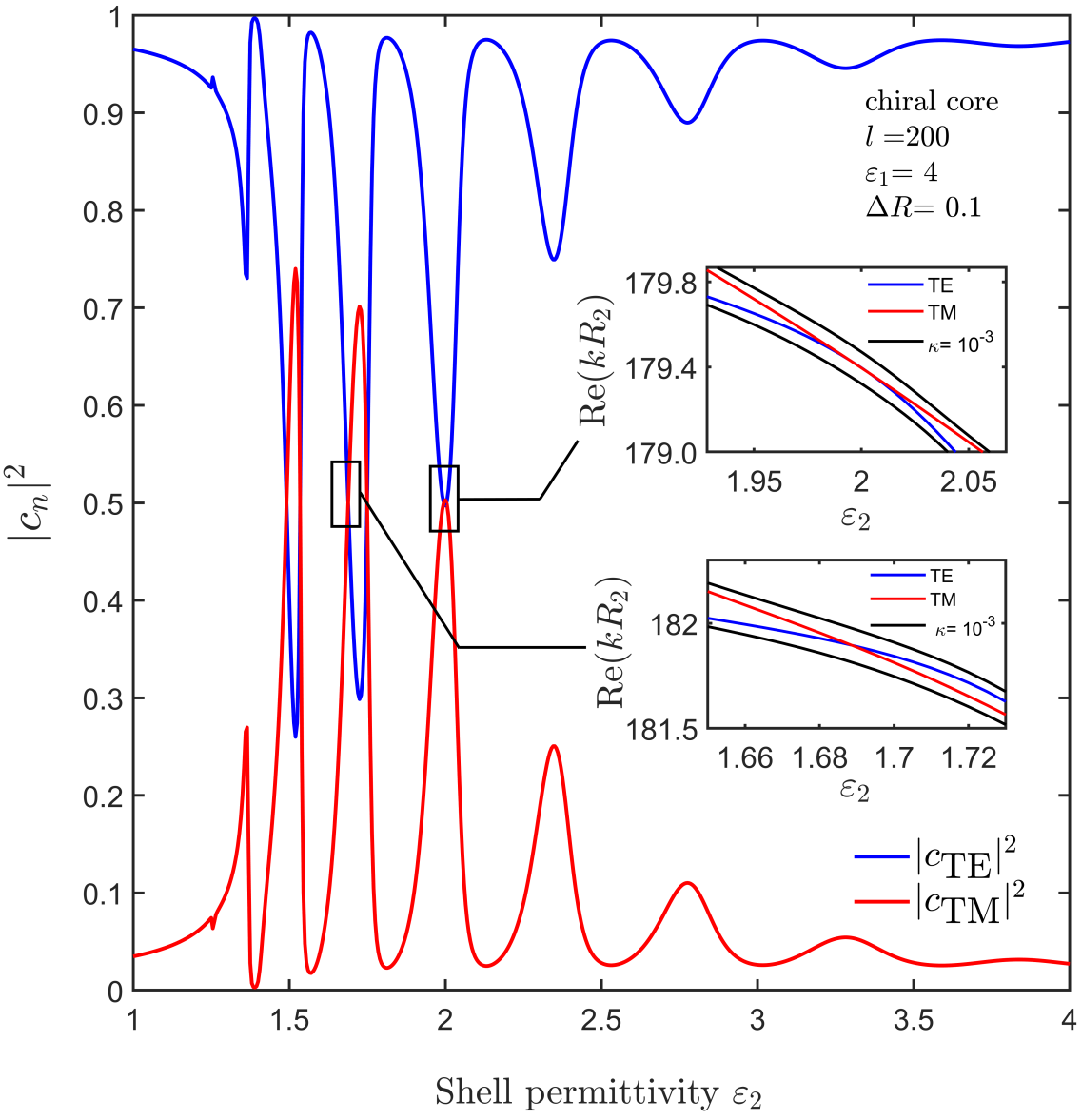

Figure 6.6. The absolute square of the expansion coefficients $|c_{\mathrm{TE}}|^2$ (blue) and $|c_{\mathrm{TM}}|^2$ (red) of the perturbed state, corresponding to the perturbed wavenumber k_+ due to chirality perturbation $\kappa = 10^{-3}$ in the core. The top inset is as in Fig. 6.3(b) and the bottom inset is as in Fig. 6.4(a), showing the real parts of the unperturbed and the perturbed wavenumbers at the selected regions.

correspond to the degenerate modes for certain l. However, for a particle placed at the north pole $\Omega_p = (0, \varphi_p)$, the only modes that contribute to the splitting are $m = m' = \pm 1$ and $m = m' = 0$, see Appendix B.2 for the matrix elements $V^{12}_{lm,l'm'}$ and for the derivation of the selection rules $m = m' = \pm 1$ and $m = m' = 0$.

In Fig. 6.7, we illustrate the perturbation by a chiral particle by placing a chiral particle of radius $R_p \approx 10^{-2} R_2$ at the north pole, $\mathbf{r}_p = (R_2, 0, 0)$, of the core-shell system. We used as a basis the same quasi-degenerate modes shown in Fig. 6.3(b) at $\varepsilon_2 = 2$, $k_1 R_2 = 179.409 - 3.08 \times 10^{-7} i$ and $k_2 R_2 = 179.408 - 3.69 \times 10^{-7} i$, having angular momentum $l = 200$ and only the modes of the magnetic quantum number $m = 1$ or $m = 0$. The splitting of such modes transforms to linear splitting in the chirality of the particle κ_p around 0.4 as shown in Fig. 6.7(a). Changing the location of the particle by a distance d, including distances towards the system, produces oscillatory splitting as shown in Fig. 6.7(b). These oscillations are roughly proportional to the oscillations of the overlap of their wavefunctions, see Fig. 6.3(e). As the particle moves away from the system, the splitting falls quickly with distance, and has a discontinuity for the case $m = 0$ at the shell surface because the matrix element in this case maintains only the normal components of the electric and magnetic fields of TE and TM polarizations. We observed that changing the chirality of the particle itself yields a more pronounced effect compared to modifying the chirality of the surrounding medium, which may potentially constrain practical applications.

6.6 Summary

We have presented linear splitting of quasi-degenerate modes in chirality. We used the RSE, recently generalized to include chiral media, to demonstrate the transition of chirality contribution in mode splitting from second-order effect to first-order, using two quasi-degenerate modes of TE and TM polarization in spherically symmetric systems.

We have employed the degeneracy conditions discussed in the previous chapter to illustrate the linear splitting of strictly degenerate modes of a magnetic sphere and the quasi-degenerate modes of a core-shell system. The linear splitting was demonstrated in

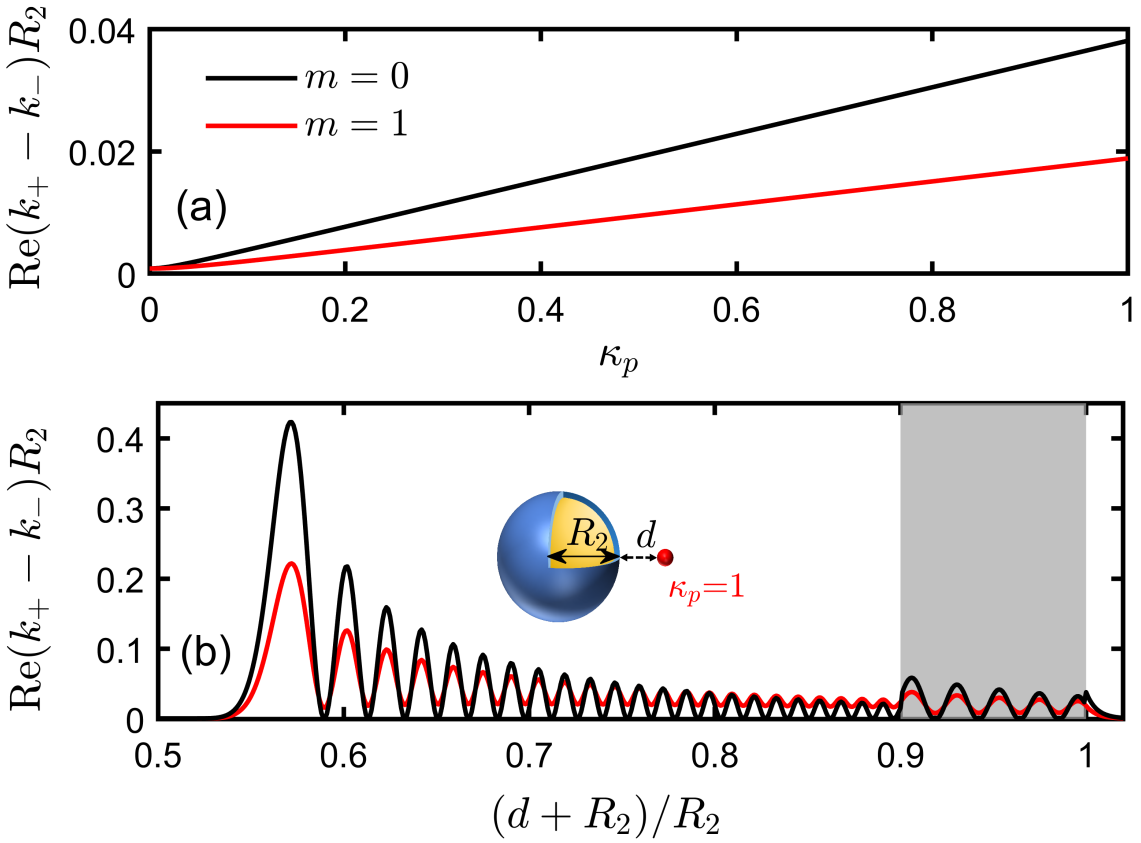

Figure 6.7. (a) The splitting of the modes, $k_1 R_2 = 179.409 - \times 10^{-7} i$ and $k_2 R_2 = 179.408 - 3.69 \times 10^{-7} i$, due to a presence of a chiral particle of radius $R_p \approx 0.01 R_2$ on the surface of the core-shell system as a function of the chirality of the particle κ_p, for the magnetic quantum numbers $m = 0$ (black) and $m = 1$ (red). (b) The splitting of the modes as the particle moves a distance d away and toward the system.

such systems due to the presence of chirality, either homogeneously inside or outside the resonators or within the shell in the case of the core-shell system. Further, we have demonstrated linear splitting due to a point-like chiral perturber which breaks the spherical symmetry. In this case, all the degenerate resonant states with different magnetic quantum number m are perturbed differently. Through selection rules of a particle placed at the north pole, only few states are perturbed by the chiral particle.

While the linear splitting of quasi-degenerate modes is handedness-blind because the modes split simultaneously and equally for both positive and negative chirality κ, the linear splitting is concentration-dependent since κ is proportional to the number of chiral molecules. Also, although the proposed systems may be challenging to be achieved experimentally, the numerical and analytical calculations may be insightful for developing novel chiral sensing schemes, contributing to the comprehension of the interaction of optical modes with chiral systems.

Chapter 7

Conclusion

7.1 Thesis Overview

The resonant states of an open optical system are the eigen solution to the source-free Maxwell's equations, considering purely outgoing boundary conditions. These states are characterized by complex wavenumbers with negative imaginary parts, resulting in the resonant state having a finite lifetime and experiencing exponential growth with distance in the region outside the system. Owing to the boundary of optical systems, orthonormality conditions have been successfully formulated, and a rigorous perturbation theory, RSE, has been developed for perturbations within the boundaries of the system where the resonant states are complete. However, developing a perturbation theory to treat perturbations in the entire space outside the system's boundaries presents a challenge. This has limited perturbation theories to first or second order for perturbations in a finite range in the vicinity of the system or to first-order perturbations in the entire space outside the system. In this thesis, we developed a rigorous theory based on the RSE and several approximations to mainly treat homogeneous perturbations in an isotropic medium surrounding an arbitrary optical system. Our theoretical framework focuses on reciprocal optical systems with a linear response.

Developing a rigorous theory for treating perturbations in the surrounding medium

was achieved through the RSE. This was accomplished by developing a transformation matrix to map the Maxwell's equations of the perturbed system into an effective system that encloses the perturbation within its boundaries, where the resonant states are complete. The RSE can then rigorously treat the resonant states in this effective system. From the proposed approaches, we distinguished two approximations: the diagonal and the simplified diagonal approximations. In the diagonal approximation, only the diagonal elements of the RSE matrix are maintained in the basis, and all the matrix elements are neglected in its simplified version.

In the case of dispersion, where the system is described by the generalized Drude-Lorentz model, the transformation scales the poles of dispersion. This requires using the infinitesimal-dispersive RSE method, which involves adding the scaled pole resonant states to the basis. However, since the scaled poles are perturbation-dependent, they need to be recalculated whenever the perturbation changes. To avoid this complication, we proposed a transformation of the original pole resonant states to generate an alternative set of fixed pole resonant states that can be used for all perturbations. For a dispersive surrounding medium, the transformation becomes state-dependent and may not work. In this case, one may transform both the unperturbed and perturbed systems and then apply the RSE to treat the effective perturbation to find the perturbed modes at least in the-first order. For chiral systems, the basis system has to be chiral to apply the transformation.

We provided an attempt to develop an alternative basis based on regularization to directly treat changes in the surrounding medium of an open optical system without the transformation as an intermediate step. We developed orthonormality conditions and Poynting's theorem for the regularized resonant states and expressed the integrals of the regularized resonant states over the infinite volume outside the system in terms of the integrals over the system volume. The regularized resonant state expansion failed to converge to the exact solution for an example of a dielectric sphere, indicating a lack of completeness in such states. Nevertheless, we formulated a regularized diagonal approximation of single mode only to calculate the shift of the regularized resonant states due to small changes in a dispersive or non-dispersive

medium surrounding the system. We proved that the first order of this approximation is identical to the first-order perturbation theory available in the literature, which is presently the best available approximation, and they both meet at the first-order with the RSE-based approach for non-dispersive surrounding medium. The regularized diagonal approximation became particularly useful for treating chiralty perturbation when the basis system is non-chiral.

We applied the RSE-based method and the other approximations—diagonal approximations, regularized, and first-order—to realistic materials, including plasmonic nanoparticles of different sizes, shapes, and materials and dielectric microresonators. We calculated perturbed modes in such systems due to changes in the surrounding medium. We evaluated the performance of each approach by calculating its accuracy relative to exact values obtained analytically or numerically.

The full RSE-based approach shows a quick convergence to the exact modes falling as N^{-3}, where N is the number of the resonant states in the basis, similar to the standard RSE method. By replacing the perturbation-dependent pole resonant states (pRSs I) with the perturbation-independent pole resonant states (pRSs II) in the basis of the infinitesimal RSE, the $1/N^3$ convergence to the exact solution was almost maintained.

Remarkably, the diagonal approximations show higher accuracy than other approximations beyond the first-order, with one order of magnitude reduction of the diagonal approximation more than its simplified version for the considered plasmonic particles described by the Drude model. The regularized diagonal approximation exhibits lower accuracy than other approximations but is nevertheless better than the first-order. For the considered example of a microresonator, all the single-mode approximations failed to accurately predict the change of the fundamental whispering gallery mode. We replaced the single-mode approximations with a local basis of whispering gallery modes, achieving considerable accuracy with only a few modes in the RSE basis.

Additionally, we employed the high accuracy of the diagonal approximation of

Drude systems to propose a method to find the integral of the normalized fields over the system's volume, which are used in the calculations of both the diagonal, regularized diagonal, and first-order approximations for arbitrarily shaped systems. Using the diagonal approximation, we accurately calculated this integral using numerically obtained wavenumbers. For a configuration of more than one system, we constructed a system of linear equations to solve for the integral for each system. Interestingly, this method enabled us to calculate the perturbed modes using the proposed approximations for a system on a substrate, which is not solvable by the standard RSE for internal perturbations or the proposed RSE-based approach for external perturbations. This is because the substrate introduces inhomogeneity in the surrounding medium.

We discussed the possibility of achieving degeneracy of TE and TM resonant states in homogeneous spherical systems of isotropic response through the analytical solution and secular equations of a simple sphere and a core-shell system. We then demonstrated quasi-degenerate whispering gallery modes in a dielectric core-shell system for different values of the shell permittivity and thickness.

Lastly, since the effect of chirality in most sensing schemes is weak due to its extremely small values, we developed a theoretical framework to convert the impact of chirality in mode shift from a second-order effect to a first-order effect. We derived a linear splitting of quasi-degenerate modes using the RSE, with a focus on spherical systems. The deduced degeneracy conditions for spherical systems were employed to provide two quasi-degenerate TE and TM modes in the basis for illustrating their linear splitting due to chirality perturbation. We considered various possibilities, including homogeneous chirality perturbation either inside or outside a magnetic sphere and a core-shell system. We also considered a perturbation by a chiral molecule, which breaks the spherical symmetry and perturbs different resonant states differently. Owing to selection rules for a particle placed at the north pole, the affected resonant states are reduced to a few states. The quasi-degenerate modes of a core-shell system exhibit linear splitting for a particle placed at the north pole. Although handedness cannot be distinguished from the linear splitting of the modes, the linear splitting

is concentration-dependent since chirality is proportional to the number of chiral molecules. The systems we suggested involve artificial materials such as solid chiral shells or chiral spheres, which may be challenging for experimental realization. Nevertheless, the calculations may provide insights for developing chiral sensing schemes and understanding the interaction of optical modes with chiral materials.

7.2 Future work

As a next step, a comprehensive analysis could be taken to develop a clear understanding of the accurate results of the diagonal approximation, especially for the results achieved for nanodimers, i.e., the bow-tie antenna or the dolmen. A rigid understanding of the diagonal approximation would also help with understanding the proposed method for calculating the integral of the square of the normalized fields based on the accuracy of the diagonal approximation.

The proposed method for calculating the integral for the normalised field requires prior information about the resonance shift, which was obtained numerically in this work. This could be examined on measured data to develop a perturbation theory for arbitrary resonators and for a larger class of perturbations without any computational loads. Additionally, the calculated fields from this approach can be compared with other normalization conditions and studied for their impact on the convergence of the RSE.

The RSE-based approach could be incorporated with the fit program used for generating Drude parameters to provide open resources for identifying the electromagnetic properties of the medium from their spectral changes.

For chiral sensing, the work can be taken to an experimental level, and the sensitivity of the chiral particle could be increased by considering polarizability of the chiral particle.

Appendix A

Dielectric slab

By considering a non-magnetic slab with thickness $2a$ and dielectric properties described by,

$$\varepsilon(z) = \begin{cases} \varepsilon_s & , |z| \leq a \\ 1 & , |z| \geq a \,, \end{cases} \tag{A.1}$$

and considering polarized electric field in the $\hat{x}$ direction with zero in-plane wavenumber k, the wave equation for the electric field has the form

$$\left[\frac{d^2}{dz^2} + \varepsilon(z)k^2\right] E(z) = 0 \,. \tag{A.2}$$

The above equation is satisfied by the general solution

$$f(z) = \begin{cases} Ae^{i\sqrt{\varepsilon_s}kz} + Be^{-i\sqrt{\varepsilon_s}kz} & \text{for } |z| < a \\ Ce^{ikz} + De^{-ikz} & \text{for } z \geq a \\ Ee^{ikz} + Fe^{-ikz} & \text{for } z \leq -a \,, \end{cases} \tag{A.3}$$

having time dependence $e^{-i\omega t}$, where $\omega = ck$, and secular equation of the form

$$\begin{aligned} Ae^{i\sqrt{\varepsilon_s}ka} + Be^{-i\sqrt{\varepsilon_s}ka} &= Ce^{ikz} + De^{-ikz}, \\ Ae^{-i\sqrt{\varepsilon_s}ka} + Be^{i\sqrt{\varepsilon_s}ka} &= Ee^{-ikz} + Fe^{ika}, \\ A\sqrt{\varepsilon_s}e^{i\sqrt{\varepsilon_s}ka} - B\sqrt{\varepsilon_s}e^{-i\sqrt{\varepsilon_s}ka} &= Ce^{ika} - De^{-ikz}, \\ A\sqrt{\varepsilon_s}e^{-i\sqrt{\varepsilon_s}ka} - B\sqrt{\varepsilon_s}e^{i\sqrt{\varepsilon_s}ka} &= Ee^{-ikz} - Fe^{ika}\,. \end{aligned} \tag{A.4}$$

The secular equation is obtained from the continuity of the tangential components of the electric and magnetic fields across the slab's boundaries. Now, considering three cases of additional boundary conditions, given by

$$D = 0\,, \qquad E = 0\,, \qquad \text{for outgoing boundary conditions}\,, \tag{A.5}$$

$$C = 0\,, \qquad F = 0\,, \qquad \text{for incoming boundary conditions}\,, \tag{A.6}$$

$$D = 0\,, \qquad F = 0\,, \qquad \text{for transparent boundary conditions}\,, \tag{A.7}$$

in the secular equation Eq. (A.4) results in quantization of the wavenumber k, with n labelling the state. For the outgoing boundary conditions, the wavenumber becomes complex with negative imaginary part:

$$k_n = \frac{1}{2a\sqrt{\varepsilon_s}}(n\pi - i\ln\alpha) \qquad \text{for } n = 0, \pm1, \pm2, \ldots, \tag{A.8}$$

with $\alpha = \frac{\sqrt{\varepsilon_s}+1}{\sqrt{\varepsilon_s}-1}$. For the incoming boundary conditions, the wavenumber takes the form

$$k_n = \frac{1}{2a\sqrt{\varepsilon_s}}(n\pi + i\ln\alpha) \qquad \text{for } n = 0, \pm1, \pm2, \ldots \tag{A.9}$$

which is also complex-valued but with real imaginary part. The wavenumber for the transparent boundary conditions is real:

$$k_n = \frac{n\pi}{2a\sqrt{\varepsilon_s}} \qquad \text{for } n = 0, \pm1, \pm2, \ldots \tag{A.10}$$

Now, by using the normalization condition for the slab [13]

$$\int_{-a}^{a} \varepsilon_s f_n f_m dz + \frac{f_n(a)\frac{df_m(a)}{dz} - f_m(-a)\frac{df_n(-a)}{dz}}{k_m^2 - k_n^2} = \delta_{nm}, \tag{A.11}$$

and k_n for the corresponding boundary conditions, one obtains the normalization constants for each case. The normalization constants in the case of outgoing boundary conditions are [13]

$$A_n = \frac{(-i)^n}{2\sqrt{a\varepsilon_s}}, \qquad C_n = \frac{e^{-ik_n a}}{\sqrt{a(\varepsilon_s - 1)}}, \tag{A.12}$$

with $B_n = (-1)^n A_n$ and $F_n = (-1)^n C_n$. The constants for the incoming boundary conditions are

$$A_n = \frac{(-i)^n}{2\sqrt{a\varepsilon_s}}, \qquad D_n = \frac{e^{ik_n a}}{\sqrt{a(\varepsilon_s - 1)}}, \tag{A.13}$$

with $B_n = (-1)^n A_n$ as in the outgoing case, and $E_n = (-1)^n D_n$. Lastly, for the transparent boundary conditions, the constants take the form

$$A_n = \frac{(-i)^n\sqrt{\alpha}}{2\sqrt{a\varepsilon_s}}, \qquad C_n = \frac{e^{-ik_n a}}{\sqrt{a(\varepsilon_s - 1)}}, \qquad E_n = (-1)^n e^{i\varphi_n} C_n, \tag{A.14}$$

where $\varphi_n = 2k_n a$.

Appendix B

Matrix elements of the RSE

B.1 Matrix elements for homogeneous chirality perturbations

Considering two resonant states of TE and TM polarizations of a non-chiral spherical system in the RSE matrix to treat chirality perturbations, the matrix elements V_{nm} become

$$V_{11} = \int_V \mathbf{E}_1 \cdot \Delta\varepsilon \mathbf{E}_1 \, d\mathbf{r} - \int_V \mathbf{H}_1 \cdot \Delta\mu \mathbf{H}_1 \, d\mathbf{r} \,, \tag{B.1}$$

$$V_{22} = \int_V \mathbf{E}_2 \cdot \Delta\varepsilon \mathbf{E}_2 \, d\mathbf{r} - \int_V \mathbf{H}_2 \cdot \Delta\mu \mathbf{H}_2 \, d\mathbf{r} \,, \tag{B.2}$$

and

$$V_{12} = V_{21} = -i \int_V \left[\mathbf{E}_1 \cdot \kappa \mathbf{H}_2 + \mathbf{H}_1 \cdot \kappa \mathbf{E}_2 \right] d\mathbf{r} \,, \tag{B.3}$$

To evaluate the matrix elements for spherical systems, we use the expansions of the electric and magnetic fields in the VSH's for TE and TM resonant states,

$$\mathbf{E}_1 = E_{1lm}(r) \boldsymbol{Y}_{1lm}(\Omega) \,, \tag{B.4}$$

$$\mathbf{H}_1 = H_{2lm}(r) \boldsymbol{Y}_{2lm}(\Omega) + H_{3lm}(r) \boldsymbol{Y}_{3lm}(\Omega) \,, \tag{B.5}$$

$$\mathbf{E}_2 = E_{2lm}(r) \boldsymbol{Y}_{2lm}(\Omega) + E_{3lm}(r) \boldsymbol{Y}_{3lm}(\Omega) \,, \tag{B.6}$$

$$\mathbf{H}_2 = H_{1lm}(r) \boldsymbol{Y}_{1lm}(\Omega) \,, \tag{B.7}$$

where the subscripts 1 and 2 refer to the TE and TM resonant states, respectively.

Using the radial functions $\mathcal{E}_{jlm}(r) = rE_{jlm}(r)$ and $\mathcal{H}_{jlm}(r) = riH_{jlm}(r)$ in Eqs. (B.4)–(B.7) and their definitions Eqs. (5.18) and (5.19) for TE and TM respectively, the matrix elements Eqs. (B.1), (B.2), and (B.3) yields

$$V_{11} = \Delta\varepsilon \int_V \psi_1(r)\psi_1(r)dr + \Delta\mu\beta^2 \int_V \left[\psi_1'(r)\psi_1'(r) + \frac{\alpha_l^2}{r^2}\psi_1(r)\psi_1(r)\right] dr\,, \quad \text{(B.8)}$$

$$V_{22} = \frac{\Delta\varepsilon}{\beta^2} \int_V \left[\psi_2'(r)\psi_2'(r) + \frac{\alpha_l^2}{r^2}\psi_2(r)\psi_2(r)\right] dr + \Delta\mu \int_V \psi_2(r)\psi_2(r)dr \quad \text{(B.9)}$$

$$V_{12} = -\kappa \int_V \left[\psi_1(r)\psi_2(r) + \psi_1'(r)\psi_2'(r) + \alpha_l^2 \frac{\psi_1(r)}{r}\frac{\psi_2(r)}{r}\right] dr\,, \quad \text{(B.10)}$$

where all degenerate modes of l' and m' are vanished by the spherical symmetry using the orthonormality of the VSHs.

Magnetic sphere

For homogeneous chirality perturbation in the magnetic sphere, the modes are strictly degenerate, i.e, $k_1 = k_2$. The matrix element V_{12} Eq. (B.10) is evaluated as [61]

$$V_{12} = -\kappa R \left[A_1^2 J_1^2(z)\left(1 - \frac{\alpha_l^2}{(nk_1R)^2}\right) + A_1^2 J_1'^2(z)\right]\,. \quad \text{(B.11)}$$

For chirality perturbation inside the sphere. For perturbation in the surrounding medium, it takes a regularized form

$$V_{12} = \kappa R \left[B_1^2 H_1^2(k_nR)\left(1 - \frac{\alpha_l^2}{(k_1R)^2}\right) + B_1^2 H_1'^2(k_nR)\right]\,. \quad \text{(B.12)}$$

Core-shell system

For homogeneous chirality perturbation in the core-shell system, the modes are quasi-degenerate. In this case, the matrix element V_{12} Eq. (B.10) is evaluate as [61]

$$V_{12} = -\kappa \left[\frac{\psi_1(r)\psi_2'(r) - \psi_1'(r)\psi_2(r)}{n(r)(k_1 - k_2)}\right]_{r_1}^{r_2}\,, \quad \text{(B.13)}$$

taking the explicit form

$$V_{12} = -\kappa \frac{A_1 J_1(z_{11}) A_2 J_2'(z_{11}) - A_1 J_1'(z_{11}) A_2 J_2(z_{11})}{n_1(k_1 - k_2)}\,, \tag{B.14}$$

for chirality perturbation inside the core, and

$$V_{12} = -\kappa \frac{K_1(z_{22}) K_2'(z_{22}) - K_1'(z_{22}) K_2(z_{22}) - K_1(z_{21}) K_2'(z_{21}) + K_1'(z_{21}) K_2(z_{21})}{n_2(k_1 - k_2)}\,, \tag{B.15}$$

for chirality perturbation in the shell. The matrix element for the perturbation outside the core-shell system is evaluated by regularization as

$$V_{12} = \kappa \frac{B_1 H_1(z_{32}) B_2 H_2'(z_{32}) - B_1 H_1'(z_{32}) B_2 H_2(z_{32})}{(k_1 - k_2)}\,. \tag{B.16}$$

B.2 Matrix elements for the point-like chiral perturber

A perturbation by a point-like chiral source, expressed as Dirac delta function $\kappa = \kappa_p V_p \delta(\mathbf{r} - \mathbf{r}_p)$, where the parameters κ_p and V_p are the chirality and volume of the particle, respectively, and $\mathbf{r}_p = (r_p, \theta_p, \varphi_p)$ is the position of the particle, breaks the spherical symmetry and results in the matrix element,

$$V^{12}_{lm,l'm'} = -i \int_V \left[\mathbf{E}^1_{lm} \cdot \kappa \mathbf{H}^2_{l'm'} + \mathbf{H}^1_{lm} \cdot \kappa \mathbf{E}^2_{l'm'} \right] d\mathbf{r}\,, \tag{B.17}$$

where subscripts 1 and 2 refer to TE and TM, respectively, with TE mode having l and m quantum numbers, and TM having $l' = l$ and m', such that

$$\mathbf{E}^1_{lm} = E_{1lm}(r) \boldsymbol{Y}_{1lm}(\Omega)\,, \tag{B.18}$$

$$\mathbf{H}^1_{lm} = H_{2lm}(r) \boldsymbol{Y}_{2lm}(\Omega) + H_{3lm}(r) \boldsymbol{Y}_{3lm}(\Omega)\,, \tag{B.19}$$

$$\mathbf{E}^2_{l'm'} = E_{2l'm'}(r) \boldsymbol{Y}_{2l'm'}(\Omega) + E_{3l'm'}(r) \boldsymbol{Y}_{3l'm'}(\Omega)\,, \tag{B.20}$$

$$\mathbf{H}^2_{l'm'} = H_{1l'm'}(r) \boldsymbol{Y}_{1l'm'}(\Omega)\,, \tag{B.21}$$

Using the radial functions $\mathcal{E}_{jlm}(r) = rE_{jlm}(r)$ and $\mathcal{H}_{jlm}(r) = riH_{jlm}(r)$ in Eqs. (B.18)–(B.21) and their definitions Eqs. (5.18) and (5.19) for TE and TM respectively, the matrix element Eq. (B.17) yields

$$V^{12}_{lm,l'm'} = -\kappa_p V_p \int \frac{1}{r^2 \sin\theta} \Big[\psi_1(r)\psi_2(r)\boldsymbol{Y}_{1lm}(\Omega)\cdot\boldsymbol{Y}_{1l'm'}(\Omega) + \psi_1'(r)\psi_2'(r)\boldsymbol{Y}_{2lm}(\Omega)\cdot\boldsymbol{Y}_{2l'm'}(\Omega) + \alpha_l^2 \frac{\psi_1(r)}{r}\frac{\psi_2(r)}{r}\boldsymbol{Y}_{3lm}(\Omega)\cdot\boldsymbol{Y}_{3l'm'}(\Omega)\Big] \tag{B.22}$$

$$\times \delta(r-r_p)\delta(\theta-\theta_p)\delta(\varphi-\varphi_p)drd\Omega\,. \tag{B.23}$$

where the degenerate modes now with the magnetic quantum number m for a certain l form the RSE matrix. Evaluating the above integral of Dirac delta function yields

$$V^{12}_{lm,l'm'} = -\kappa_p V_p \frac{1}{r_p^2} \Big[\psi_1(r_p)\psi_2(r_p)\boldsymbol{Y}_{1lm}(\Omega_p)\cdot\boldsymbol{Y}_{1l'm'}(\Omega_p) + \psi_1'(r_p)\psi_2'(r_p)\boldsymbol{Y}_{2lm}(\Omega_p)\cdot\boldsymbol{Y}_{2l'm'}(\Omega_p) + \alpha_l^2 \frac{\psi_1(r_p)}{r_p}\frac{\psi_2(r_p)}{r_p}\boldsymbol{Y}_{3lm}(\Omega_p)\cdot\boldsymbol{Y}_{3l'm'}(\Omega_p)\Big]\,, \tag{B.24}$$

having the following explicit forms of vector spherical harmonics,

$$\boldsymbol{Y}_{1lm}(\Omega_p) = \frac{C_{lm}}{\alpha_l}\left[\chi_m(\varphi_p)\frac{dP_l^{|m|}(\cos\theta_p)}{d\theta}\hat{\boldsymbol{\varphi}} - \frac{1}{\sin\theta_p}P_l^{|m|}(\cos\theta_p)\frac{d\chi_m(\varphi_p)}{d\varphi}\hat{\boldsymbol{\theta}}\right]\,, \tag{B.25}$$

$$\boldsymbol{Y}_{2lm}(\Omega_p) = \frac{C_{lm}}{\alpha_l}\left[\chi_m(\varphi_p)\frac{dP_l^{|m|}(\cos\theta_p)}{d\theta}\hat{\boldsymbol{\theta}} + \frac{1}{\sin\theta_p}P_l^{|m|}(\cos\theta_p)\frac{d\chi_m(\varphi_p)}{d\varphi}\hat{\boldsymbol{\varphi}}\right]\,, \tag{B.26}$$

$$\boldsymbol{Y}_{3lm}(\Omega_p) = \chi_m(\varphi_p)P_l^{|m|}(\cos\theta_p)\hat{\boldsymbol{r}}\,, \tag{B.27}$$

where $C_{lm} = \sqrt{\frac{2l+1}{2}\frac{(l-|m|)!}{(l+|m|)!}}$. All degenerate modes corresponding to m in this case should be taken into account in calculating the perturbed modes. However, for a particle situated at the north pole $\Omega_p = (0, \varphi_p)$, all degenerate modes uncoupled from the basis except for $|m| = 1$ and $m = 0$. We prove such selection rules imposed by placing the particle at the north pole in the following.

To evaluate the VSHs at the north pole, we need to evaluate both the associated

Legendre polynomial $P_l^{|m|}(\cos\theta_p)$ and its derivative $\frac{dP_l^{|m|}(\cos\theta_p)}{d\theta}$ at $\theta_p = 0$ as well as the azimuthal dependence $\chi_m(\varphi_p)$ and its derivative $\frac{d\chi_m(\varphi_p)}{d\varphi}$. The azimuthal dependence and its derivative are straightforward, and the definition of $\chi_m(\varphi)$ is given by Eq. (5.6). For $P_l^{|m|}(\cos\theta_p)$ at $\theta_p = 0$, we know that [68]

$$P_l^m(1) = \begin{cases} 1\,, & \text{if } m = 0 \\ 0\,, & \text{otherwise}\,. \end{cases} \tag{B.28}$$

Now, the first derivative of $P_l^{|m|}(\cos\theta)$ with respect to θ is given by [68]

$$\frac{dP_l^m(\cos\theta)}{d\theta} = \frac{l\cos\theta P_l^m(\cos\theta) - (l+m)P_{l-1}^m(\cos\theta)}{\sqrt{1-\cos^2\theta}}\,, \tag{B.29}$$

where

$$P_l^m(\cos\theta) = (-1)^m \left(1-\cos^2\theta\right)^{m/2} \frac{d^m}{d\cos^m\theta} P_l(\cos\theta)\,, \tag{B.30}$$

and P_l is the Legendre polynomial. The derivative Eq. (B.29) at $\theta_p = 0$ is zero for all choices of m except for $|m| = 1$. For $|m| = 1$, one needs to evaluate $\frac{dP_l(1)}{d\cos\theta}$ and $\frac{dP_{l-1}(1)}{d\cos\theta}$. These values can be obtained with the help of the generating function [68],

$$\sum_{l=0}^{\infty} P_l(\cos\theta)t^l = (1-2xt+t^2)^{-\frac{1}{2}} \tag{B.31}$$

which can be expanded to compare coefficients. This helps to obtain the values of $\frac{dP_l(1)}{d\cos\theta}$ and $\frac{dP_{l-1}(1)}{d\cos\theta}$ to be used in Eq. (B.29) to find $\frac{dP_l^1(1)}{d\theta}$. This evaluation leads to the following,

$$\frac{dP_l^m(1)}{d\theta} = \begin{cases} \frac{l(l+1)}{2}\,, & \text{if } m = \pm 1 \\ 0\,, & \text{otherwise}\,, \end{cases} \tag{B.32}$$

As a result from Eqs. (B.28) and (B.32), for a particle at the north pole, all degenerate modes do not contribute except for $m = m' = 1$, $m = m' = -1$ and

$m = m' = 0$. The matrix element $V^{12}_{lm,l'm'}$ for $m = m' = 1$ then can be written simply as

$$V^{12}_{lm,l'm'} = -\kappa_p V_p \frac{l(l+1)}{8\pi} \frac{\cos\varphi_p}{r_p^2} \left[\psi_1(r_p)\psi_2(r_p)\psi_1'(r_p)\psi_2'(r_p)\right] , \tag{B.33}$$

Similarly, for $m = -1$, the matrix element in this case is

$$V^{12}_{lm,l'm'} = -\kappa_p V_p \frac{l(l+1)}{8\pi} \frac{\sin\varphi_p}{r_p^2} \left[\psi_1(r_p)\psi_2(r_p)\psi_1'(r_p)\psi_2'(r_p)\right] . \tag{B.34}$$

Lastly, for $m = 0$, the only surviving term of the matrix element in Eq. (B.24) is the third term when $m' = 0$:

$$V^{12}_{lm,l'm'} = -\kappa_p V_p \frac{l(l+1)}{4\pi} \frac{1}{r_p^2} \left[\alpha_l^2 \frac{\psi_1(r_p)}{r_p} \frac{\psi_2(r_p)}{r_p}\right] . \tag{B.35}$$

The table below summarizes the values of the functions $\frac{dP_l^{|m|}(1)}{d\theta}$, $\chi_m(\varphi_p)$, $P_l^{|m|}(1)$, and $\frac{d\chi_m}{d\varphi}(\varphi_p)$ at the north pole for $m = \pm 1$ and $m = 0$.

m	$\frac{dP_l^{\lvert m\rvert}(1)}{d\theta}$	$\chi_m(\varphi_p)$	$P_l^{\lvert m\rvert}(1)$	$\frac{d\chi_m}{d\varphi}(\varphi_p)$
1	$\frac{l(l+1)}{2}$	$\pi^{-1/2}\cos\varphi_p$	0	$-\pi^{-1/2}\sin\varphi_p$
-1	$\frac{l(l+1)}{2}$	$\pi^{-1/2}\sin\varphi_p$	0	$\pi^{-1/2}\cos\varphi_p$
0	0	$(2\pi)^{-1/2}$	1	0

Table B.1. The functions in the vector spherical harmonics at $\Omega_p = (0, \varphi_p)$, where $\Omega_p = (0, \varphi_p)$ is the location of the chiral particle.

Appendix C

More results

C.1 Effective-pole resonant states generated by Bessel function

C.2 Application of regularized diagonal approximation to refractive index sensing

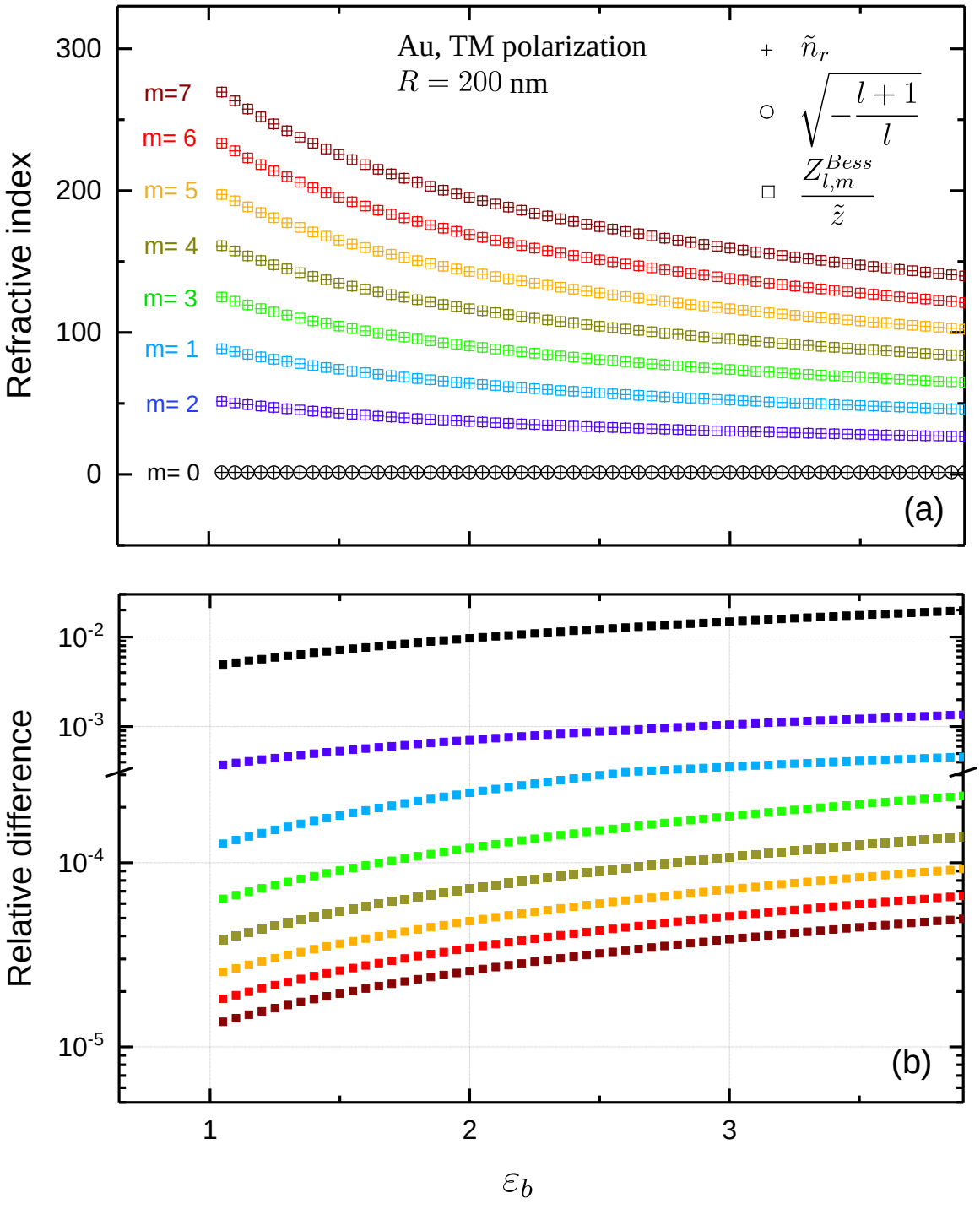

Figure C.1. (a) The imaginary part of refractive index of the first few pRSs in TM polarization of a gold nanosphere of radius $R = 200\,\text{nm}$ described by Drude model as functions of the permittivity of the surrounding medium ε_b, calculated exactly, via Eq. (2.60) ($\tilde{n}_r$, crosses), and by using the Bessel function Eq. (2.65) and Eq. (2.66). (b) The relative error for the approximation shown in (a).

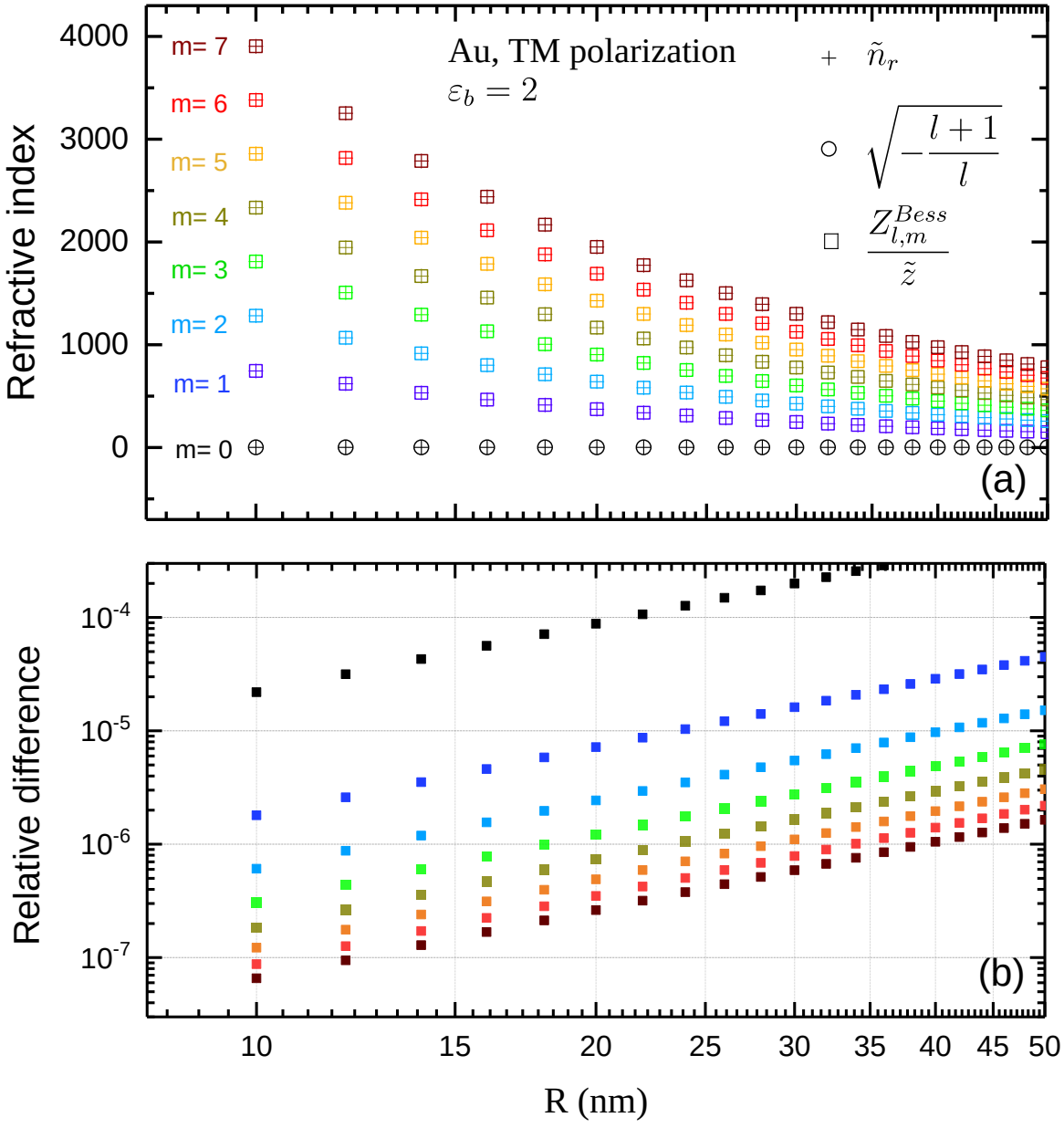

Figure C.2. As Fig. C.1 but for the dependence on the sphere radius R, for $\varepsilon = 2$.

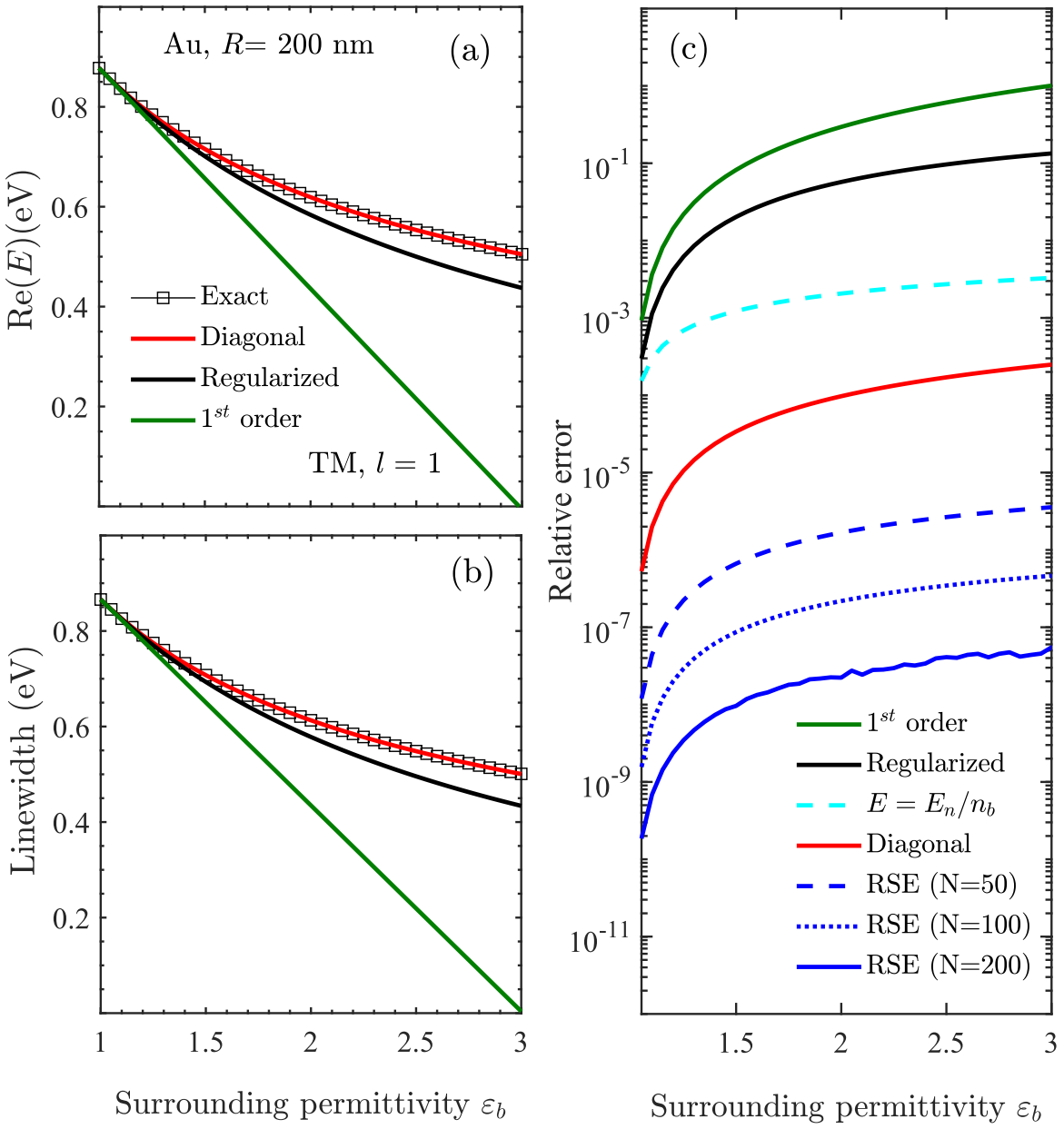

Figure C.3. (a) Resonance energy (Re E), (b) linewidth (-2Im E), and (c) relative error of the complex energy E of the fundamental surface plasmon mode of a gold nanosphere (R = 200 nm) as functions of the background permittivity ε_b, calculated analytically (thin black lines with open squares), using the diagonal dispersive RSE (red lines), regularized diagonal (black line), and first-order approximation (green lines). (c) Relative error of the first-order (green), regularized diagonal (black), simple diagonal (cyan), and diagonal approximation (solid red line), as well as of the full RSE with $N = 50$ (dashed blue), 100 (dotted blue) and 200 (solid blue line).

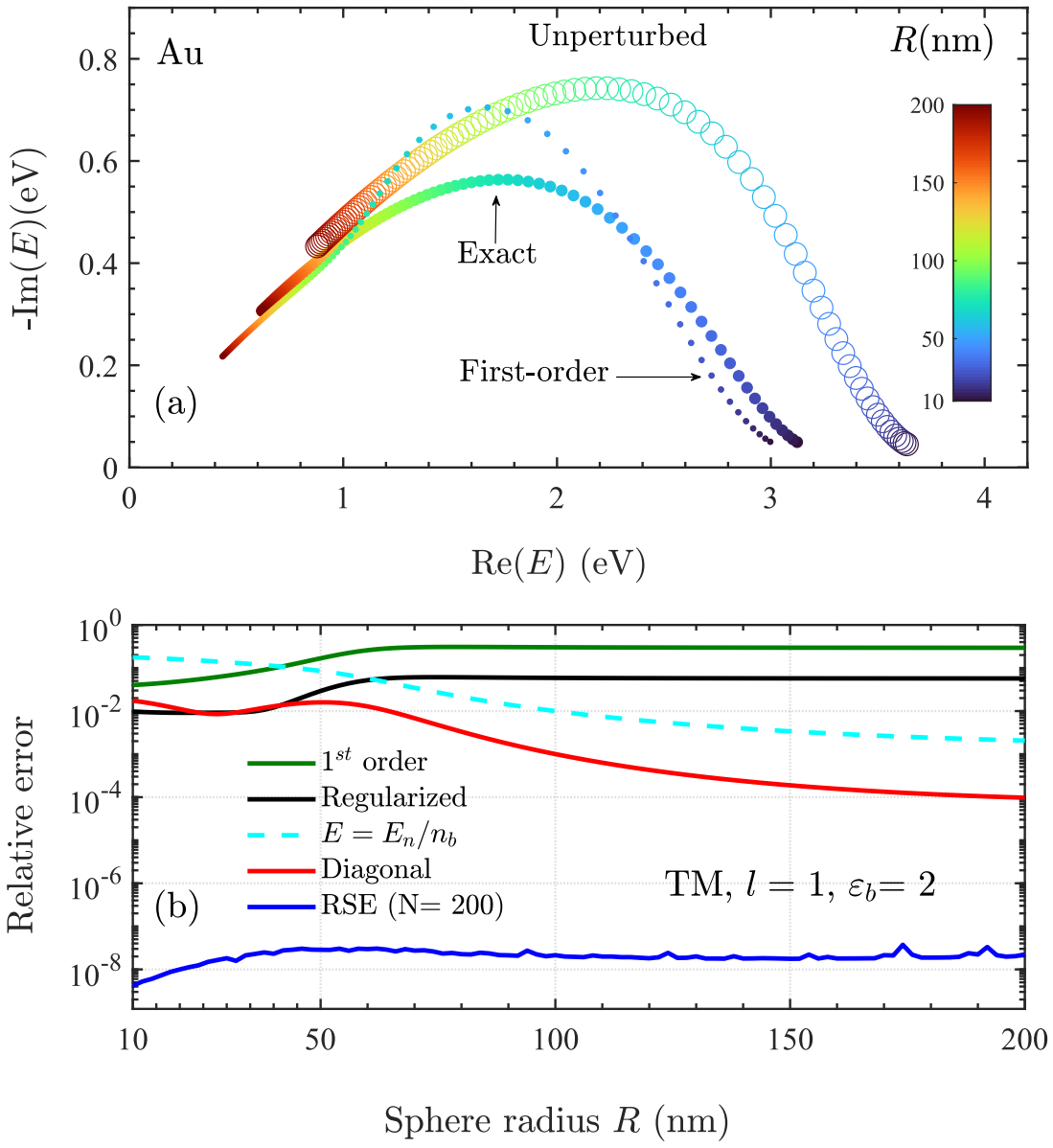

Figure C.4. (a) Complex energy of the fundamental surface plasmon mode of a gold nanosphere surrounded by vacuum (unperturbed) and by a dielectric with $\varepsilon_b = 2$ (exact and first-order) as functions of the sphere radius R given by the color code. (b) Relative error of first-order (green), regularized diagonal (black) simple diagonal (cyan), and diagonal approximation (red), as well as of the full RSE (blue line), as functions of R.

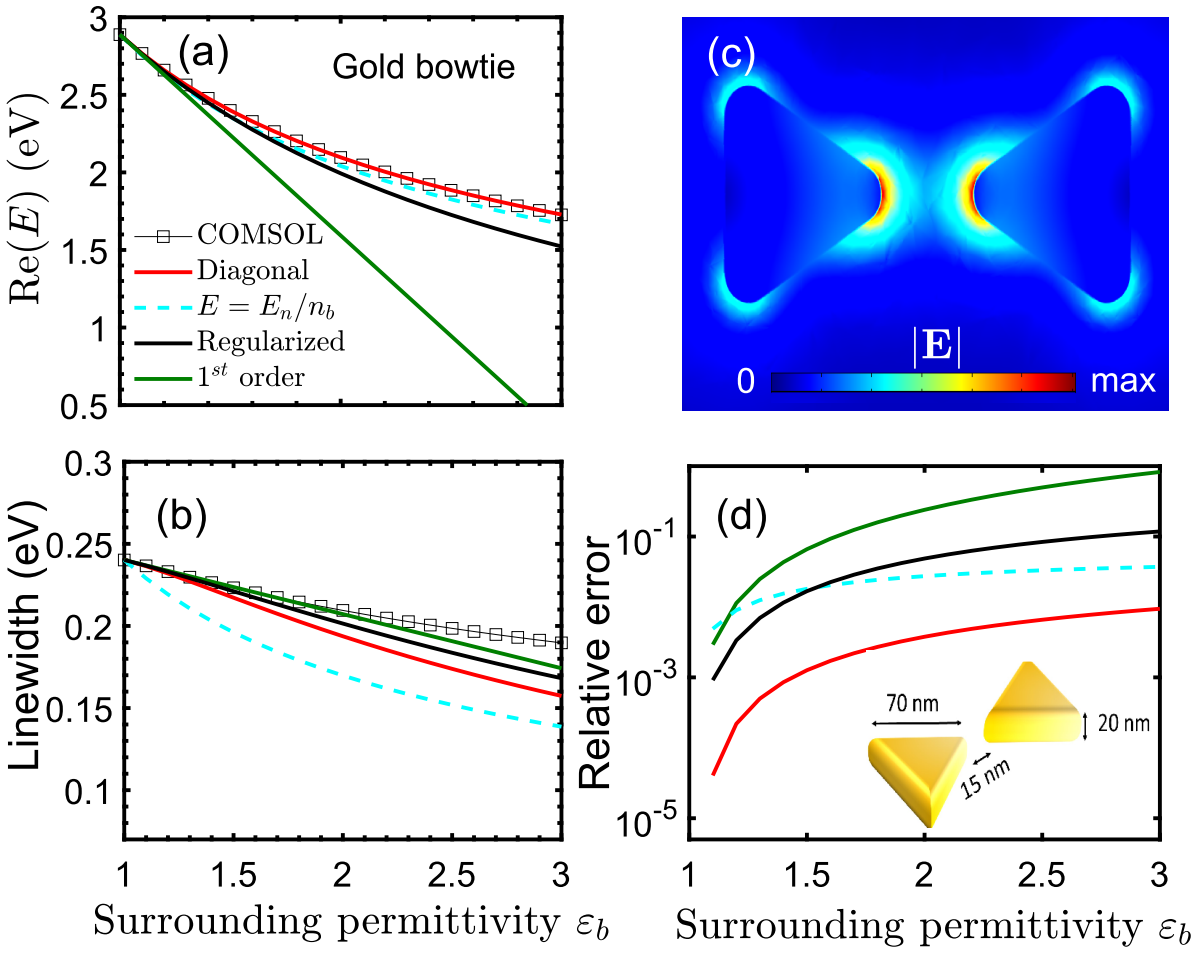

Figure C.5. (a) Resonance energy ($\mathrm{Re}\, E$) and (b) linewidth of a gold bow-tie antenna mode as functions of the permittivity of the surrounding medium ε_b, calculated using COMSOL [73] (black squares), diagonal dispersive RSE (red), regularized diagonal (black line), and the first-order approximations (green). (c) Electric field of the unperturbed mode. (d) Error of the first-order approximation (green), regularized diagonal (black), simple diagonal (cyan), and diagonal approximation (red) relative to COMSOL data. The inset shows schematics and dimensions of the system, with corners rounded to arcs with a radius of 8 nm.

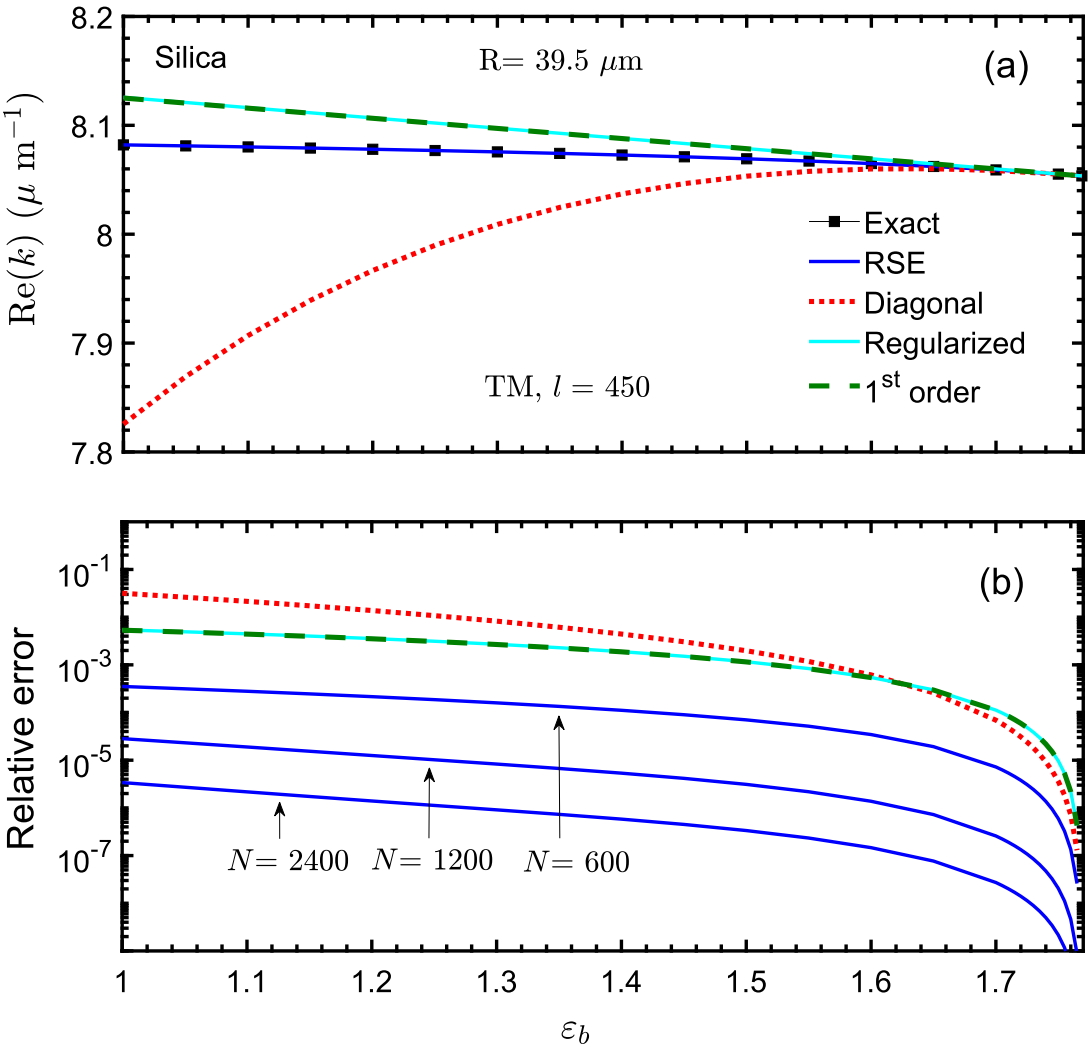

Figure C.6. (a) Real part and (b) relative error of the wave number k of the $l = 450$ TM fundamental WGM of a silica micro-sphere as functions of the background permittivity ε_b, calculated exactly (black line with squares), using the full RSE with different basis sizes N as given, using the diagonal ($N = 1$) RSE (dotted red lines), regularized diagonal (cyan), and first-order (dashed green) approximations.

Bibliography

[1] M. A. Butler, "Fiber optic sensor for hydrogen concentrations near the explosive limit", Journal of the Electrochemical Society **138**, L46 (1991).

[2] T. Koschinsky **and** L. Heinemann, "Sensors for glucose monitoring: technical and clinical aspects", Diabetes/metabolism research and reviews **17**, 113–123 (2001).

[3] W. D. Wilson, "Analyzing biomolecular interactions", Science **295**, 2103–2105 (2002).

[4] H. Altug, S.-H. Oh, S. A. Maier **and** J. Homola, "Advances and applications of nanophotonic biosensors", Nature nanotechnology **17**, 5–16 (2022).

[5] E. Herkert, F. Sterl, N. Strohfeldt, R. Walter **and** H. Giessen, "Low-cost hydrogen sensor in the ppm range with purely optical readout", ACS sensors **5**, 978–983 (2020).

[6] A. Unger **and** M. Kreiter, "Analyzing the performance of plasmonic resonators for dielectric sensing", The Journal of Physical Chemistry C **113**, 12243–12251 (2009).

[7] S. Arnold, M. Khoshsima, I. Teraoka, S. Holler **and** F. Vollmer, "Shift of whispering-gallery modes in microspheres by protein adsorption", Optics Letters **28**, 272–274 (2003).

[8] M. Doost, "Resonant state expansion applied to open optical systems", phdthesis (Cardiff University, 2014).

[9] C. Sauvan, T. Wu, R. Zarouf, E. A. Muljarov **and** P. Lalanne, "Normalization, orthogonality, and completeness of quasinormal modes of open systems: the case of electromagnetism", Optics Express **30**, 6846–6885 (2022).

[10] C. Sauvan, J. P. Hugonin, I. S. Maksymov **and** P. Lalanne, "Theory of the spontaneous optical emission of nanosize photonic and plasmon resonators", Physical Review Letters **110**, 237401 (2013).

[11] S. V. Lobanov, W. Langbein **and** E. A. Muljarov, "Resonant-state expansion of three-dimensional open optical systems: light scattering", Physical Review A **98**, 033820 (2018).

[12] T. Weiss **and** E. A. Muljarov, "How to calculate the pole expansion of the optical scattering matrix from the resonant states", Physical Review B **98**, 085433 (2018).

[13] E. A. Muljarov, W. Langbein **and** R. Zimmermann, "Brillouin-wigner perturbation theory in open electromagnetic systems", Europhysics Letters **92**, 50010 (2010).

[14] M. B. Doost, W. Langbein **and** E. A. Muljarov, "Resonant-state expansion applied to three-dimensional open optical systems", Physical Review A **90**, 013834 (2014).

[15] E. A. Muljarov **and** W. Langbein, "Exact mode volume and purcell factor of open optical systems", Physical Review B **94**, 235438 (2016).

[16] E. A. Muljarov **and** T. Weiss, "Resonant-state expansion for open optical systems: generalization to magnetic, chiral, and bi-anisotropic materials", Optics Letters **43**, 1978–1981 (2018).

[17] M. Doost, W. Langbein **and** E. Muljarov, "Resonant-state expansion for a simple dispersive medium", arXiv preprint arXiv:1508.03851 (2015).

[18] E. A. Muljarov **and** W. Langbein, "Resonant-state expansion of dispersive open optical systems: creating gold from sand", Physical Review B **93**, 075417 (2016).

[19] S. V. Lobanov, G. Zoriniants, W. Langbein **and** E. A. Muljarov, "Resonant-state expansion of light propagation in nonuniform waveguides", Physical Review A **95**, 053848 (2017).

[20] P. T. Leung **and** K. M. Pang, "Completeness and time-independent perturbation of morphology-dependent resonances in dielectric spheres", Journal of the Optical Society of America B **13**, 805–817 (1996).

[21] J. Yang, H. Giessen **and** P. Lalanne, "Simple analytical expression for the peak-frequency shifts of plasmonic resonances for sensing", Nano Letters **15**, 3439–3444 (2015).

[22] A. Gras, W. Yan **and** P. Lalanne, "Quasinormal-mode analysis of grating spectra at fixed incidence angles", Optics Letters **44**, 3494–3497 (2019).

[23] W. Yan, P. Lalanne **and** M. Qiu, "Shape deformation of nanoresonator: a quasinormal-mode perturbation theory", Physical Review Letters **125**, 013901 (2020).

[24] Z. Sztranyovszky, W. Langbein **and** E. A. Muljarov, "First-order perturbation theory of eigenmodes for systems with interfaces", arXiv:2205.13041 (2022).

[25] S. Both, "Theory of resonant light-matter interactions in nanophotonic sensing", PhD thesis (University of Stuttgart, 2022).

[26] S. Both **and** T. Weiss, "First-order perturbation theory for changes in the surrounding of open optical resonators", Optics Letters **44**, 5917–5920 (2019).

[27] T. Weiss, M. Schäferling, H. Giessen, N. A. Gippius, S. G. Tikhodeev, W. Langbein **and** E. A. Muljarov, "Analytical normalization of resonant states in photonic crystal slabs and periodic arrays of nanoantennas at oblique incidence", Physical Review B **96**, 045129 (2017).

[28] M. Mesch, T. Weiss, M. Schäferling, M. Hentschel, R. S. Hegde **and** H. Giessen, "Highly sensitive refractive index sensors with plasmonic nanoantennas – utilization of optimal spectral detuning of fano resonances", ACS Sensors **3**, 960–966 (2018).

[29] Y. Chen, W. Chen, X. Kong, D. Wu, J. Chu **and** C.-W. Qiu, "Can weak chirality induce strong coupling between resonant states?", Physical Review Letters **128**, 146102 (2022).

[30] G. Gamow, *The quantum theory of the atomic nucleus* (US Atomic Energy Commission, Division of Technical Information Extension, 1963).

[31] A. Bohm, M. Gadella **and** G. B. Mainland, "Gamow vectors and decaying states", American Journal of Physics **57**, 1103–1108 (1989).

[32] G. García-Calderón **and** R. Peierls, "Resonant states and their uses", Nuclear Physics A **265**, 443–460 (1976).

[33] K. M. Lee, P. T. Leung **and** K. M. Pang, "Dyadic formulation of morphology-dependent resonances. i. completeness relation", Journal of the Optical Society of America **16**, 1409–1417 (1999).

[34] S. Both **and** T. Weiss, "Resonant states and their role in nanophotonics", Semiconductor Science and Technology **37**, 013002 (2021).

[35] A. Tanimu **and** E. A. Muljarov, "Resonant-state expansion applied to one-dimensional quantum systems", Physical Review A **98**, 022127 (2018).

[36] D. Givoli, "Non-reflecting boundary conditions", Journal of computational physics **94**, 1–29 (1991).

[37] Z. Sztranyovszky, W. Langbein **and** E. A. Muljarov, "Optical resonances in graded index spheres: a resonant-state-expansion study and analytic approximations", Physical Review A **105**, 033522 (2022).

[38] J. D. Jackson, *Classical electrodynamics*, 3rd ed. (Wiley, New York, NY, 1999).

[39] I. Lindell, A. Sihvola, S. Tretyakov **and** A. J. Viitanen, *Electromagnetic waves in chiral and bi-isotropic media* (Artech House, 1994).

[40] T. G. Mackay **and** A. Lakhtakia, *Electromagnetic anisotropy and bianisotropy: a field guide* (World Scientific, 2010).

[41] T. Dray **and** C. A. Manogue, *The geometry of vector calculus*, [Online; accessed November-2023], 2012.

[42] A. Baz, Y. B. Zeldovich **and** A. Perelomov, *Scattering, reactions and decay in non-relativistic quantum mechanics (translated from the russian by the israel program for scientific translations, jerusalem 1969).*

[43] H. Lai, P. Leung, K. Young, P. Barber **and** S. Hill, "Time-independent perturbation for leaking electromagnetic modes in open systems with application to resonances in microdroplets", Physical Review A **41**, 5187 (1990).

[44] P. Leung, S. Liu **and** K. Young, "Completeness and time-independent perturbation of the quasinormal modes of an absorptive and leaky cavity", Physical Review A **49**, 3982 (1994).

[45] P. T. Kristensen, C. Van Vlack **and** S. Hughes, "Generalized effective mode volume for leaky optical cavities", Optics letters **37**, 1649–1651 (2012).

[46] P. T. Kristensen **and** S. Hughes, "Modes and mode volumes of leaky optical cavities and plasmonic nanoresonators", ACS Photonics **1**, 2–10 (2014).

[47] R.-C. Ge, P. T. Kristensen, J. F. Young **and** S. Hughes, "Quasinormal mode approach to modelling light-emission and propagation in nanoplasmonics", New Journal of Physics **16**, 113048 (2014).

[48] G. G. Calderón, "An expansion of continuum wave functions in terms of resonant states", Nuclear Physics A **261**, 130–140 (1976).

[49] M. B. Doost, W. Langbein **and** E. A. Muljarov, "Resonant state expansion applied to two-dimensional open optical systems", Physical Review A **87**, 043827 (2013).

[50] N. Moiseyev, *Non-hermitian quantum mechanics* (Cambridge University Press, 2011).

[51] J. P. Hugonin **and** P. Lalanne, "Perfectly matched layers as nonlinear coordinate transforms: a generalized formalization", Journal of the Optical Society of America A **22**, 1844–1849 (2005).

[52] P. Lalanne, W. Yan, A. Gras, C. Sauvan, J.-P. Hugonin, M. Besbes, G. Demésy, M. Truong, B. Gralak, F. Zolla **and** A. Nicolet, "Quasinormal mode solvers for resonators with dispersive materials", Journal of the Optical Society of America A **36**, 686–704 (2019).

[53] T. Wu, D. Arrivault, W. Yan **and** P. Lalanne, "Modal analysis of electromagnetic resonators: user guide for the man program", Computer Physics Communications **284**, 108627 (2023).

[54] P. T. Leung, S. Y. Liu, S. S. Tong **and** K. Young, "Time-independent perturbation theory for quasinormal modes in leaky optical cavities", Physical Review A **49**, 3068–3073 (1994).

[55] E. Muljarov **and** W. Langbein, "Comment on "normalization of quasinormal modes in leaky optical cavities and plasmonic resonators"", Physical Review A **96**, 017801 (2017).

[56] Y. B. Zel'dovich, "Contribution to the theory of unstable states", Zhur. Eksptl'. i Teoret. Fiz. **39** (1960).

[57] R. C. Mcphedran **and** B. Stout, "'killing mie softly': analytic integrals for complex resonant states", Quarterly Journal of Mechanics and Applied Mathematics **73**, 119–139 (2020).

[58] J.-P. Berenger, "A perfectly matched layer for the absorption of electromagnetic waves", Journal of computational physics **114**, 185–200 (1994).

[59] S. G. Johnson, "Notes on perfectly matched layers (pmls)", arXiv preprint arXiv:2108.05348 (2021).

[60] J. A. Stratton, *Electromagnetic theory*, **volume** 33 (John Wiley & Sons, 2007).

[61] E. A. Muljarov, "Full electromagnetic green's dyadic of spherically symmetric open optical systems and elimination of static modes from the resonant-state expansion", Physical Review A **101**, 053854 (2020).

[62] M. R. Foreman, J. D. Swaim **and** F. Vollmer, "Whispering gallery mode sensors", Advances in optics and photonics **7**, 168–240 (2015).

[63] H. S. Sehmi, W. Langbein **and** E. A. Muljarov, "Applying the resonant-state expansion to realistic materials with frequency dispersion", Physical Review B **101**, 045304 (2020).

[64] A. Elsherbeni **and** V. Demir, *The finite-difference time-domain method for electromagnetics with matlab simulations* (SciTech Pub., 2009).

[65] M. B. Doost, W. Langbein **and** E. A. Muljarov, "Resonant-state expansion applied to planar open optical systems", Physical Review A **85**, 023835 (2012).

[66] H. S. Sehmi, W. Langbein **and** E. A. Muljarov, "Optimizing the drude-lorentz model for material permittivity: method, program, and examples for gold, silver, and copper", Physical Review B **95**, 115444 (2017).

[67] P. B. Johnson **and** R. W. Christy, "Optical constants of the noble metals", Physical Review B **6**, 4370–4379 (1972).

[68] M. Abramowitz **and** I. A. Stegun, *Handbook of mathematical functions with formulas, graphs, and mathematical tables*, **volume** 55 (US Government printing office, 1948).

[69] T. Weiss, M. Mesch, M. Schäferling, H. Giessen, W. Langbein **and** E. A. Muljarov, "From dark to bright: first-order perturbation theory with analytical mode normalization for plasmonic nanoantenna arrays applied to refractive index sensing", Physical Review Letters **116**, 237401 (2016).

[70] J. Yang, H. Giessen **and** P. Lalanne, "Simple analytical expression for the peak-frequency shifts of plasmonic resonances for sensing", Nano Letters **15**, 3439–3444 (2015).

[71] S. F. Almousa **and** E. A. Muljarov, "Exact theory and approximations for optical resonators in a changing external medium", Physical Review B **107**, L081401 (2023).

[72] L. M. Payne, W. Albrecht, W. Langbein **and** P. Borri, "The optical nanosizer – quantitative size and shape analysis of individual nanoparticles by high-throughput widefield extinction microscopy", Nanoscale **12**, 16215–16228 (2020).

[73] Modal Analysis of Nanoresonators (MAN-7.1), [Online; accessed March-2022] (https://www.lp2n.institutoptique.fr/light-complex-nanostructures).

[74] Q. Bai, M. Perrin, C. Sauvan, J.-P. Hugonin **and** P. Lalanne, "Efficient and intuitive method for the analysis of light scattering by a resonant nanostructure", Optics express **21**, 27371–27382 (2013).

[75] W. Yan, R. Faggiani **and** P. Lalanne, "Rigorous modal analysis of plasmonic nanoresonators", Physical Review B **97**, 205422 (2018).

[76] COMSOL Multiphysics Programming Reference Manual, [Online; accessed March-2024] (https://doc.comsol.com).

[77] T. Wu, A. Baron, P. Lalanne **and** K. Vynck, "Intrinsic multipolar contents of nanoresonators for tailored scattering", Physical Review A **101**, 011803 (2020).

[78] R. Faggiani, A. Losquin, J. Yang, E. M**r**arsell, A. Mikkelsen **and** P. Lalanne, "Modal analysis of the ultrafast dynamics of optical nanoresonators", ACS Photonics **4**, 897–904 (2017).

[79] M. D. Baaske, M. R. Foreman **and** F. Vollmer, "Single-molecule nucleic acid interactions monitored on a label-free microcavity biosensor platform", Nature Nanotechnology **9**, 933–939 (2014).

[80] F. Vollmer **and** D. Yu, **editors**, *Optical whispering gallery modes for biosensing* (Springer International Publishing, 2020).

[81] A. Baz', Y. Zel'dovich **and** A. Perelomov, *Scattering, reactions and decay in nonrelativistic quantum mechanics* (U. S. Department of Commerce, Washington, D. C., 1969).

[82] I. Staude, A. E. Miroshnichenko, M. Decker, N. T. Fofang, S. Liu, E. Gonzales, J. Dominguez, T. S. Luk, D. N. Neshev, I. Brener **and** Y. Kivshar, "Tailoring directional scattering through magnetic and electric resonances in subwavelength silicon nanodisks", ACS nano **7**, 7824–7832 (2013).

[83] S. Vincent, X. Jiang, P. Russell **and** F. Vollmer, "Thermally tunable whispering-gallery mode cavities for magneto-optics", Applied Physics Letters **116** (2020).

[84] S. Both, M. Schäferling, F. Sterl, E. A. Muljarov, H. Giessen **and** T. Weiss, "Nanophotonic chiral sensing: how does it actually work?", ACS Nano **16**, 2822–2832 (2022).

[85] B. Vennes **and** T. C. Preston, "Morphology-dependent resonances in homogeneous and core-shell nonspherical particles", Physical Review A **104**, 033512 (2021).

[86] M. G. Silveirinha, "Trapping light in open plasmonic nanostructures", Physical Review A **89**, 023813 (2014).

[87] G. B. Arfken, H. J. Weber **and** F. E. Harris, *Mathematical methods for physicists: a comprehensive guide* (Academic press, 2011).

[88] E. A. Muljarov **and** T. Weiss, "Resonant-state expansion generalized to magnetic, chiral, and bi-anisotropic open optical systems and metamaterials", **in**: the 9th international conference on metamaterials, photonic crystals and plasmonics (2018).

[89] S. S. Oh **and** O. Hess, "Chiral metamaterials: enhancement and control of optical activity and circular dichroism", Nano Convergence **2**, 1–14 (2015).

[90] J. S. Siegel, "Single-handed cooperation", Nature **409**, 777–778 (2001).

[91] L. A. Nguyen, H. He **and** C. Pham-Huy, "Chiral drugs: an overview", International journal of biomedical science: IJBS **2**, 85 (2006).

[92] R. W. Smithells **and** C. G. Newman, "Recognition of thalidomide defects.", Journal of Medical Genetics **29**, 716–723 (1992).

[93] P. Ferenci, "Diagnosis and current therapy of wilson's disease", Alimentary Pharmacology & Therapeutics **19**, 157–165 (2004).

[94] M. Schäferling, *Chiral nanophotonics: chiral optical properties of plasmonic systems*, Springer Series in Optical Sciences (Springer International Publishing, 2016).

[95] A. O. Govorov, Z. Fan, P. Hernández, J. M. Slocik **and** R. R. Naik, "Theory of circular dichroism of nanomaterials comprising chiral molecules and nanocrystals: plasmon enhancement, dipole interactions, and dielectric effects.", Nano letters **10 4**, 1374–82 (2010).

[96] A. O. Govorov **and** Z. Fan, "Theory of chiral plasmonic nanostructures comprising metal nanocrystals and chiral molecular media.", Chemphyschem : a European journal of chemical physics and physical chemistry **13 10**, 2551–60 (2012).

[97] S. F. Almousa, T. Weiss **and** E. A. Muljarov, "Employing quasidegenerate optical modes for chiral sensing", Physical Review B **109**, L041410 (2024).